

**NAVAL POSTGRADUATE SCHOOL**  
**Monterey, California**



**THESIS**

**DESIGN AND METHOD FOR THE EVALUATION  
OF THE COKING RESISTANCE OF SWIRL  
PLATES OF THE E-2C AIRCRAFT FUEL  
NOZZLES**

by

Vassilios P. Vassiloyanakopoulos

March 1996

Thesis Advisor:

J.Perkins

Approved for public release; distribution is unlimited.

19960620 116

DTIC QUALITY INSPECTED 1

REPORT DOCUMENTATION PAGE			Form Approved OMB No. 0704	
Public reporting burden for this collection of information is estimated to average 1 hour per response, including the time for reviewing instruction, searching existing data sources, gathering and maintaining the data needed, and completing and reviewing the collection of information. Send comments regarding this burden estimate or any other aspect of this collection of information, including suggestions for reducing this burden, to Washington headquarters Services, Directorate for Information Operations and Reports, 1215 Jefferson Davis Highway, Suite 1204, Arlington, VA 22202-4302, and to the Office of Management and Budget, Paperwork Reduction Project (0704-0188) Washington DC 20503.				
1. AGENCY USE ONLY (Leave blank)		2. REPORT DATE March 1996	3. REPORT TYPE AND DATES COVERED Master's Thesis	
4. TITLE AND SUBTITLE Design and method for the evaluation of the coking resistance of swirl plates of the E-2C aircraft fuel nozzles			5. FUNDING NUMBERS	
6. AUTHOR(S): Vassilios P.Vassiloyanakopoulos				
7. PERFORMING ORGANIZATION NAME(S) AND ADDRESS(ES) Naval Postgraduate School Monterey CA 93943-5000			8. PERFORMING ORGANIZATION REPORT NUMBER	
9. SPONSORING/MONITORING AGENCY NAME(S) AND ADDRESS(ES)			10. SPONSORING/MONITORING AGENCY REPORT NUMBER	
11. SUPPLEMENTARY NOTES The views expressed in this thesis are those of the author and do not reflect the official policy or position of the Department of Defense or the U.S. Government.				
12a. DISTRIBUTION/AVAILABILITY STATEMENT Approved for public release; distribution is unlimited			12b. DISTRIBUTION CODE	
13. ABSTRACT (maximum 200 words) The extensive coking observed on the swirl plates of the fuel nozzles of the E-2C HAWKEYE aircraft is the initiative of this investigation. A testing rig reproducing the shut down procedure of the engine was designed and a method for the evaluation of the resistance in coking for different types of swirl plates is presented. The method is based on measurements of weight increase and holes closure, and on microscopic examination. It can be applied to the evaluation of any suggested modification of swirl plates in the future and provides the NAVY with a reliable easy to use and modify experimental set-up able to produce comparative data. Results for two different types of swirl plates with different surface finish are presented, together with conclusions and comments arising from the experimental results and the design process. Recommendations for future search objectives to the problem are also presented.				
14. SUBJECT TERMS : Coking of swirl plates, surface finish, weight measurements, hole's closure, optical examination			15. NUMBER OF PAGES 123	
			16. PRICE CODE	
17. SECURITY CLASSIFICATION OF REPORT Unclassified	18. SECURITY CLASSIFICATION OF THIS PAGE Unclassified	19. SECURITY CLASSIFICATION OF ABSTRACT Unclassified	20. LIMITATION OF ABSTRACT UL	



Approved for public release; distribution is unlimited.

**DESIGN AND METHOD FOR THE EVALUATION OF THE COKING  
RESISTANCE OF SWIRL PLATES OF THE E-2C AIRCRAFT FUEL NOZZLES**

Vassilios P. Vassiloyanakopoulos  
Lieutenant Junior Grade, Hellenic Navy  
B.S., Hellenic Naval Academy, 1989

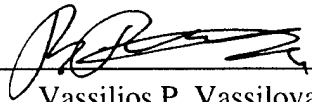
Submitted in partial fulfillment  
of the requirements for the degree of

**MASTER OF SCIENCE IN MECHANICAL ENGINEERING**

from the

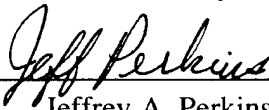
**NAVAL POSTGRADUATE SCHOOL  
March 1996**

Author:

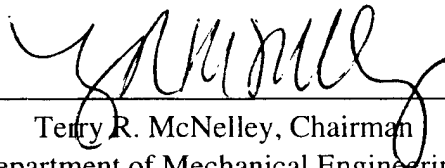


Vassilios P. Vassiloyanakopoulos

Approved by:



Jeffrey A. Perkins



Terry R. McNelley, Chairman  
Department of Mechanical Engineering





## ABSTRACT

The extensive coking observed on the swirl plates of the fuel nozzles of the E-2C HAWKEYE aircraft is the initiative of this investigation. A testing rig reproducing the shut down procedure of the engine was designed and a method for the evaluation of the resistance in coking for different types of swirl plates is presented. The method is based on measurements of weight increase and holes closure, and on microscopic examination. It can be applied to the evaluation of any suggested modification of swirl plates in the future and provides the NAVY with a reliable easy to use and modify experimental set-up able to produce comparative data. Results for two different types of swirl plates with different surface finish are presented, together with conclusions and comments arising from the experimental results and the design process. Recommendations for future search objectives relative to the problem are also presented.



## TABLE OF CONTENTS

I. INTRODUCTION .....	1
A. GENERAL .....	1
B. GAS TURBINES AND DEPOSITS.....	2
C. DEPOSITS ON SWIRL PLATES.....	4
D. BACKGROUND.....	9
E. OBJECTIVES.....	10
F. WEIGHT AND FLOW MEASUREMENTS.....	11
II. EXPERIMENTAL PROCEDURE.....	13
A. EXPERIMENTAL SET-UP.....	13
B. DATA EXTRACTION.....	20
C. SAFETY FEATURES.....	25
III. RESULTS AND DISCUSSION.....	27
A. GENERAL.....	27
B. WEIGHT MEASUREMENTS.....	27
C. OPTICAL MICROSCOPY EXAMINATION.....	32
D. SEM EXAMINATION.....	52
E. FLOW - CLOSURE OF HOLES MEASUREMENTS.....	67
IV. CONCLUSIONS AND RECOMMENDATIONS.....	73
A. CONCLUSIONS.....	73
B. RECOMMENDATIONS.....	75
APPENDIX A: CORROSION AND DEPOSITS IN GAS TURBINES.....	77
APPENDIX B: CHEMICAL FACTORS .....	81

APPENDIX C: COATED SWIRL PLATES SUGGESTION.....	85
APPENDIX D: ISENTROPIC FLOW AND FLOW MEASUREMENTS.....	89
APPENDIX E: COMPUTER PROGRAMMING DESCRIPTION.....	97
APPENDIX F: PRINCIPLES FOR A PROPOSED GRADING SYSTEM ON THE COKING RESISTANCE OF SWIRL PLATES.....	103
LIST OF REFERENCES.....	107
INITIAL DISTRIBUTION LIST.....	109

## LIST OF FIGURES

1. Physical factors participating in the deposition accumulation.....	4
2. Schematic of dual fuel nozzle.....	5
3. Side view of the dual fuel nozzle- Schematic of the swirl plate.....	6
4. Temperature-Time profile of the swirl plates at the soak back conditions	8
5. Schematic of the experimental set up for the Nozzle Project.....	14
6. Schematic of the data flow in the control program used.....	17
7. Temperature- Time profile for the swirl plates in 30 min. cycles.....	18
8. Temperature- Time profile obtained from the testing rig (repeatable cycles).....	19
9. Schematic of the "positions" of the swirl plate.....	21
10. Schematic of the flow measurements experimental set-up.....	22
11. Calibration curve of pressure transducer.....	24
12. Weight increase vs. cycles performed for A22 and A'26.....	29
13. Weight increase vs. cycles performed for A27 and B18.....	31
14. Optical picture 12 o' clock, 80 cycles, A'26 (a) and A22 (b).....	34
15. Optical picture 3 o' clock, 80 cycles, A'26 (a) and A22 (b).....	35
16. Optical picture 3 o' clock, virgin, B18 (a) and A27 (b).....	36
17. Optical picture 3 o' clock, 25 cycles, B18 (a) and A27 (b).....	37
18. Optical picture 3 o' clock, 50 cycles, B18 (a) and A27 (b).....	38
19. Optical picture 3 o' clock, 75 cycles, B18 (a) and A27 (b).....	39
20. Optical picture 3 o' clock, 100 cycles, B18 (a) and A27 (b).....	40
21. Optical picture 3 o' clock, 125 cycles, B18 (a) and A27 (b).....	41
22. Optical picture 3 o' clock, 150 cycles, B18 (a) and A27 (b).....	42

23. Optical picture 6 o' clock, virgin , B18 (a) and A27 (b).....	43
24. Optical picture 6 o' clock, 25 cycles, B18 (a) and A27 (b).....	44
25. Optical picture 6 o' clock 50 cycles, B18 (a) and A27 (b).....	45
26. Optical picture 6 o' clock, 75 cycles, B18 (a) and A27 (b).....	46
27. Optical picture 6 o' clock, 100 cycles, B18 (a) and A27 (b).....	47
28. Optical picture 6 o' clock, 125 cycles, B18 (a) and A27 (b).....	48
29. Optical picture 6 o' clock, 150 cycles, B18 (a) and A27 (b).....	49
30. Optical picture 2 o' clock 75 cycles A27.....	50
31. Optical picture 2 o' clock 100 cycles A27.....	50
32. Optical picture 2 o' clock 125 cycles A27.....	51
33. Optical picture 2 o' clock 150 cycles A27.....	51
34. SEM picture 12 o' clock, virgin A22 (a) and A'26 (b).....	54
35. SEM picture 12 o' clock, virgin A22 (a) and A'26( b) (high magnification).....	55
36. SEM picture 12 o' clock, virgin B18 (a) and A22 (b).....	56
37. SEM picture 12 o' clock, virgin B18 (a) and A22 (b) (high magnification).....	57
38. SEM picture 12 o' clock, 50 cycles, B18 (a) and A22 (b).....	58
39. SEM picture 12 o' clock, 100 cycles, B18 (a) and A22 (b).....	59
40. SEM picture 12 o' clock, 150 cycles, B18 (a) and A22 (b).....	60
41. SEM picture 3 o' clock, 50 cycles, B18 (a) and A22 (b).....	61
42. SEM picture 3 o' clock, 100 cycles, B18 (a) and A22 (b).....	62
43. SEM picture 3 o' clock, 150 cycles, B18 (a) and A22 (b).....	63
44. SEM picture 6 o' clock, 50 cycles, B18 (a) and A22 (b).....	64
45. SEM picture 3 o' clock, 100 cycles, B18 (a) and A22 (b).....	65

46. SEM picture 3 o' clock, 150 cycles, B18 (a) and A22 (b).....	66
47. Flow characteristic curves for A22 swirl plate.....	68
48. Flow characteristic curves for B18 swirl plate.....	69
49. Average percentage hole closure of swirl plates vs. cycles performed...	71
50. Schematic representation of a Jet Engine.....	77
51. Deposition on combustion chamber.....	79
52. Rate of deposits accumulation in gas turbines burning Bunker C fuel...	80
53. How coke forms (Heat break up followed by molecular growth from fragments .....	86
54. Coke does not grow if fragments can disperse.....	86
55. Surface microcavities contain fragments and permit coke to grow.....	87
56. Sulfur or oxygen in fluid react with the metal atoms to form surface microcavities.....	87
57. GE's suggestion of coating film on the surface.....	88
58. Compressible flow through a duct (a) real fluid velocity, (b) one dimensional approximation.....	89
59. Area ratio vs. Mach number for isentropic flow of a perfect gas with $k=1.4$ .....	91
60. Various pressure and Mach number configurations for flow through a nozzle.....	92
61. Area ratio vs. Mach number for subsonic flow.....	92
62. Operation of converging nozzle: (a) nozzle geometry, (b) pressure distribution and (c) mass flow vs. back pressure.....	93
63. Schematic of operational principle of flow meter.....	95
64. Operation of coils in the flow meter.....	96



65. Schematic of the programme used in controlling the furnace.....	97
66. Schematic of the data display screen.....	100
67. Temperature- Time profile for the swirl plates and the furnace.....	101

# I. INTRODUCTION

## A. GENERAL

The U.S.NAVAIR is currently investigating a major problem experienced in the T56-A-427 turbine engine types of Allison Engine Co. The engine has been used in the NAVY E-2C (HAWKEYE) aircraft since 1987 [Ref. 1]. Fuel coking was evident on the swirl plates of the fuel nozzles in engines operating with JP5 fuel. Some of the swirl plates have been reported to become severely plugged with coke, and so they had to be immediately replaced [Ref. 2]. Investigation of the problem has shown that coking occurs at significant rates when the fuel nozzle interiors are subjected to temperatures above 320F during thermal soak back. This condition occurs within seconds of shut down from High Speed Ground Idle (HSGI) in which case the temperature remains within the range 350-400F for approximately 30-50 minutes [Ref. 3]. The most annoying fact in the described situation is that the cycle for refurbishing of the fuel nozzles is less than a tenth (10%) of the operational limit set by the US Navy at the range of 3000 hours [Ref. 3, 4]. A statistical study performed by Allison has shown that at least one swirl plate will be blocked in 30 % of the operated engines after 200 hours and this percentage rises to up to 80% for 800 hours [Ref. 5]. As can be understood, this situation results to severe demands on maintenance support and is crucial for the effectiveness of the turbine and the availability and operational ability of the aircraft. The Navy is looking for the most reliable and economic solution to face this problem, since E-2C still remains the major early warning and control aircraft of the US Navy and represents an important unit on aircraft carriers [Ref. 1].

## **B. GAS TURBINES AND DEPOSITS**

The general problem of coking depositions in gas turbines, as well as in boilers, is not new. Numerous studies have already been submitted over the past four decades, in an attempt to explain the problem and suggest solutions. Most of these studies were concerned with the chemical reactions forming depositions. These reactions, prove to be very complex, so that quite different results have been obtained from different studies.

A description of the problem of the coking is given in [Ref. 6]. According to this study, deposits in gas turbines go hand in hand with corrosion, while also upsetting the aerodynamic condition in the case of gases required to translate to kinetic energy and flow conditions through the swirl plates. Three major factors are considered to be involved in the formation of deposits :

1. Temperature of metal and gas stream.
2. Composition of substances in contact with the metal surfaces and the nature of these surfaces.
3. Aerodynamic considerations, involving gas and particle velocity and size consist of deposited particles.

These problematic factors have been proved already severe enough in themselves to have taxed the capabilities of engineers and chemists for the past decades. Although advances have been made in understanding a few of the complex chemical and physical relationships involved, the overall problem still needs complete solution, as deposits in gas turbines continue to cause problems in the efficiency and maintenance of these devices.

W. T. Reid [Ref. 6] suggests that both physical and chemical mechanisms take part in the formation and accumulation of deposits. Among the physical factors mentioned are :

1. Molecular Diffusion, in which very tiny particles move with velocities approaching that of gas molecules.
2. Brownian Motion, in which somewhat larger particles (up to  $1\mu\text{m}$ ) behave as discrete pieces of matter during the " random walk" motion imparted by collision with gas molecules [Ref. 7].
3. Turbulent Diffusion, in which even larger particles (larger than  $1\mu\text{m}$ ) entering a boundary layer are propelled through a laminar sublayer by velocities imparted by the turbulent gas layer between the laminar sublayer and the bulk gas stream.
4. Inertial Impaction, in which, still larger particles receive sufficient kinetic energy from the main gas stream for them to penetrate a boundary layer or the turbulent region or to follow a different path from the gas stream.

In the following Figure 1, we can see the effect of each of the above mentioned factors in the deposit accumulation.

A special case, involving build-up of deposits, can be based on vapour diffusion or condensation. Considering the fact that the number of small particles in the gas stream entering the boundary layer will be too small to account for any appreciable mass of deposits, the presence of these particles can be attributed to the condensation of vapour being transported into the boundary layer [Ref. 6].

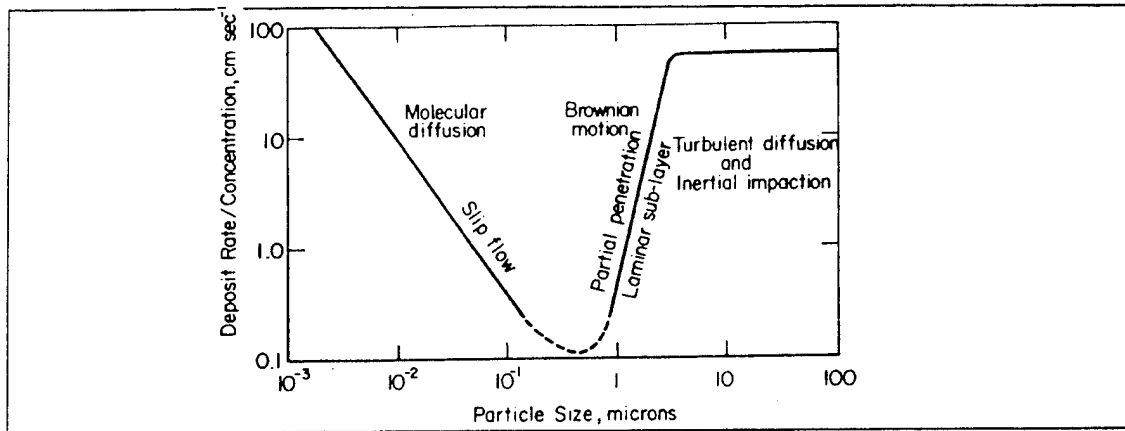


Figure 1: Physical Factors participating in the deposition accumulation (From [6]).

Considering the chemical factors, W. T. Reid [Ref. 6] includes :

1. Sintering characteristics of the deposits, referring to the particle's coalescence with the surface at elevated temperatures. Factors like chemical composition, time-temperature history during combustion, atmosphere conditions where the engine is working etc., can contribute to this mechanism. The formation of a liquid phase is likely to ensure adherence of the deposits on the metal's surface.
2. Chemical reactions, which can be either autoxidation (at temperatures 500F and below) or pyrolysis (at temperatures of 900F and higher) with an intermediate regime for the range of temperatures in between [Ref. 8, Appendix B].

### C. DEPOSITS ON SWIRL PLATES

The fuel nozzles that are currently in use in the T56-A-427 gas turbine are Dual Entry Nozzles (also known as double orifice nozzles). In general the function of a fuel nozzle, according to [Ref. 9], is to create a highly atomised, accurately shaped spray of fuel, suitable for rapid mixing and combustion with the primary air stream under varying conditions of fuel and air flow. The Dual Entry Nozzle was developed to double the flow range of the previous designed nozzles and to maintain a practically constant spray cone

angle throughout a wide operating range. Schematic representation of such a nozzle can be seen in Figures 2, 3. The nozzle features two concentric orifices and swirl chambers . The inner swirl chamber and its small orifice serve for primary flows and with increasing the fuel flow requirements, fuel flow passes through tangential grooves into the annular swirl chamber ahead of the main orifice. When the secondary flow starts, at high fuel requirements, the atomisation of the secondary fuel is assisted by the energy of the fully developed primary spray with which it blends [Ref. 10].

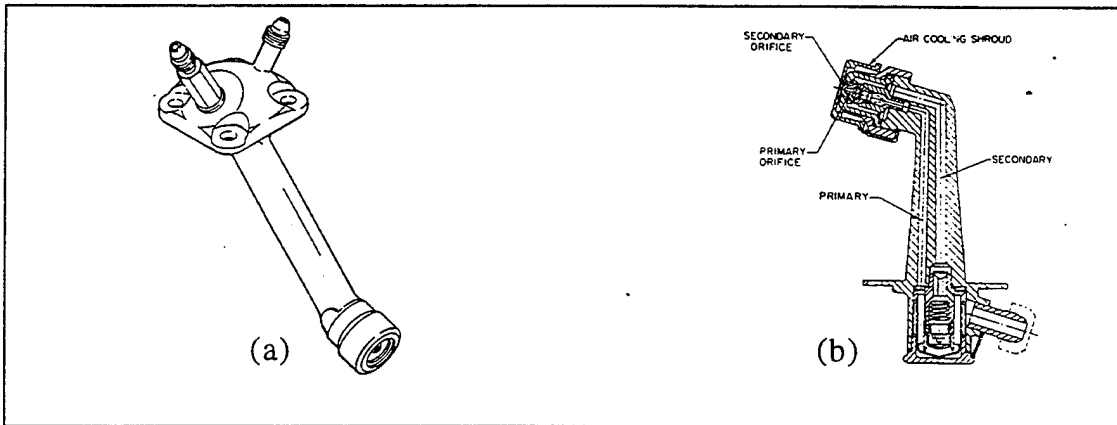


Figure 2: Schematic of Dual Fuel nozzle ((a) from [11] and (b) from [10] ).

When the flow and pressure requirements are decreased below 125 psi (which is the case when the engine is shut down), a small amount of fuel is trapped in the line between the valve and the swirl plate. Based on calculations made from engineering drawings, the estimated volume of the trapped in the internal main circuit is only a few cubic centimetres [Ref. 3].

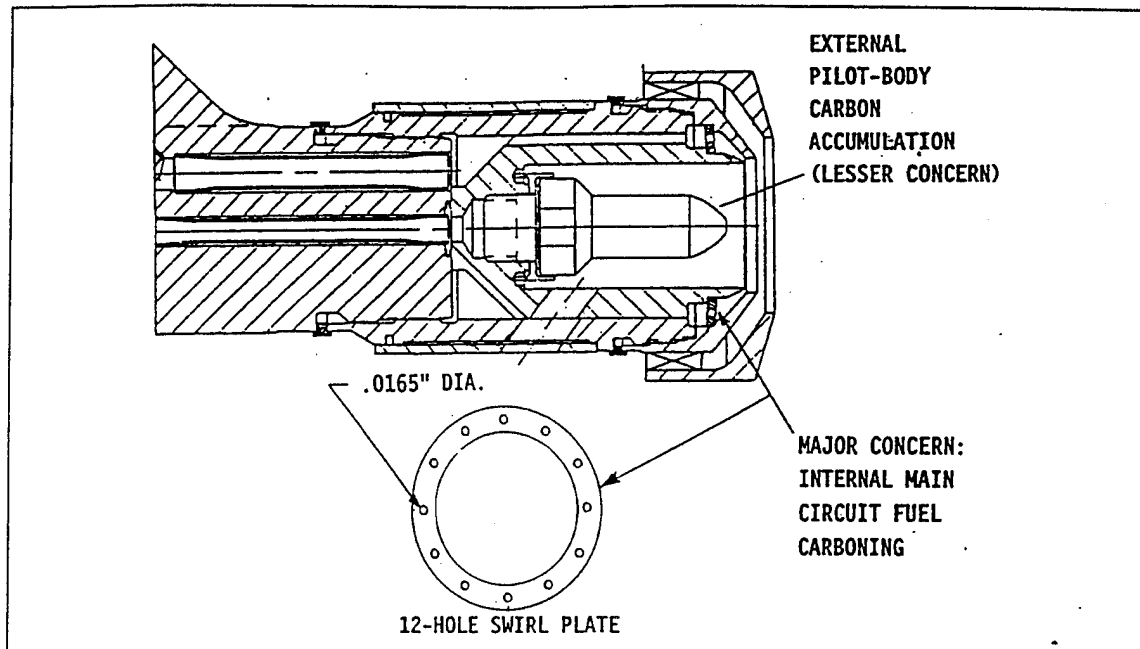


Figure 3 : Side view of the Dual Fuel Nozzle schematic of the swirl plate (from [12]).

While the formation of depositions in gas turbines is usually associated with excessive fuel temperature, the High Speed Ground Idle operation, followed by shutting down the engine, has been found to be characterised by comparatively lower temperatures. Heat transfer work performed on A-427 fuel nozzles by Allison Engines Co. with the co-operation of NAVAIR [Ref. 2], have shown that the temperature range which the swirl plates were experiencing was at the range of 340 to 370 -390 F [Ref. 3]. Using these studies, NAVAIR suggested a critical temperature -time profile [Ref. 13] and this was the guiding profile used in the experiments of the present study. The profile can be seen in Figure 4.

Considering these temperatures (below 500 F) the main chemical mechanism that dominates the reactions is autoxidation [Ref. 8, Appendix B]. The result of this behaviour is thermal degradation of the trapped fuel and formation of solid deposits on the swirl

plates . According to Prof. Crooks [Ref. 3] the process of formation of these deposits is known to be enhanced by the presence of copper ions and oxygen, resulting in the formation of what are conveniently classified as "gums ". According to [Ref. 14], gums are high molecular weight compounds containing hydrogen, carbon, oxygen and usually sulfur and nitrogen. They may occur in refined fuels in either soluble or insoluble forms. The soluble forms are expected to cause trouble when thin film of fuel is exposed to air. This fuel then, evaporates, leaving gum deposits [Ref. 3]. Although fuel specifications do not differentiate, between soluble and insoluble gums, they do limit the existence and occasionally the potential, of gums [Ref. 14, 15]. The gums observed on the swirl plates were soluble in organic solvents such as heptane or acetone.



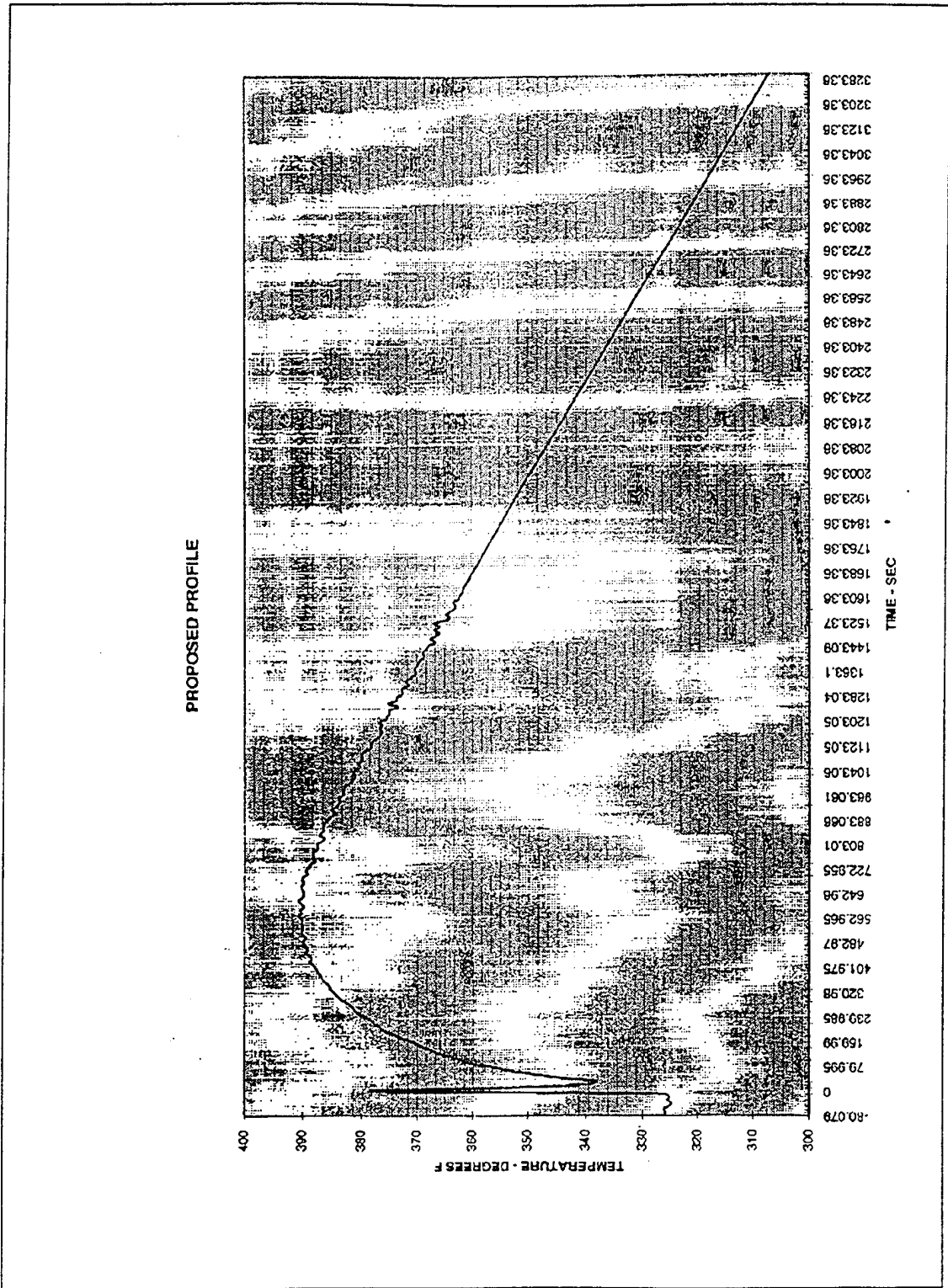


Figure 4: Temperature Time profile of the swirl plates at soak back condition (from [13]).

## D. BACKGROUND

In the attempt to find a solution to the problem several ideas have been presented which can be summarised as follows:

1. The adoption of Low Speed Ground Idle (LSGI) as a shutdown procedure was initially proposed as an interim solution. This approach has some disadvantages from a safety standpoint, especially in the case of aircraft carriers. It is always preferable to shut off the engine and halt propeller motion as soon as possible after landing on the carrier deck, rather than using a cooling down period, such as the LSGI shutdown procedure [Ref. 3]. Despite this limitation, since LSGI shutdown has been proved to be effective in decreasing the amount of depositions, it is currently used as an interim procedure as the search for a more permanent solution is continued.
2. The use of a Purge System (Low Pressure Fuel Purge System), to expel with air pressure the trapped fuel before the swirl plates [Ref. 16]. The system was suggested by the manufacturer Allison Engine Co., but has not been adopted by the NAVY due to the enormous cost of its maintenance, an expected increase in the weight of the aircraft, and the time required to be installed [Ref. 4, 17].
3. The use of different types of swirl plates, than those already in use. The standard swirl plates manufactured by Parker Co., are made from Type 347 stainless steel. In our studies these are termed as A type; they do not have any special surface finish treatment. Proposed solutions include the following improved types of swirl plates that would hopefully proved to be more effective in resisting coking accumulation than the A type:
  - a) The A' type with polished surface (using a 30 micron finish, performed by Allison).
  - b) The B type with polished surface and polished holes surface ( by Du Pont).

Coated swirl plates which are swirl plates coated with a thin protective film of  $Ta_2O_5$  or a ceramic coating. A more detailed description of this kind of swirl plates with information related to their production is given in Appendix C. [Ref. 12, 18, 3]. These three types of swirl plates are in accordance with the suggestion of Prof. Roy Crooks based on the concept that coking problems in general may be alleviated by improvement in surface finish and the use of coating films resistant to the adhesion of coke [Ref. 3].

## E. OBJECTIVES

The objectives of this project can be summarised as follows:

1. To design a testing rig that would be used to simulate the soak back condition that the gas turbine experiences as soon as the normal shut down is performed. The test rig must be able to work for two different swirl plates at the same time so that a comparison under the same conditions to be possible.
2. To provide NAVAIR with the respective experimental data, concerning deposits accumulation rate and the effect that these depositions have in the swirl plates performance, as far as the holes closure concerns
3. To perform optical and SEM investigation on the swirl plates in order to get comparative data between swirl plates of different types.

The success in achieving these objectives will provide the NAVY with a safe easy to use and modify experimental set-up, one that can be used to justify the degree of effectiveness of all kind of similar with above mentioned suggestions. With the appropriate data available and easily reproducible the Navy will have an additional guide for the optimum solution.

It should be mentioned that the problem of coking of swirl plates includes many parameters which could alter the data obtained according to the focus of the investigation. In this project the focus was in determining the effect that the surface finish of the swirl plates has upon the amount of coking and the closure of holes. The temperature - time profile was kept constant, as was the fuel used (JP 5) and the amount of air in the rig (no ventilation method was used). By changing any of these other major parameters, data could be obtained according to a different focus of interest.

## F. WEIGHT AND FLOW MEASUREMENTS

An effective way to measure the deposition rate accumulated on the different types of swirl plates was to measure the increase in their weight, namely by performing a periodic measurement. In order to measure closure of the swirl plates holes due to the deposits, which is very important for the fuel flow through them, a safe way is to perform a flow measurement of a gas passed through the nozzles, with an accurate flow meter calibrated to work for this specific gas. For this calculation, the isentropic flow model is adopted.

In general, frictionless adiabatic or isentropic flow is an ideal that cannot be reached in the flow of real gases. It can be approached, however, in flow through transition, nozzles and venturi meters, where friction effects are minor owing to the short distances travelled, and heat transfer is minor because the changes that a particle (air molecules) undergoes are slow enough to keep the velocity and temperature gradients small [Ref. 19].

Adopting the isentropic flow model we get:

For the gas mass flow rate  $\hat{m} = \rho Sv$  (1) where  
 $\hat{m}$  : mass flow rate

$\rho$  : density of gas

$S$  : area through which the gas flows

$v$  : velocity of gas stream

Considering ideal gas  $\rho = \frac{P}{RT}$  (2) where

P : pressure of gas (gage)

R : gas constant

T : temperature

From (1) and (2) and considering that the speed of sound is  $a = \sqrt{\gamma RT}$  (3)

we get  $\frac{\dot{m}}{S} = P \left(\frac{\gamma}{a}\right) \sqrt{\frac{\gamma}{RT}}$  (4)  $(\gamma = \frac{C_p}{C_v})$  (5)

For the pressures and temperatures measured at a specific point we get

$$T_o = T \left[ 1 + \frac{\gamma-1}{2} M^2 \right] \quad (6)$$

$$P_o = P \left[ 1 + \frac{\gamma-1}{2} M^2 \right]^{\frac{\gamma}{\gamma-1}} \quad (7)$$

where the '0' subscript denotes stagnation values

$$\text{Finally we get } \frac{\dot{m}}{S} = \frac{P_o}{\sqrt{T_o}} \sqrt{\frac{\gamma}{R}} \left[ 1 + \frac{\gamma-1}{2} M^2 \right]^{\frac{\gamma+1}{2(\gamma-1)}} \quad (8)$$

In our case, while the air is passing through the swirl plates holes, we can assume sonic flow ( $M=1$ ) following the similarity with the case of the nozzle neck (Appendix D).

By denoting the area of the holes of the virgin swirl plate by  $S_1$  and for the used swirl plate, after 1,2,3... experimental cycles performed, by  $S_1, S_2, S_3, \dots$ , we can calculate the average closure of the swirl plate's holes.

The percent average closure after the completion of the  $j^{\text{th}}$  cycle for the different types of swirl plates will be:

$$\phi_J = \frac{S_J - S_1}{S_1} \cdot 100 \quad (9) \quad J=1, 2, 3, \dots$$

## II. EXPERIMENTAL PROCEDURE

### A. EXPERIMENTAL SET-UP

Maxwell Smith [Ref. 15] reasonably suggests that in regard to aviation the research has kept ahead of demand in the matter of quality. Development work of this kind, to be successful, is entirely dependent on the availability of means in order to predict or even better determine whether the new products will give satisfactory performance. By using test rigs, full scale engine bench tests or flight trials can be avoided. Rigs can be located in laboratories where necessary research personnel and analytical equipment are ready to hand. Also, they can be operated twenty four hours a day, seven days a week and get results more quickly [Ref. 15].

The design concept was to reproduce actual soak back conditions for the fuel on the swirl plates by simulating the suggested temperature-time profile. The original test rig, designed by Professor Roy Crooks of the Naval Postgraduate School [Ref. 3], provided the basis for design of a new nozzle test rig. The factors that lead to the need for a new design were safety factors and the attempt to follow the temperature-time profile with a more easy to use furnace, instead of the oven that had been previously used. The experimental set-up includes the following:

1. A box furnace (220V of NEY Co., series II model 2-525)
2. Two fuel pumps (Zippettes ) activated with attached relays
3. Two three way valves controlled by two regulators (WHITEY)
4. Two, Dual Entry Fuel Injection Nozzles

5. A computer (PC) controlling the cycles and the data acquisition programme.

On the following Figure 5 a schematic of the experimental set-up can be seen.

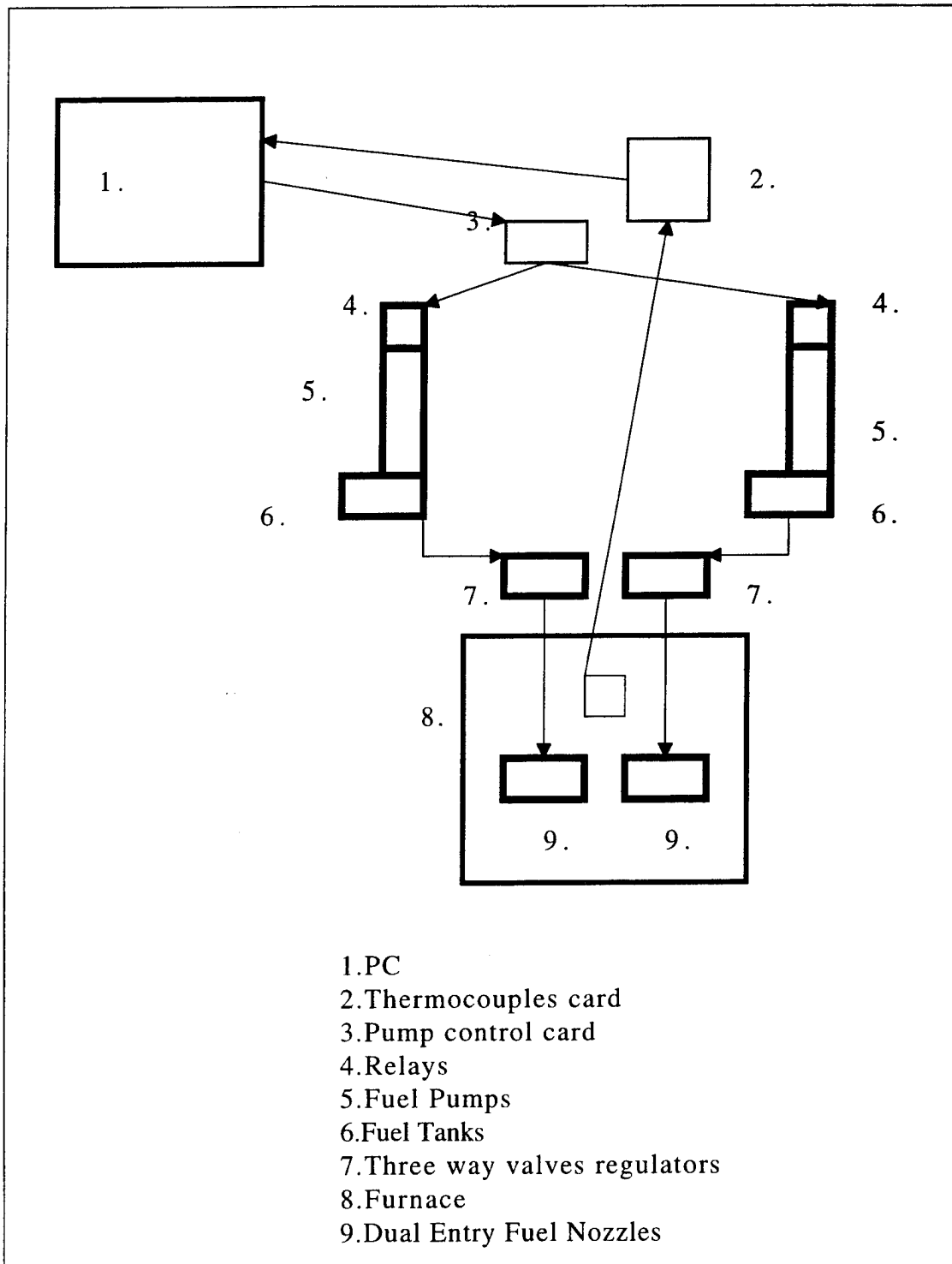


Figure 5 : Schematic of the experimental set-up for the Nozzle Project.

The data acquisition programme allows the user to view on the screen the following parameters of the cycle operation :

1. The temperature of each of the swirl plates and of the furnace from the respectively attached thermocouples.
2. The time and the number of cycles that the program is at any instant (time measured in seconds).
3. The temperature time profile of the swirl plates. Additionally the values of the temperature measured by the thermocouples are saved and transferred in separate files, that can be retrieved for the control of the temperature time profile.

The system is designed to cycle automatically while monitored and regulated by the computer through the LABTECH NOTEBOOK package [Ref. 20]. This package includes Block Menus which are control functions available to the user so that by changing the parameters in them, they can be used for different applications. The Icon View is an additional feature offered in order to have a schematic representation of the program written, with a data flow of the program. A schematic of the program used in the application can be seen in Figure 6.

As currently configured, each cycle consists of the following events in order to simulate the actual soak-back conditions:

1. The three way valve to the simulator nozzle opens.
2. A fixed quantity of fuel is injected into the fuel line and drains into the nozzle.
3. The valve closes.
4. The simulator nozzle is heated to normal operating conditions which for the swirl plate temperature refer to 370 to 380 F. The suggested profile determines the rate of the temperature increase of the swirl plates.
5. The simulator nozzles are cooled to 350F again following a cooling rate suggested by the profile.



6. Step (1) is repeated again.

The new developed design of the rig gave the opportunity to use two fuel nozzles at the same time. In this way the data extraction was faster in order to get comparable results for two different types of swirl plates placed on each nozzle and be exposed to the same conditions.

While in the original test rig a 50 minutes temperature time profile had been used, the new design has used a 30 minutes cycle. In this way it was possible to produce the deposition for the swirl plates and at the same time double the rate of data accomplished. On Figures 7 and 8 the temperature-time profile that was achieved with the new testing rig can be seen.

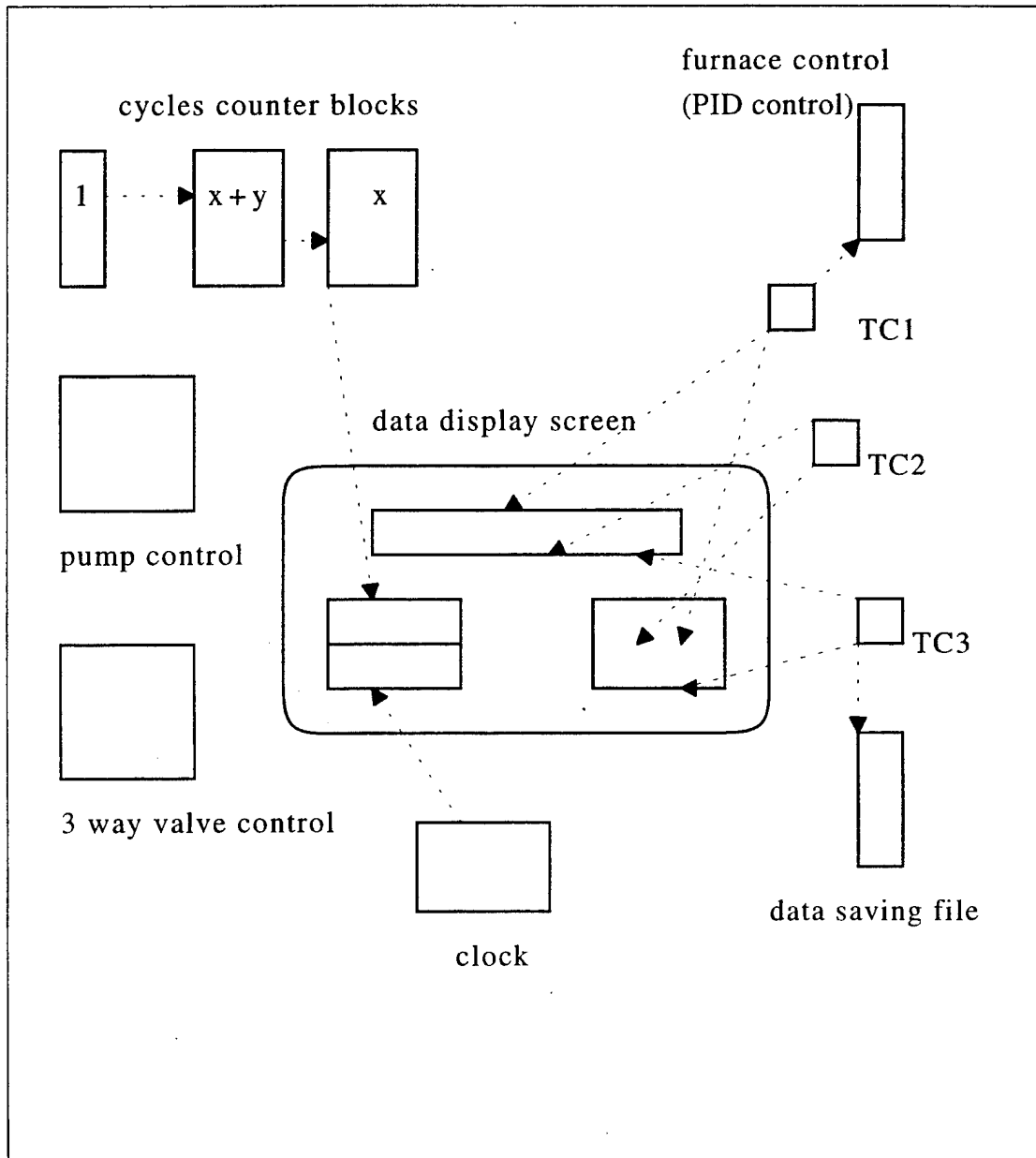


Figure 6: Schematic of the data flow in the control programme used.

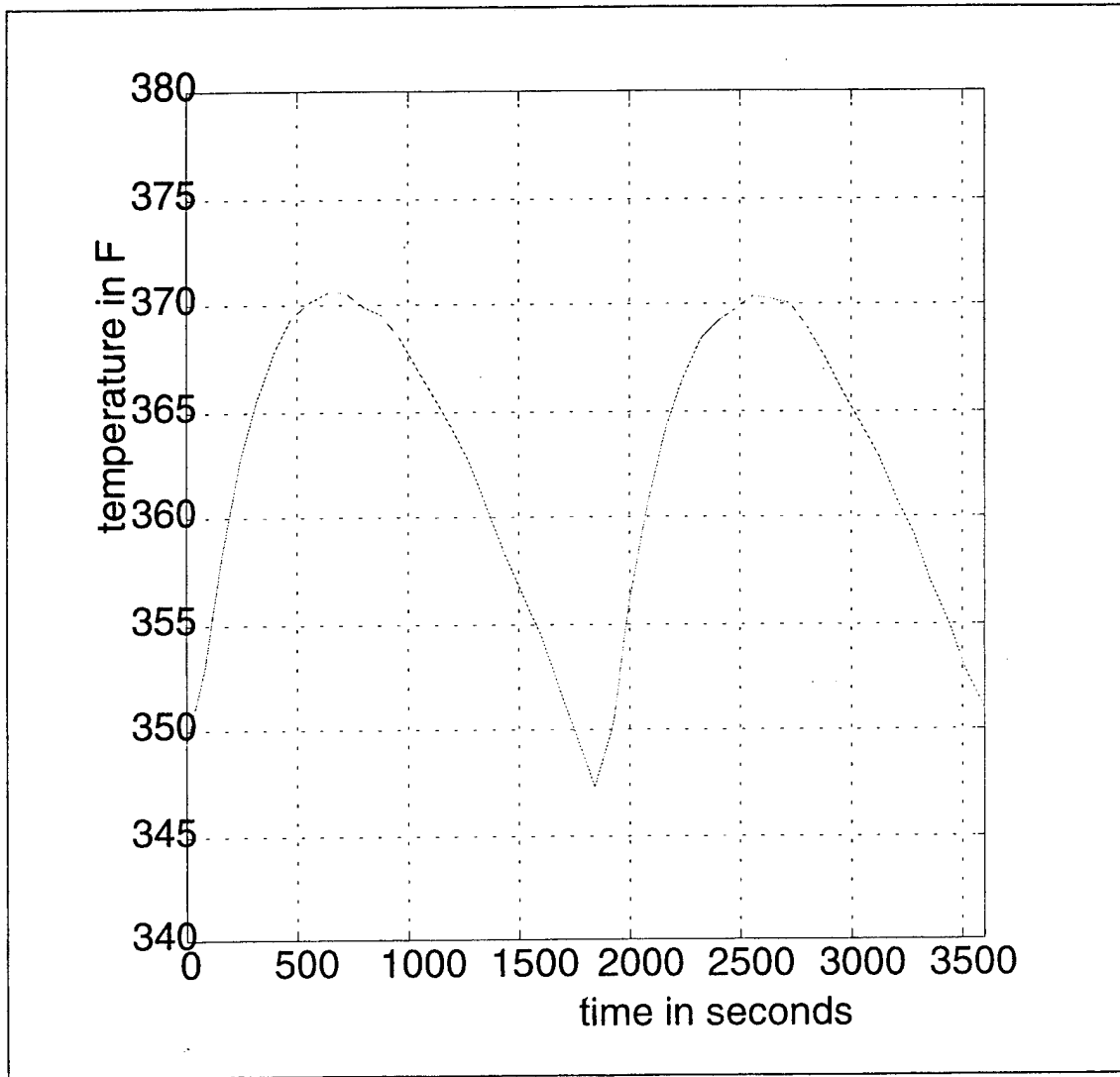


Figure 7: Temperature - Time profile for the swirl plates in two 30 minutes cycles.

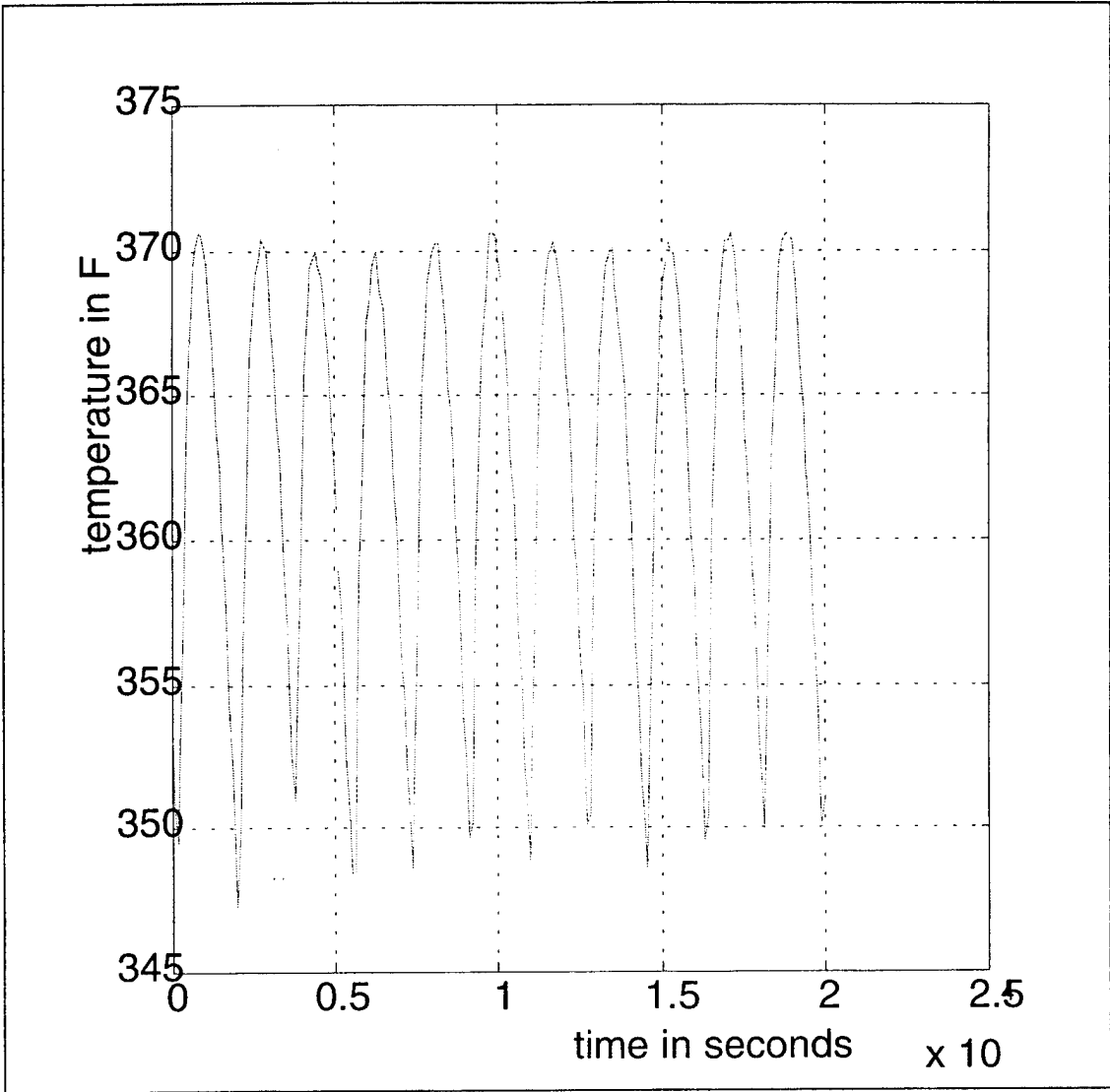


Figure 8: Temperature -Time profile obtained from the testing rig (repeatable cycles).

## **B. DATA EXTRACTION**

Weight measurements: Every 25 cycles (or every 12.5 hours of rig's operation), both swirl plates had been carefully weighted in an METTLER AT balance apparatus. The results were then compared with the initial weight of the virgin (unused swirl plates). According to this data, plots of weight with respect to the cycles performed (which can be directly associated with the same number of shut downs of the engine), was able to be produced and so give results comparable to the rate of accumulation of deposits in between the different types of the swirl plates.

Optical Microscopy Examination: In order to be able to recognise the swirl plates holes position, so as to explore whether the positioning of the hole is important in the coking accumulation, a nomenclature has been followed to distinct the several holes. A notch on the surface of the swirl plate was used to indicate the 12 o' clock position and similarly the 3, 6, 9 o' clock positions were also indicated. Every 24 cycles the swirl plates were examined with the optical microscope. If no specific features were seen in a hole, pictures of the 12, 3, 6, 9 o' clock were taken and saved in the respective name nomenclature of their position and number of cycles. Pictures of the surface of the swirl plate were also taken each time and also of any additional hole with some interesting feature depending on the deposition within that hole. Figure 9 shows a schematic of the swirl plate's hole position nomenclature.

SEM investigation: This was similar to the optical microscope investigation as far as the pictures taken and was performed after every 50 cycles. In both cases (optical and SEM) the pictures were compared with the pictures of the virgin (unused) swirl plates.

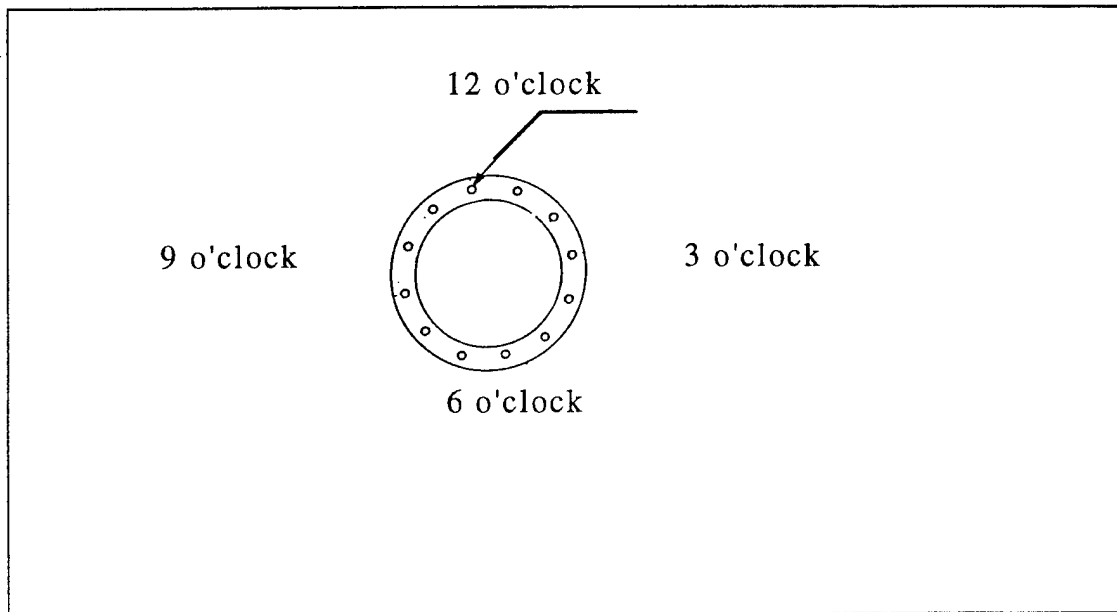


Figure 9: Schematic of the "positions" of the swirl plate (after [11]).

Flow measurements : In order to perform the flow measurements a Top-Trak, digital, electronically driven flow meter, has been used. A piping is connecting the valve of an oxygen bottle with the flow meter which is in series with a fuel injection nozzle with the swirl plate attached to it. On the following Figure 10 we can see the set-up designed in order to perform the flow measurements. This specific set-up includes:

1. Oxygen Bottle Cylinder, with Regulator attached to it (MATHESON Model 3062A). Two pressure gages were attached to the regulator (0-7500 psi and 0-5000 psi) in order to control the pressure in the bottle and the pressure of the gas coming through the piping.
2. Flow indicator with an additional pressure gage and a humidity filter attached to it (ARROW).
3. A digital flow meter calibrated to work with air (TOP RECK).
4. A pressure transducer connected with a voltmeter for the exact measure of air pressure .

5. A Dual Entry Fuel Nozzle identical to the ones used in the rig.
6. A Thermocouple connected at the Fuel Nozzle in order to measure the temperature of the air flowing through it.

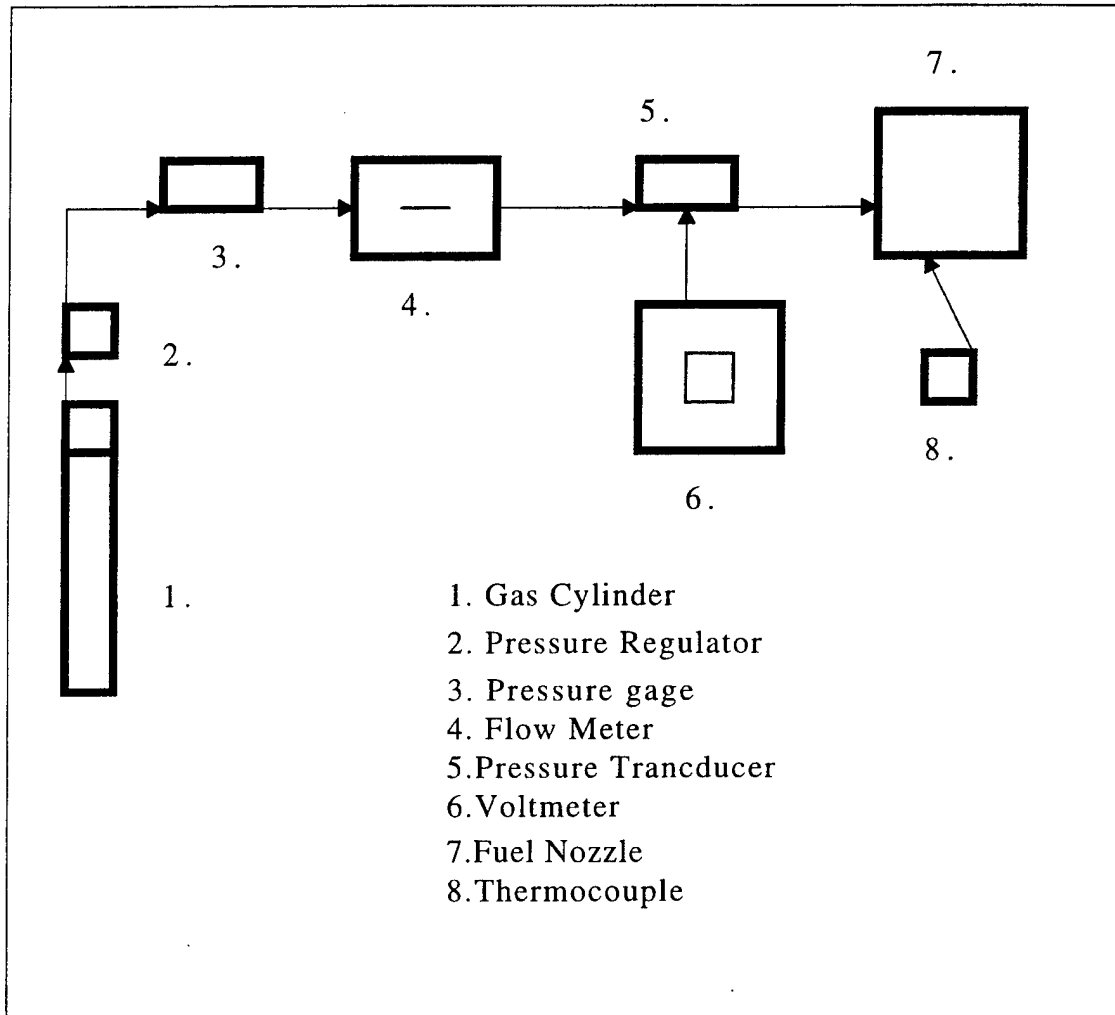


Figure 10 : Schematic of the flow measurement experimental set-up.

For the calculations required the following numbers have been considered in the case of air treated as an ideal gas :

$$\gamma = \frac{c_p}{c_v} = 1.4 \quad \rho = 1.292 \text{ kgr/m}^3 \quad R = 287 \text{ J/KgK}$$

By substituting these numbers in (7) we get the relation which will be used for the calculation of the area of the swirl plates holes.

$$S = \frac{\hat{m} \cdot \sqrt{T_0}}{0.04042 \cdot P_0} \quad (10) \quad \text{where } \hat{m} \text{ is the flow rate in kgr/sec}$$

$T_0$  is the temperature in Kelvins

$P_0$  absolute pressure in Pascals

S surface of swirl plate holes in  $\text{m}^2$

For the more accurate calculation of the gage pressure (P) the pressure transducer is used according to the calibration chart of its adjustment and with linear interpolation for intermediate values of voltage. On Figure 11 the calibration curve and the equation of the linear curve fit for the data points can be seen. The absolute pressure is at any time calculated by adding the atmospheric pressure at the time of the measurement was performed. (Details of the design method are given in Appendix D).



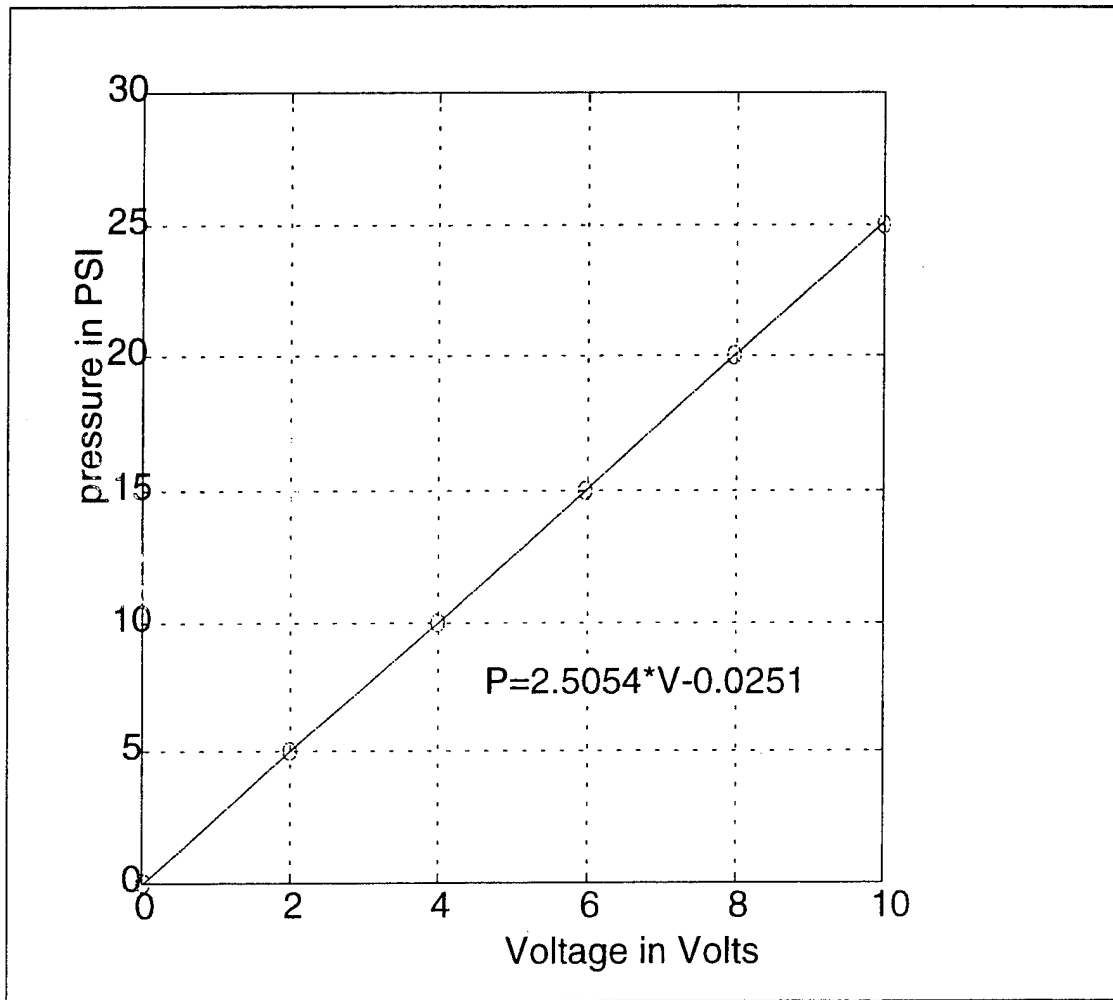


Figure 11 : Calibration curve of the pressure transducer

$P=2.5054*V-0.0251$  where P : pressure in psi  
V : Voltage in Volts

psi	0.00	25.00	0.00	5.00	10.00	15.00	20.00	25.00	15.00	5.00	0.00
Volts	0.016	10.00	0.023	2.00	3.99	5.99	7.99	10.00	5.99	2.01	0.023

Table 1: Calibration data for pressure transducer

### **C. SAFETY FEATURES**

As mentioned earlier, a major reason for the redesign of the nozzle test rig were considerations of lab safety. The new design has safety features that allow the operation of the rig without continuous personnel attendance. For instance if the programme, for any reason, fails to control the temperature, the furnace will turn off automatically as soon as it reaches a pre-set by the user maximum temperature [Ref. 21]. The furnace is also positioned within a fume hood of the Corrosion Lab in the Mechanical Engineering Building. In this way, the possibility of fumes leakage is minimised with the most effective available way, so that the personnel working the rig would not be affected from the fuel fumes.



### III. RESULTS AND DISCUSSION

#### A. GENERAL

Some of the results presented in this section have come from the old testing rig. They were taken in account only as far as the accumulation rate of deposits in the holes of the swirl plates, and not for closure measurements via the flow measurement method, because at that time the latter was in the process of being set up. Despite this fact, the data from the old rig can be used to lead to some conclusions relative to the different behaviour among the different types of swirl plates.

The newly designed test rig has provided data for the comparative behaviour of A and B types of swirl plates. This data was also used in calculations of the closure in the swirl plates holes together with the information associated with the coking accumulation rate and the optical and SEM examination.

#### B. WEIGHT MEASUREMENTS

##### a) A vs. A'

A22 and A'27 were the two swirl plates that were used in the old testing rig. On Figure 10 we can see the results of the weight measurements plotted based on the data shown on Tables 2 and 3. No significant difference in the accumulation rate of coking between the two swirl plates can be justified from the data obtained.

b) A vs. B

A27 and B18 were compared using the newly designed testing rig. On Figure 11 the results of these weight measurement are presented based on the data shown on Tables 4 and 5. A comparison of the data reveals that there is a significantly lower deposition accumulation rate on the B18 swirl plate.

Cycles performed	0	27	54	81
Weight [mg]	762.3	762.99	763.19	763.47
Weight increase	-	0.26	0.46	0.74

Table 2 : Weight measurements for A'26 (50 min. cycles, old testing rig )

Cycles Performed	0	27	54	81
Weight [mg]	822.27	822.51	822.67	822.89
Weight increase	-	0.24	0.4	0.68

Table 3 : Weight measurements for A22 (50 min. cycles, old testing rig )

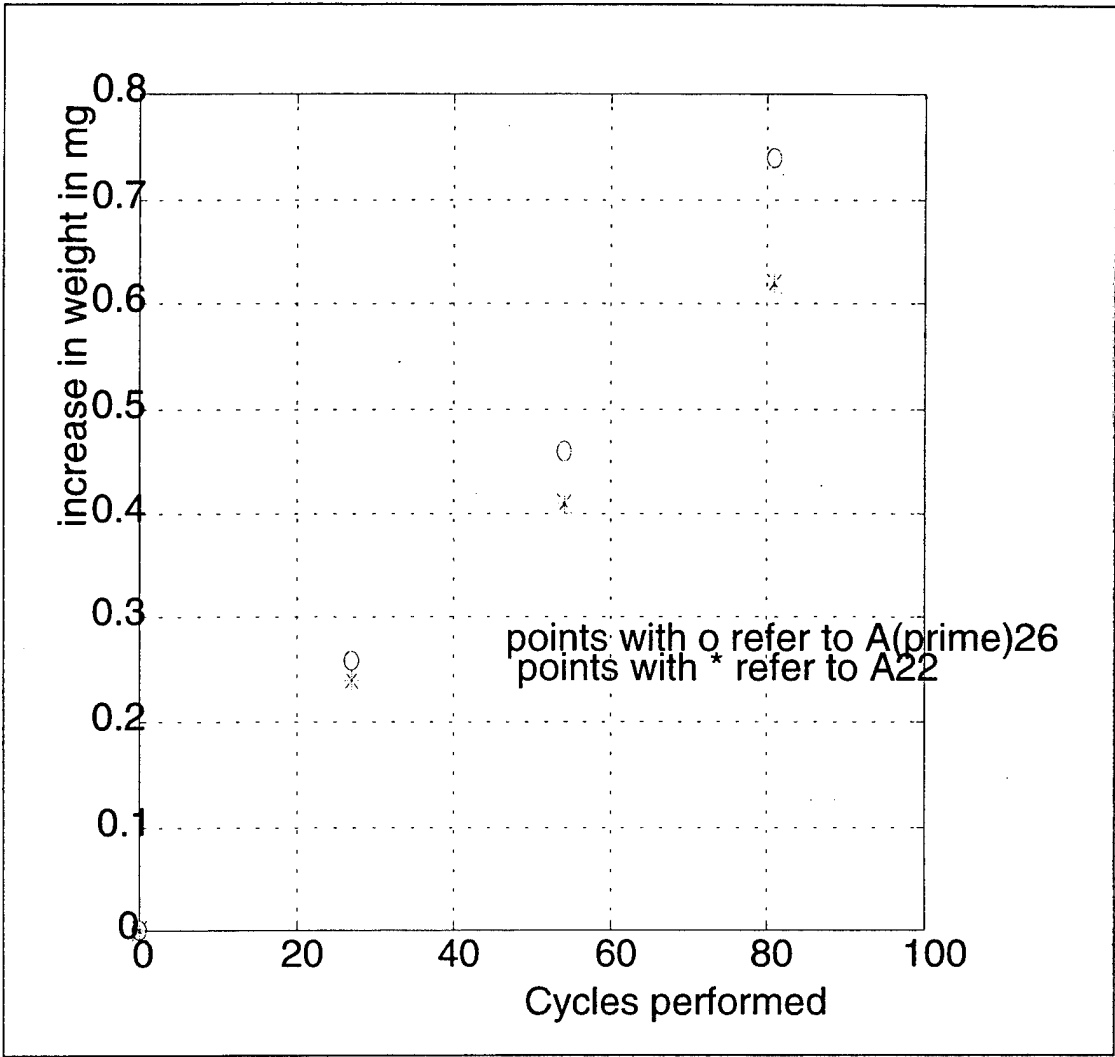


Figure 12: Weight increase vs cycles performed for A22 and A'26

Cycles	0	24	50	75	100	125	150
Weight [mg]	826.3	826.93	827.18	827.4	827.52	827.7	827.9
Weight increase	-	0.66	0.88	1.1	1.22	1.4	1.6

Table 4 : Weight measurements of A27 (30 min. cycles, new testing rig )

Cycles	0	24	50	75	100	125	150
Weight [mg]	852.5	852.74	852.91	852.95	853.01	853.16	853.33
Weight increase	-	0.24	0.41	0.45	0.51	0.65	0.8

Table 5 : Weight measurements of B18 (30 min. cycles, new testing rig )

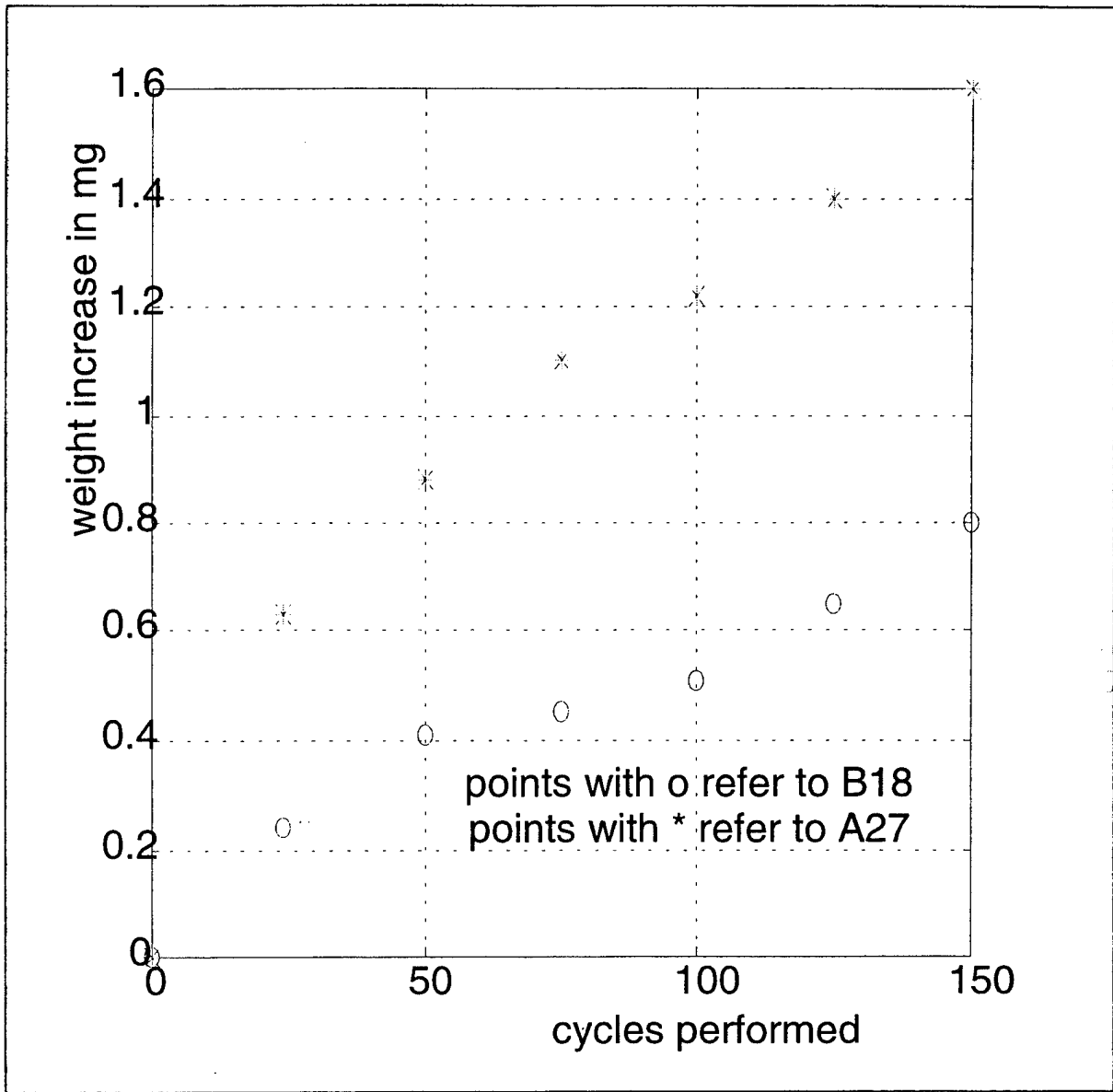


Figure 13: Weight increase vs cycles performed for A27 and B18



### C. OPTICAL MICROSCOPY EXAMINATION

Examination of the swirl plates was performed with an optical microscope that was equipped with a camera adjusted to co-operate with the IMAGE PRO software package [Ref. 22]. The pictures were taken and saved as digital (.tif) files in the computer from where they can be retrieved and copied to any printer. This is a relatively new way of taking optical pictures and has been proved to be extremely useful and quite easy to use. In case where there was no need for high resolution, the features could be seen in a simple printer's printout. In cases where a detailed optical picture was needed more highly equipped printers can be used to get the maximum benefit from the digital picture.

In Figures 13 and 14 optical pictures of the swirl plates holes at the 12 and 3 o'clock position according to the nomenclature described in the experimental procedure section can be seen, with the (a) pictures referring to the A'26 swirl plate and the (b) pictures to the A22, all being captioned underneath with the respective number of cycles been performed. These were the swirl plates that were tested using the old testing rig. No significant amount of coking can be justified around the holes surface for both types. The number of cycles performed are not enough for reliable conclusions on the coking around the holes. No significant difference can be justified; however the A' type seems to have slightly less amount of coking.

In Figures 15 through 28 optical pictures of B18 and A27 swirl plates can be seen. (Again (a) pictures are associated with B18 and (b) pictures with A27 type). Figures 15 through 21, show the 3 o'clock position, while Figures 22 through 28 the 6 o'clock position all in increasing performed cycles order from 0 cycles to 150 cycles. As can be

seen from these pictures the coking is again evident around the holes of the swirl plates and comparing the behaviour of the A type with the B type, a significantly lower coking accumulation is evident on the B type.

In Figures 29 through 32 pictures of the 2 o'clock position of the A27 swirl plate can be seen. The spiky coking deposition observed after the 75 cycles were performed was the important feature of this group of pictures. This observation is in accordance with similar observations made by Prof. Roy Crooks concerning the shape of the depositions in the swirl plates holes. The experiment, however, has shown that these depositions can break relatively easy as can be justified from the absence of the spiky deposition at the last picture (Figure 29) taken after the flow measurement has been performed.

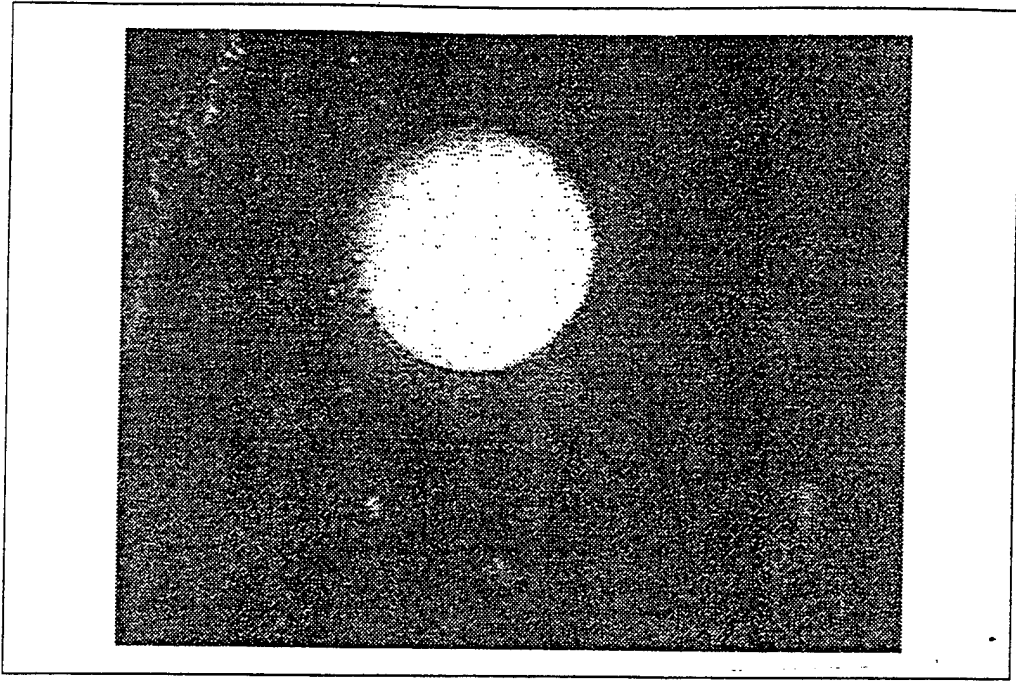


Figure 14 (a) : Optical picture A'26, 12 o'clock, 80 cycles

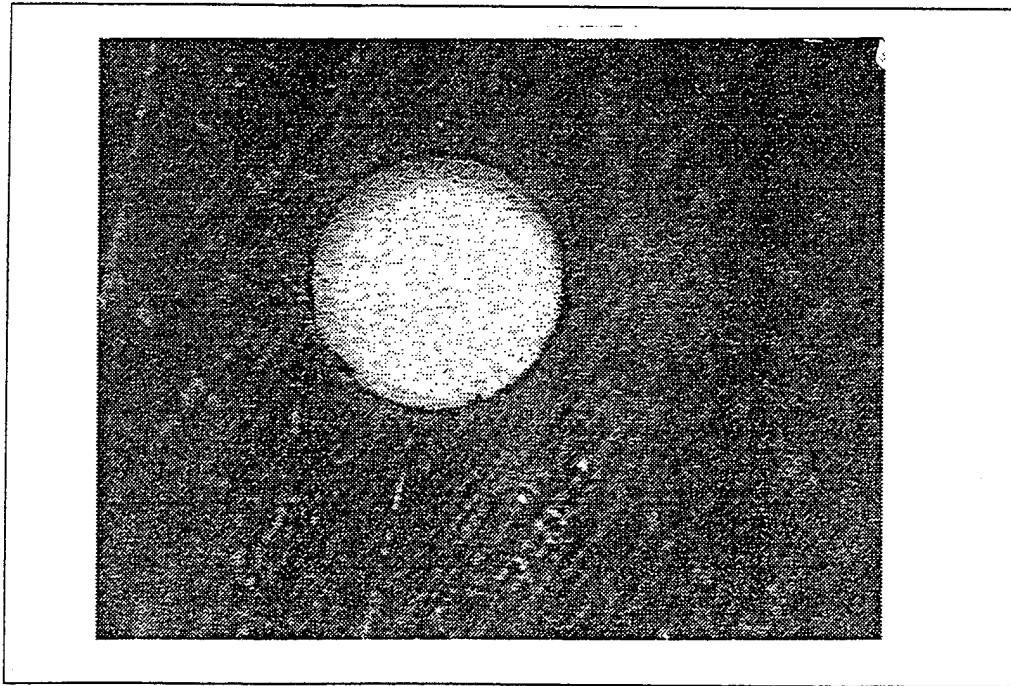


Figure 14 (b) Optical picture A22, 12 o'clock, 80 cycles

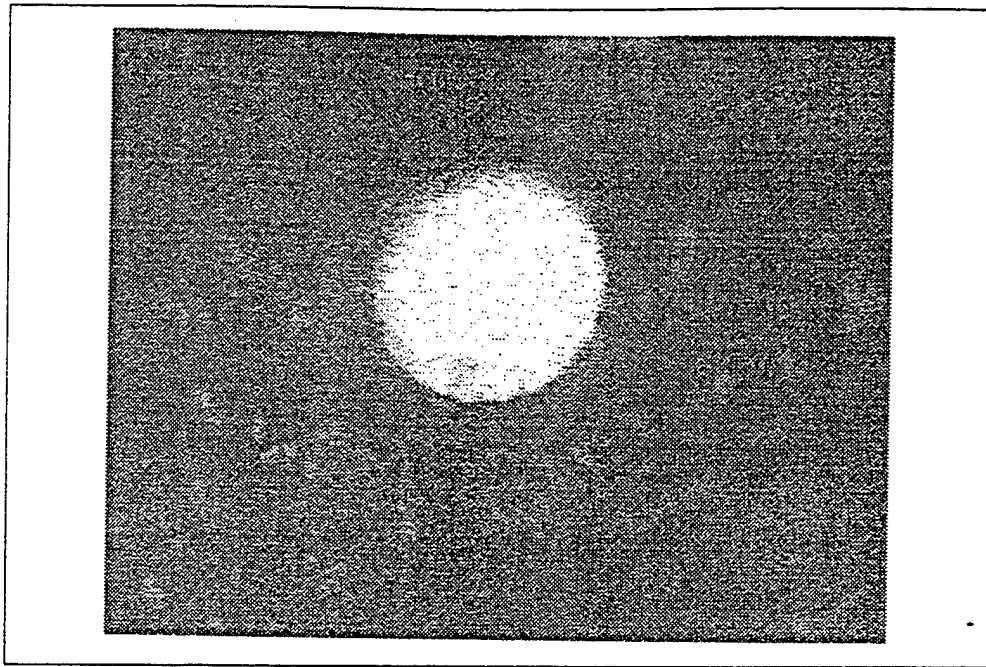


Figure 15 (a) : Optical picture A'26, 3 o' clock, 80 cycles.

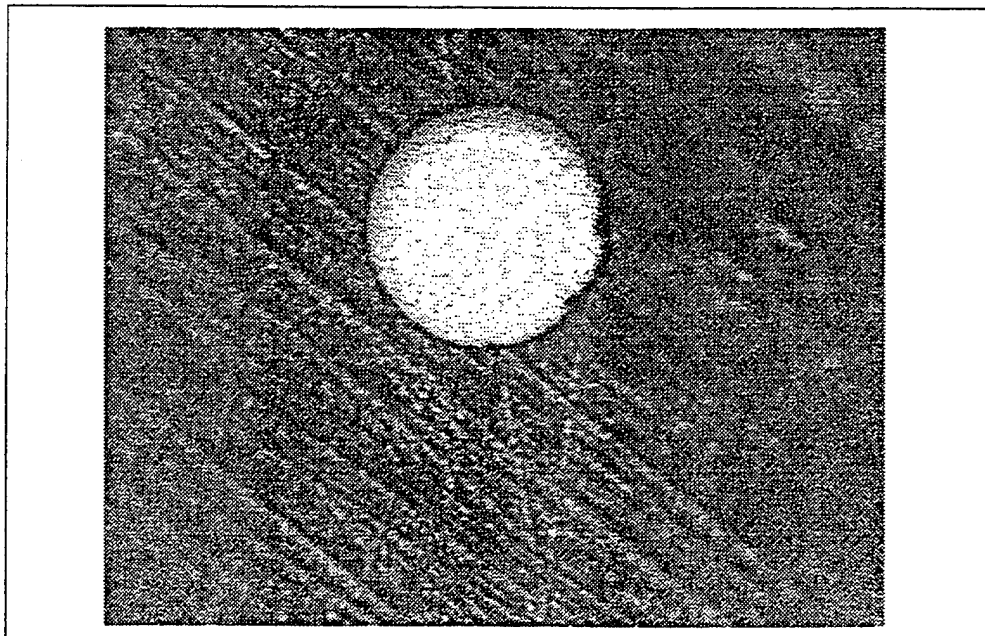


Figure 15 (b) : Optical picture A22, 3 o'clock, 80 cycles.

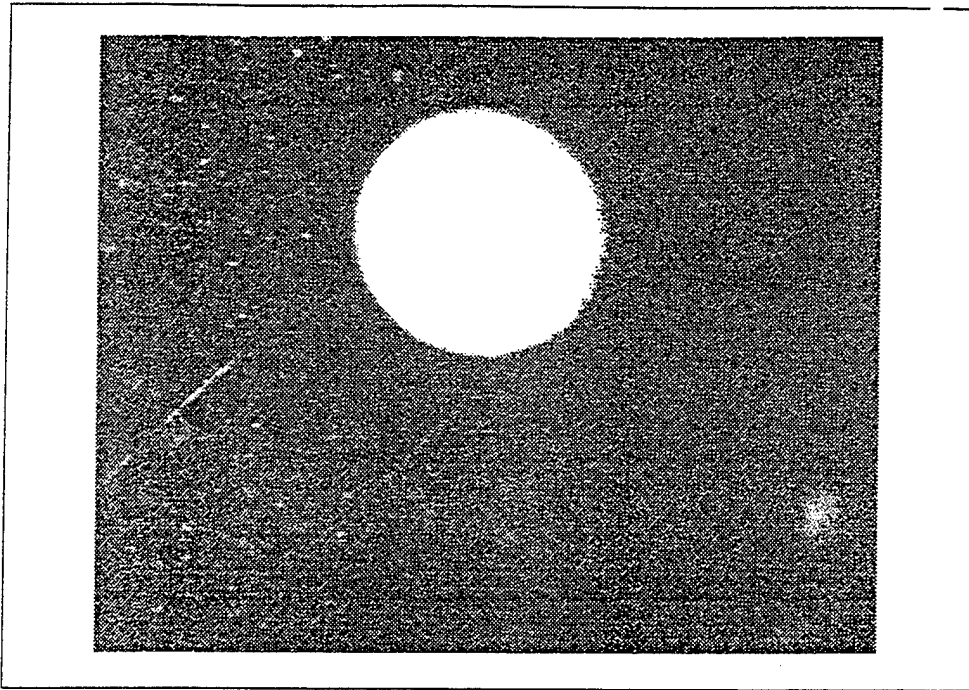


Figure 16 (a) : Optical picture virgin B18, 3 o' clock.

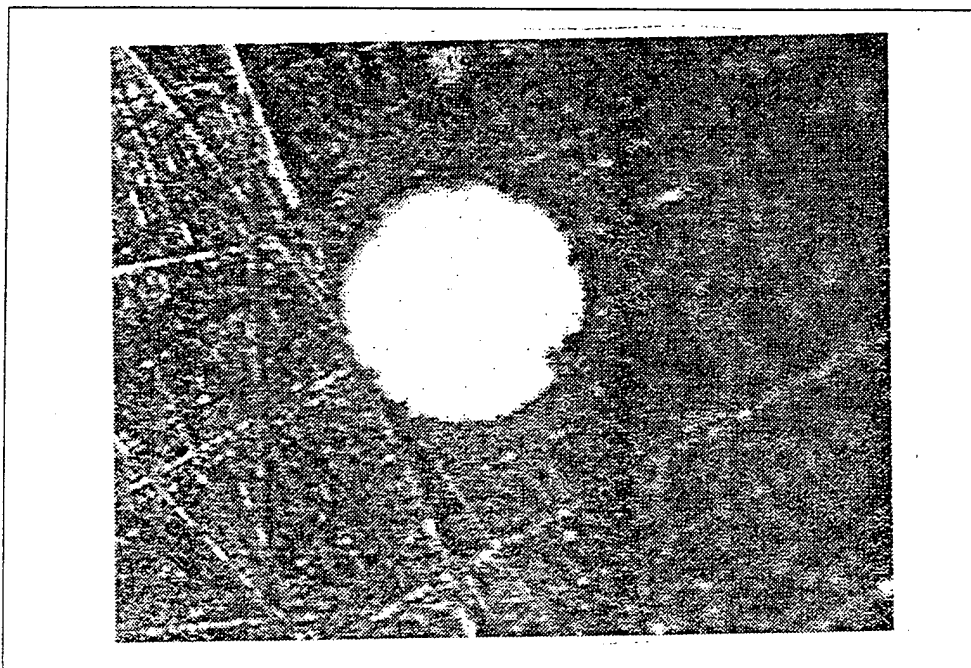


Figure 16 (b) : Optical picture virgin A27, 3 o' clock.

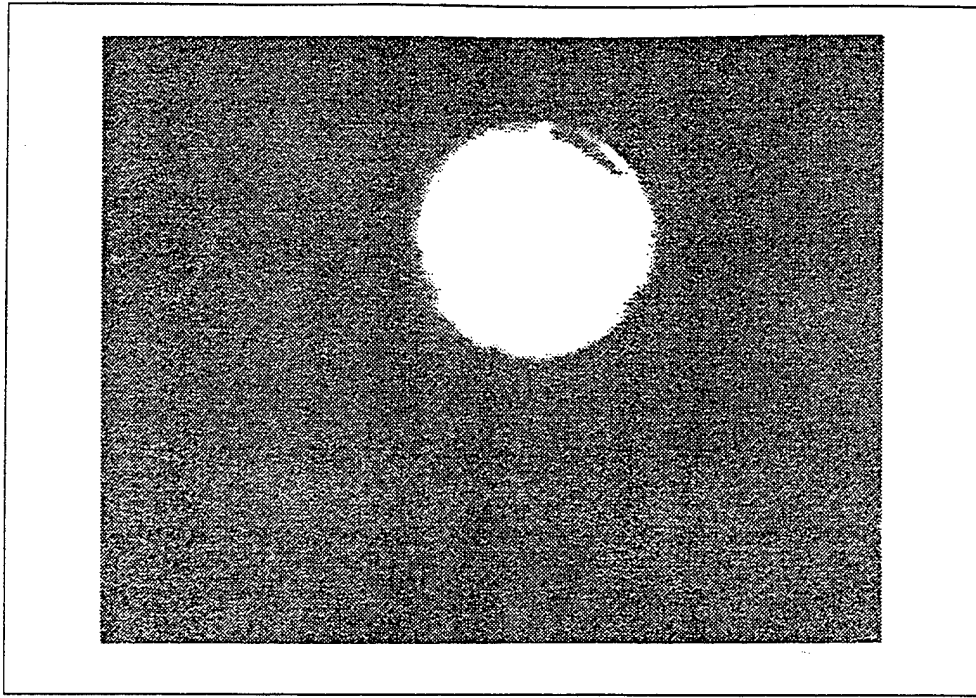


Figure 17 (a) : Optical picture B18, 3 o' clock, 25 cycles

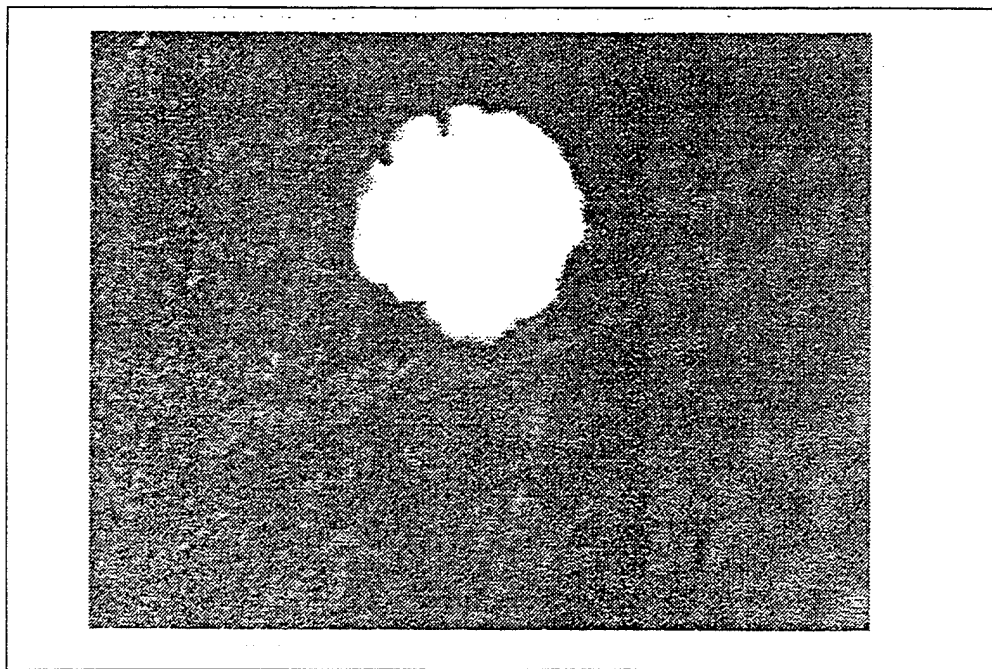


Figure 17 (b) : Optical picture A27, 3 o' clock, 25 cycles

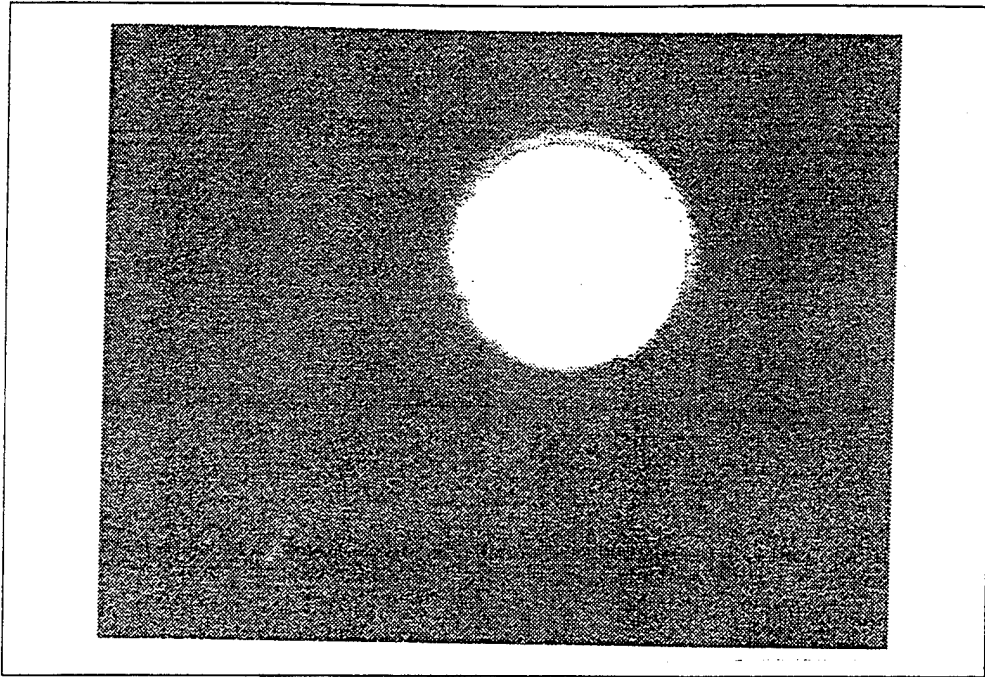


Figure 18 (a) : Optical picture B18, 3 o' clock, 50 cycles.

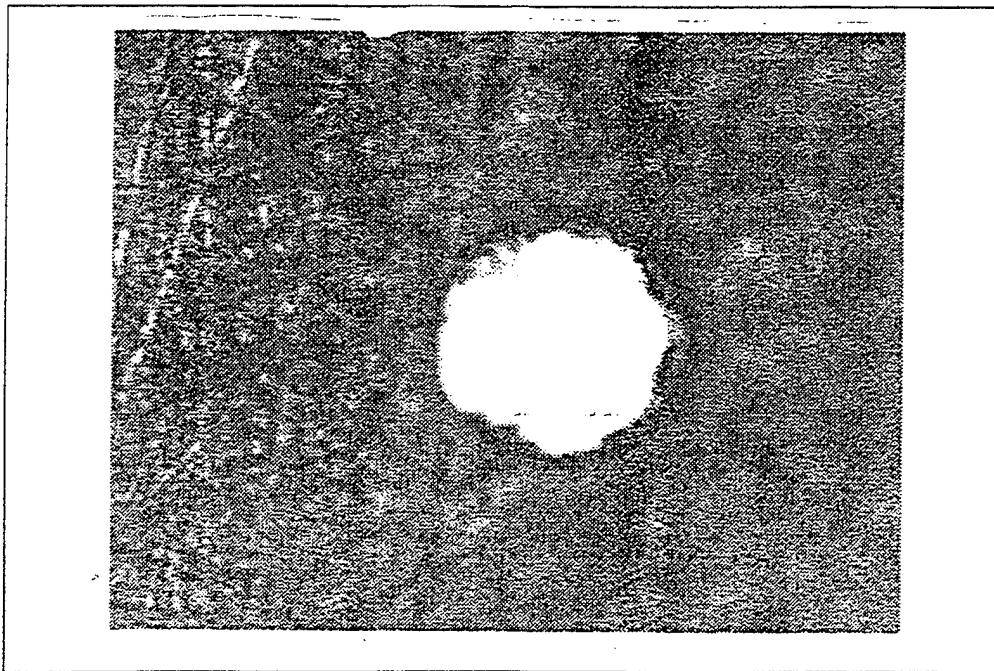


Figure 18 (b) : Optical picture A27, 3 o' clock, 50 cycles.



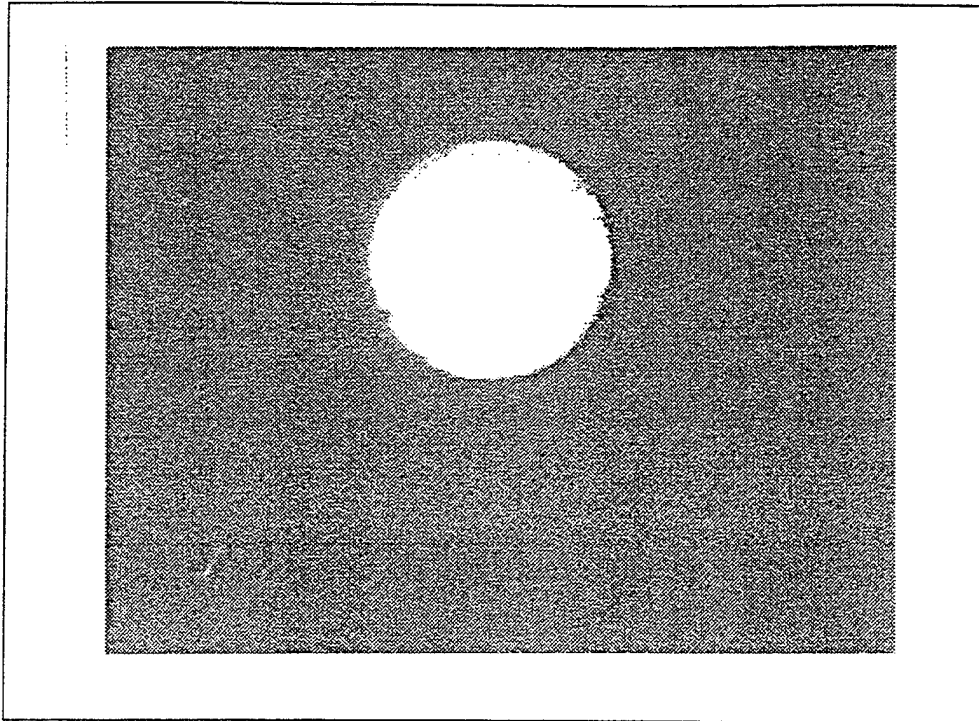


Figure 19 (a) : Optical picture B18, 3 o' clock, 75 cycles.

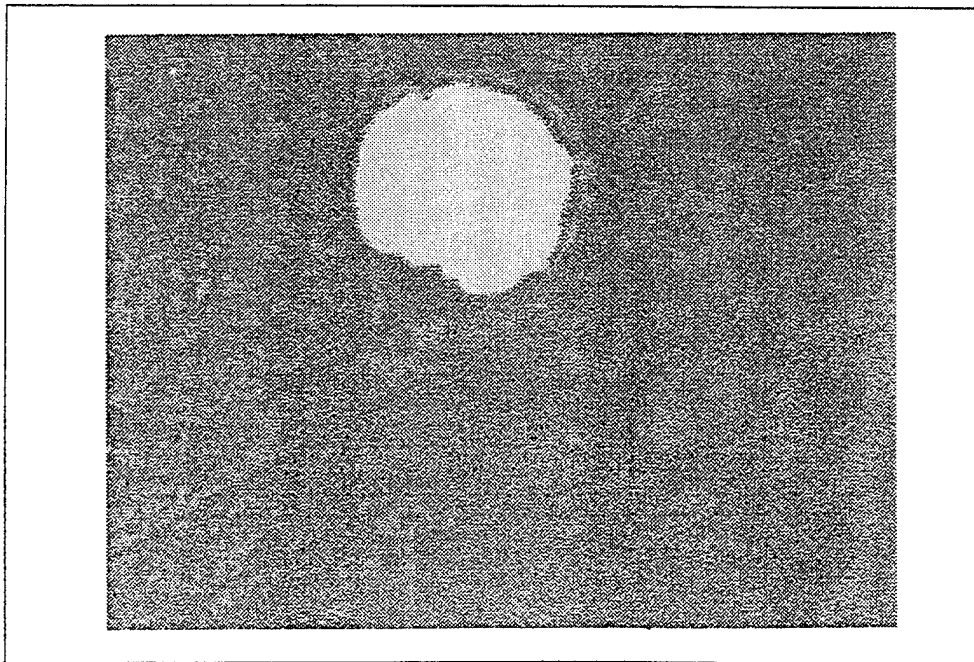


Figure 19 (b) : Optical picture A27, 3 o' clock, 75 cycles.



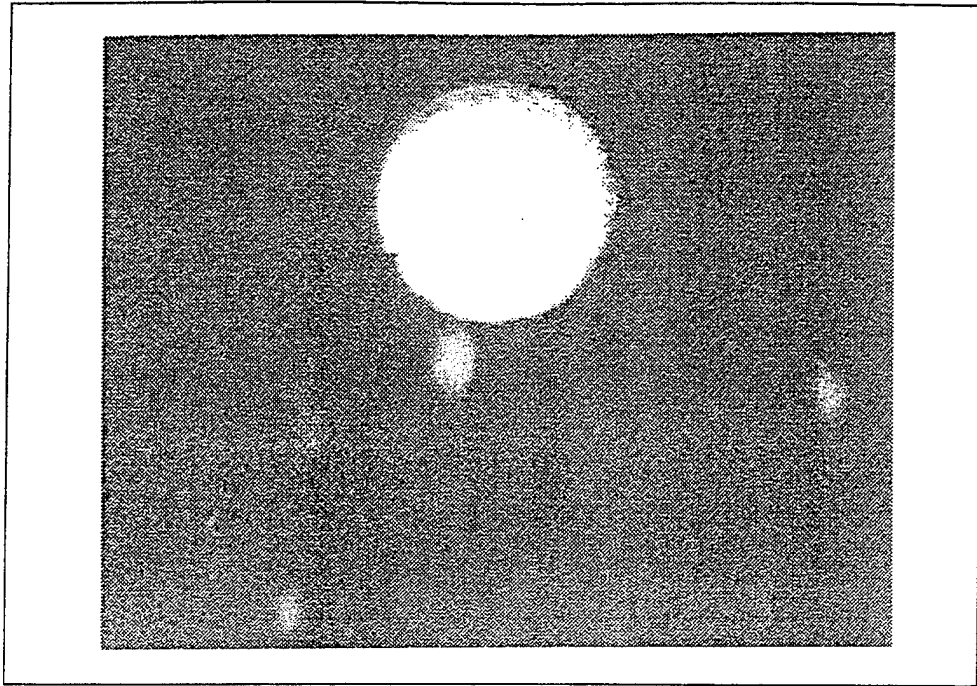


Figure 20 (a): Optical picture B18, 3 o' clock, 100 cycles.

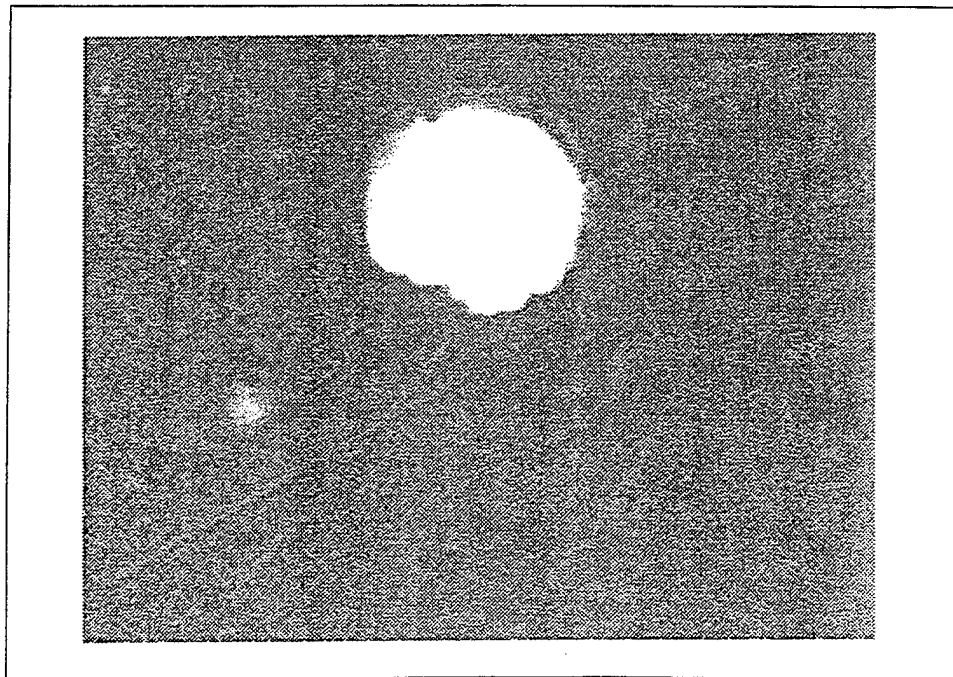


Figure 20 (b) : Optical picture A27, 3 o' clock, 100 cycles.

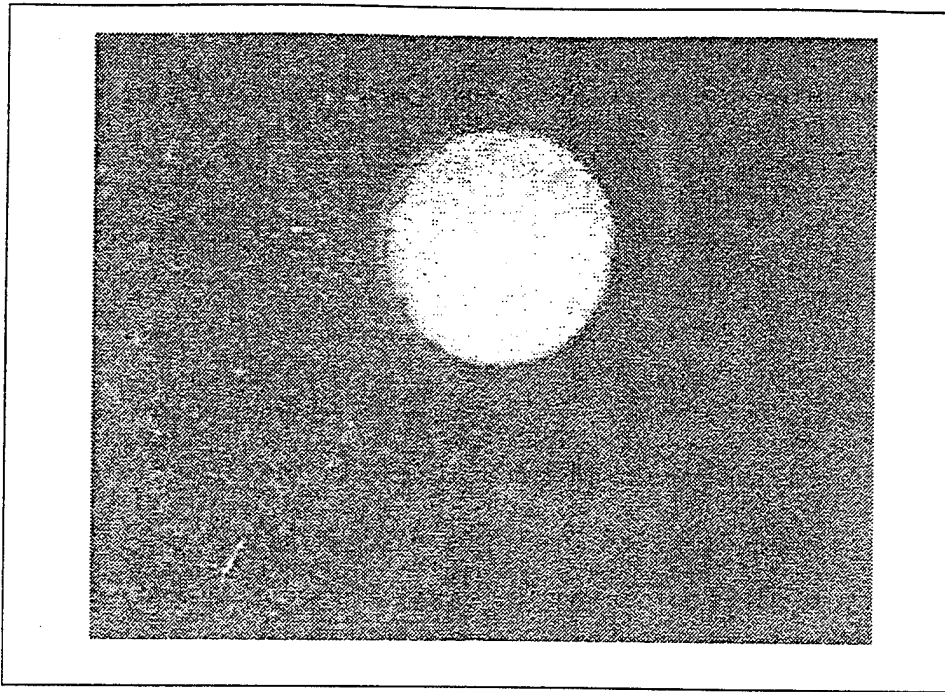


Figure 21 (a) : Optical picture B18, 3 o' clock, 125 cycles.

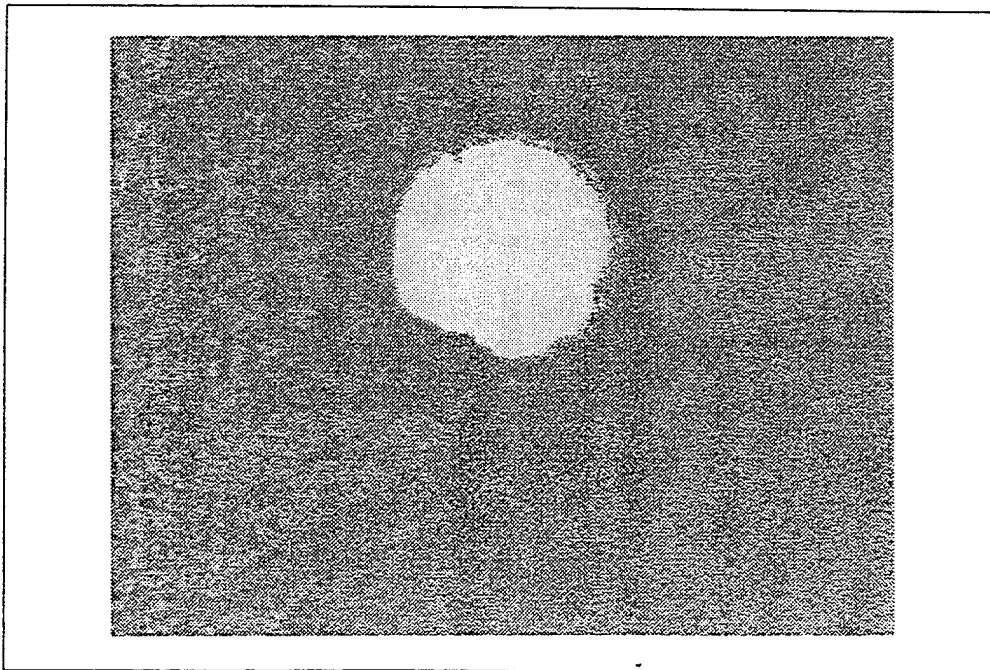


Figure 21 (b) : Optical picture A27, 3 o' clock, 125 cycles.

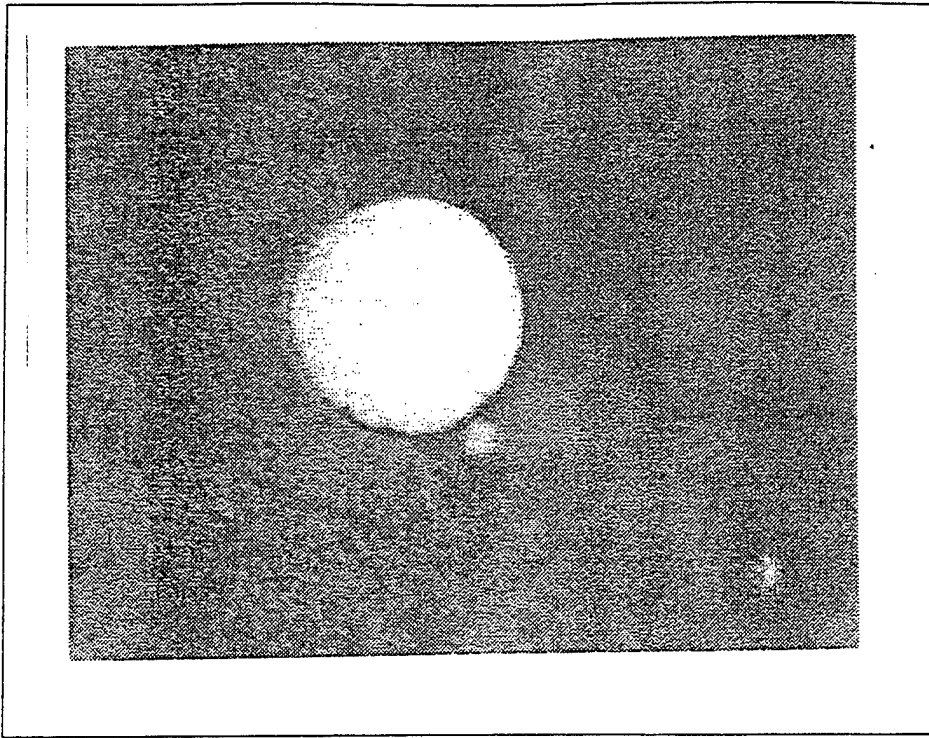


Figure 22 (a) : Optical picture B18, 3 o'clock, 150 cycles

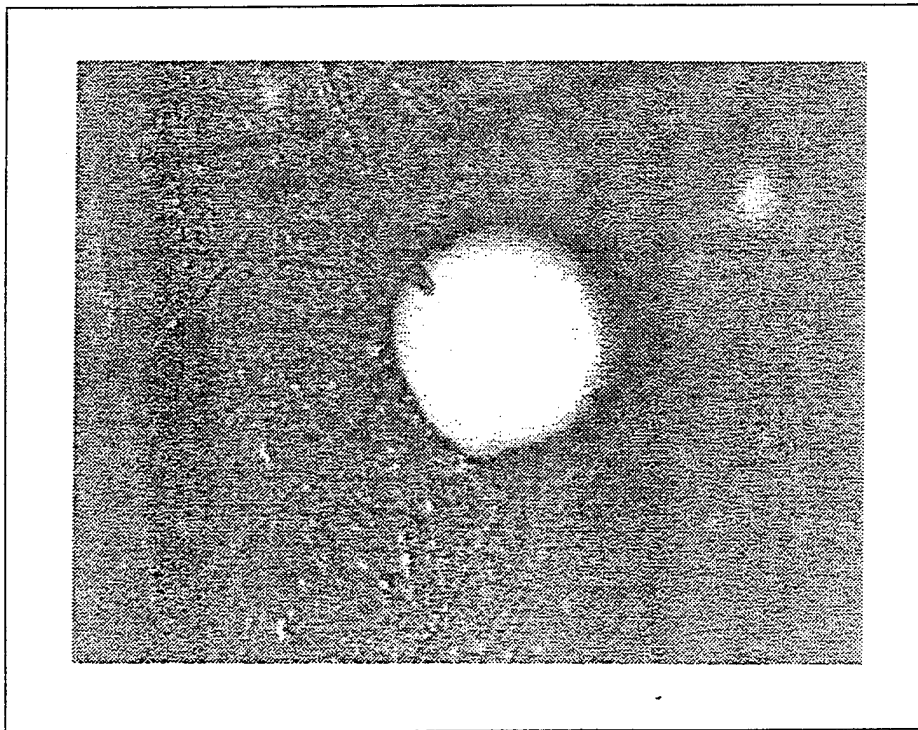


Figure 22 (b) : Optical picture A27, 3 o'clock, 150 cycles

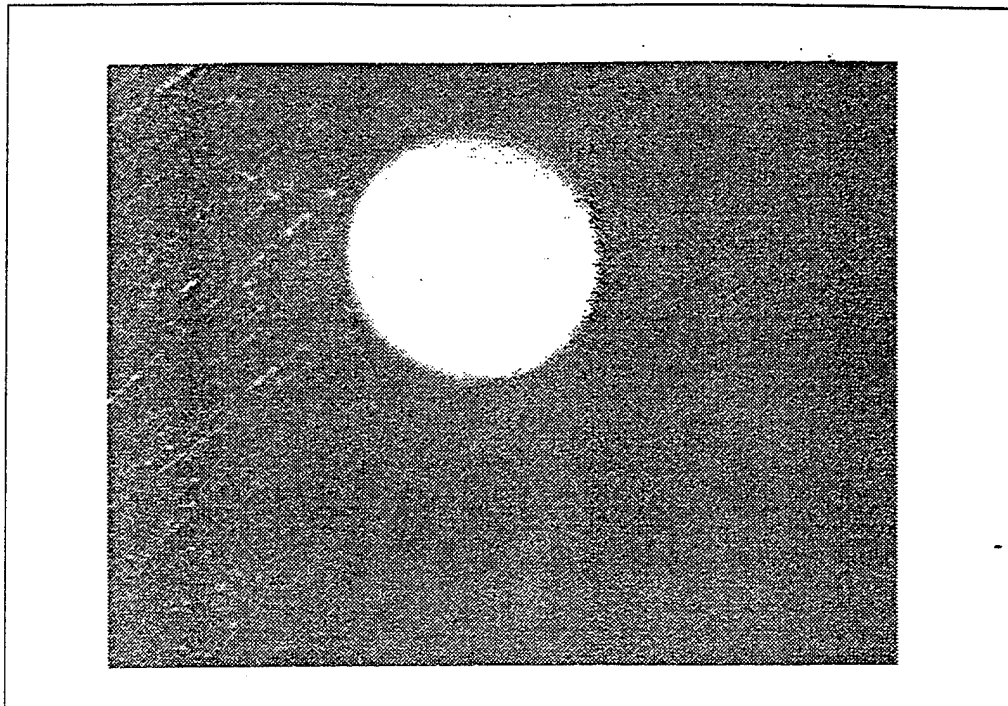


Figure 23 (a) : Optical picture B18 virgin, 6 o' clock

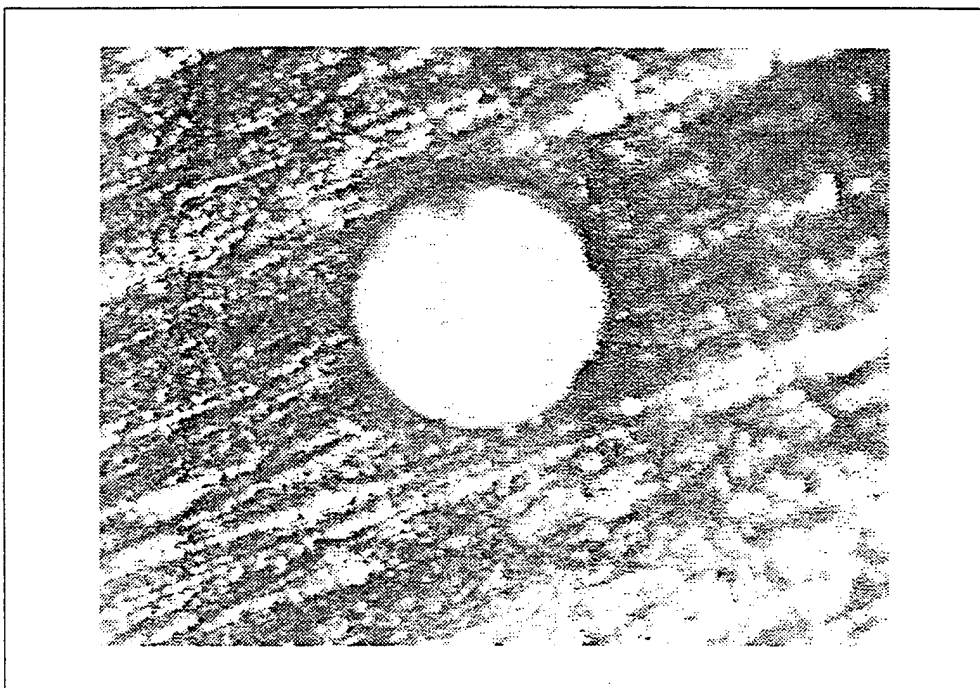


Figure 23 (b) : Optical picture A27 virgin, 6 o' clock



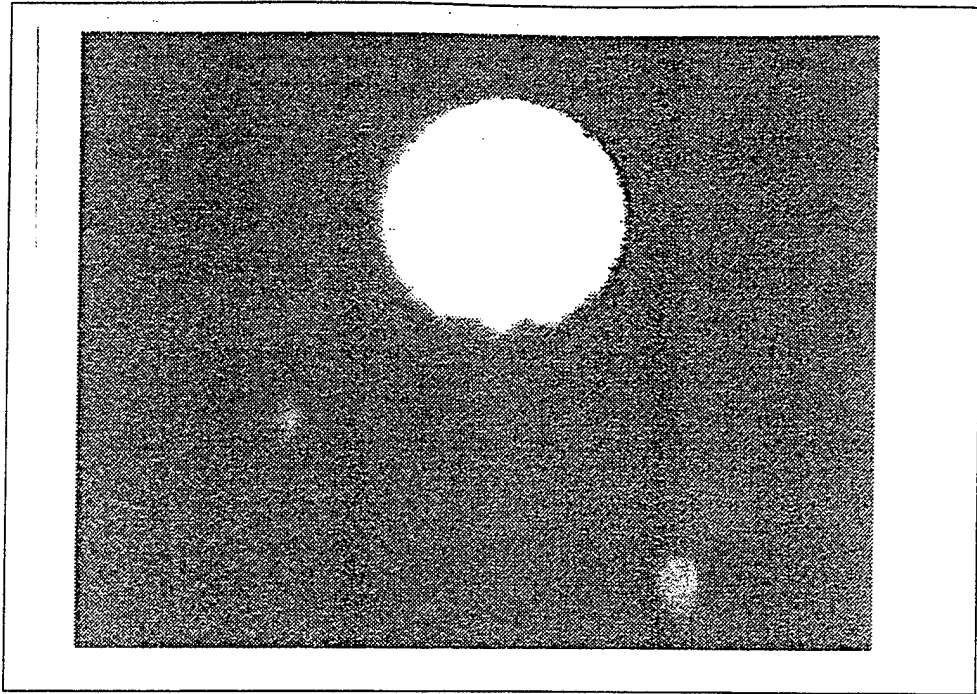


Figure 24 (a) : Optical picture B18, 6 o' clock, 25 cycles

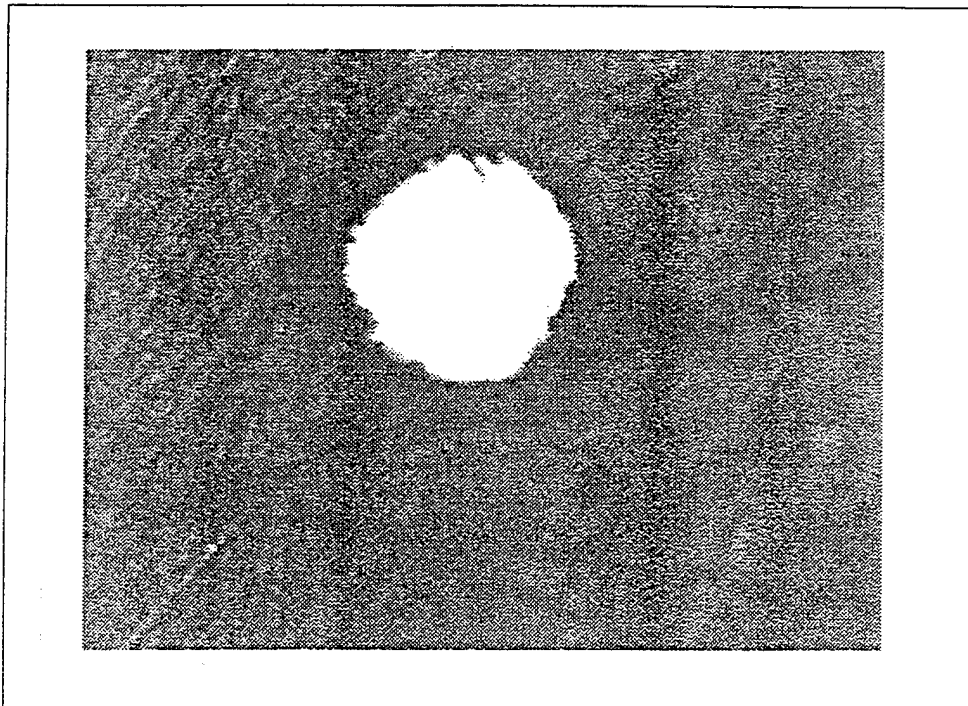


Figure 24 (b) : Optical picture A27, 6 o' clock, 25 cycles

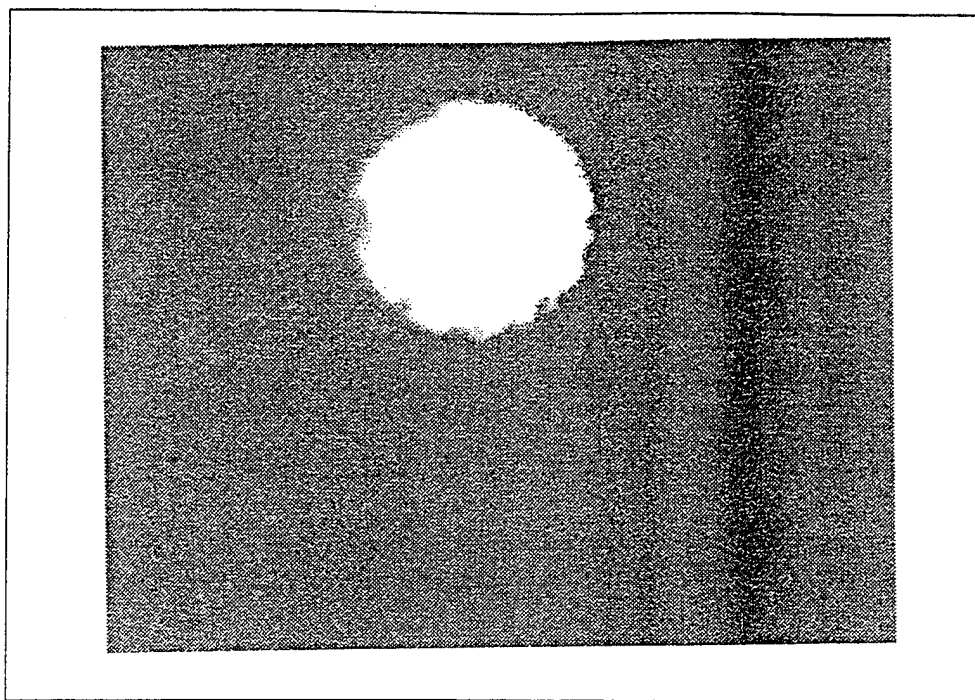


Figure 25 (a) : Optical picture B18, 6 o' clock, 50 cycles

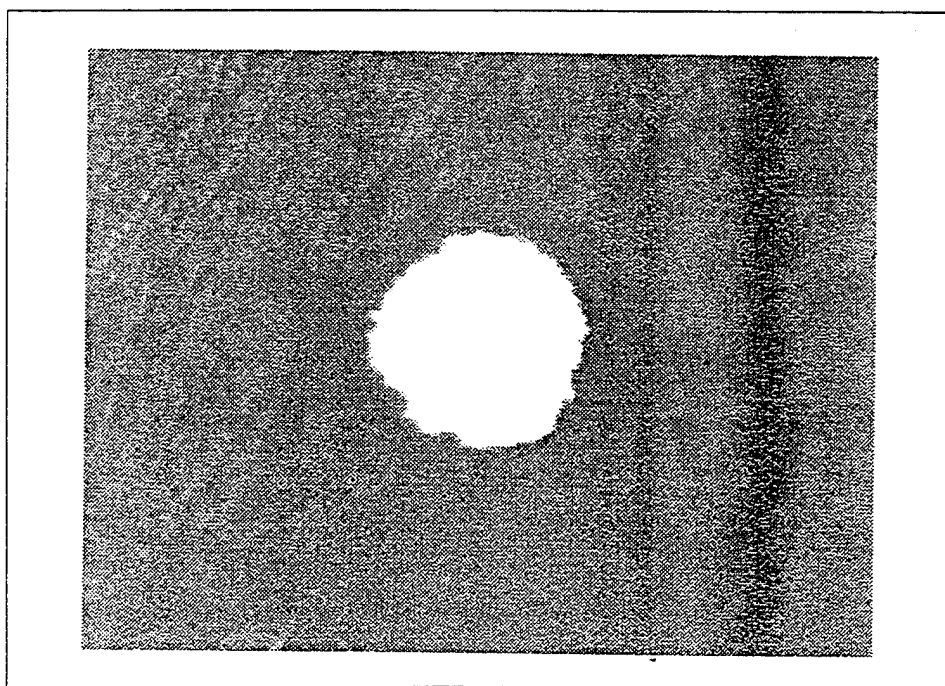


Figure 25 (b) : Optical picture A27, 6 o' clock, 50 cycles

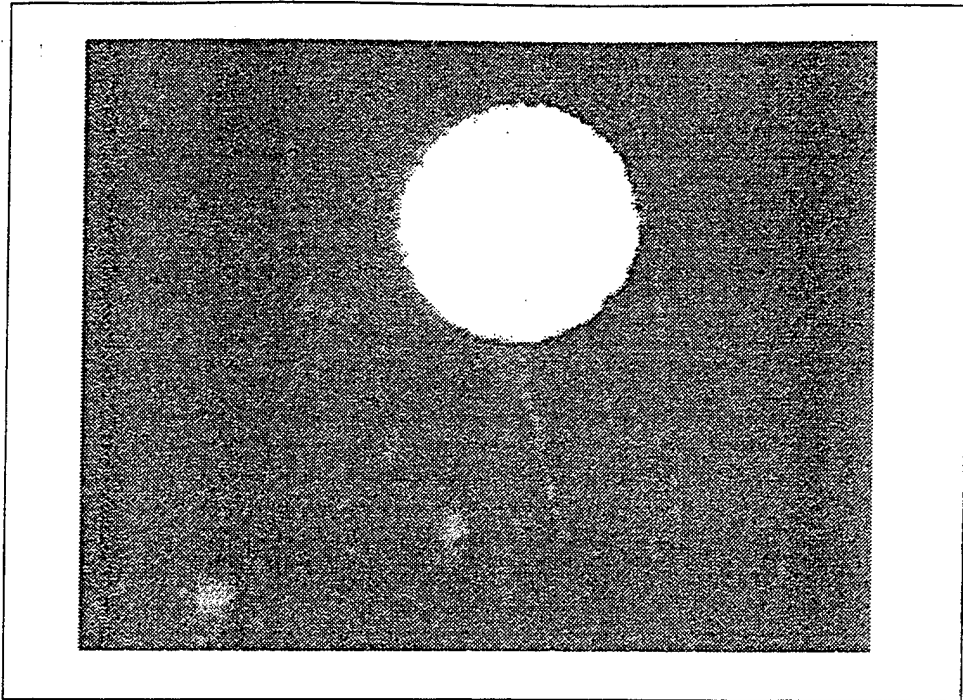


Figure 26 (a) : Optical picture B18, 6 o' clock, 75 cycles

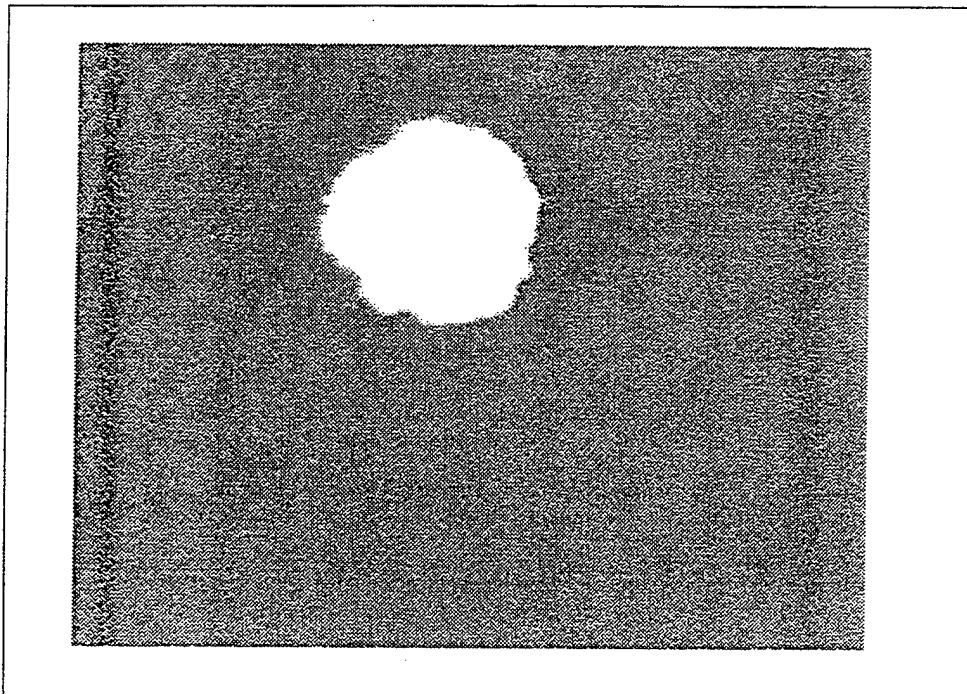


Figure 26 (b) : Optical picture A27, 6 o' clock, 75 cycles

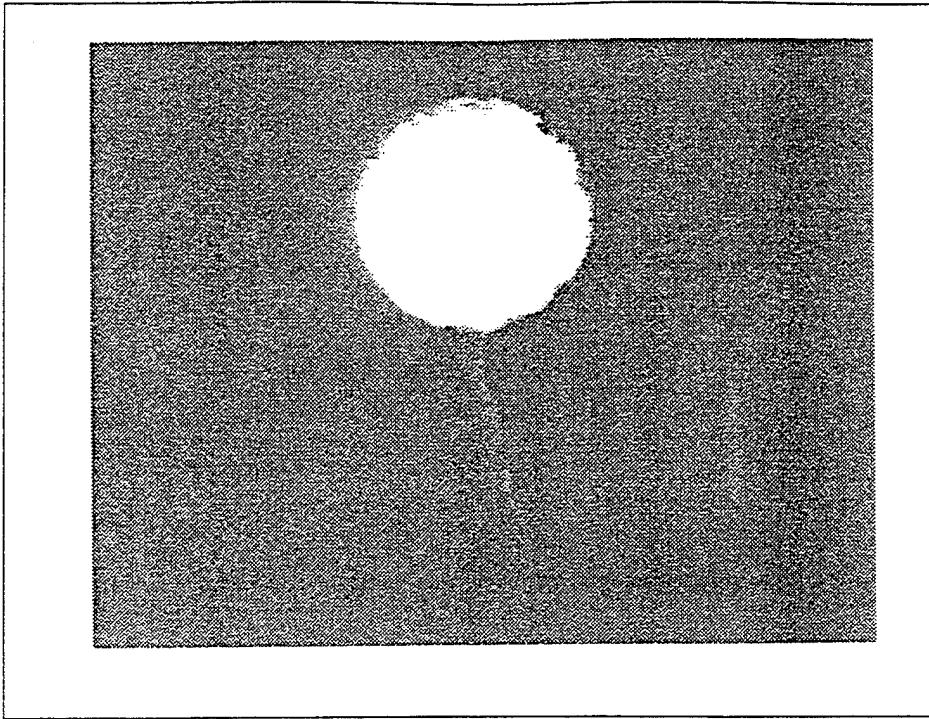


Figure 27 (a) : Optical picture B18, 6 o' clock, 100 cycles

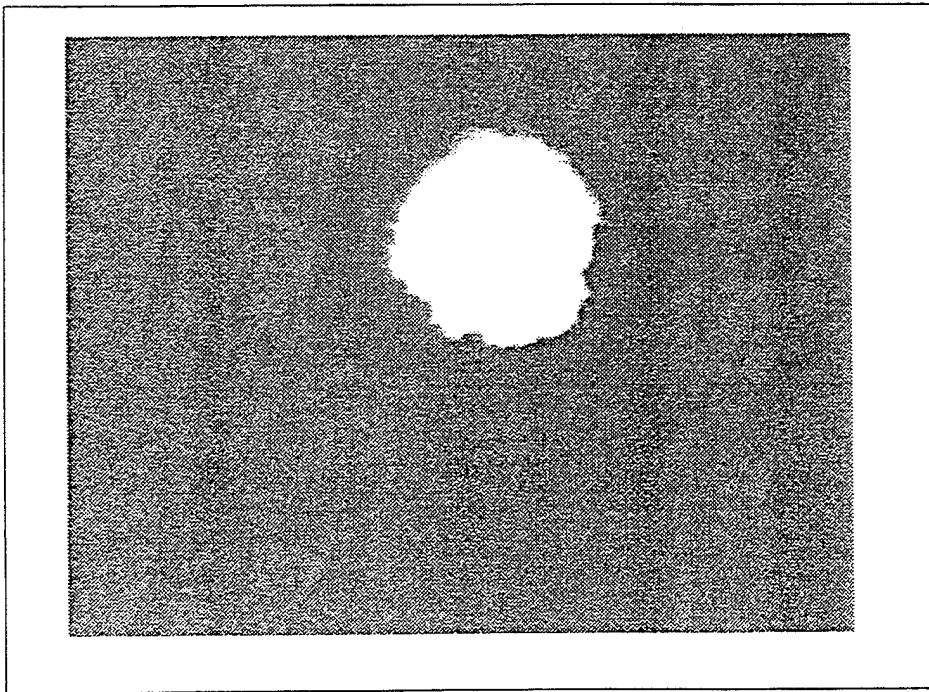


Figure 27 (b) : Optical picture A27, 6 o' clock, 100 cycles



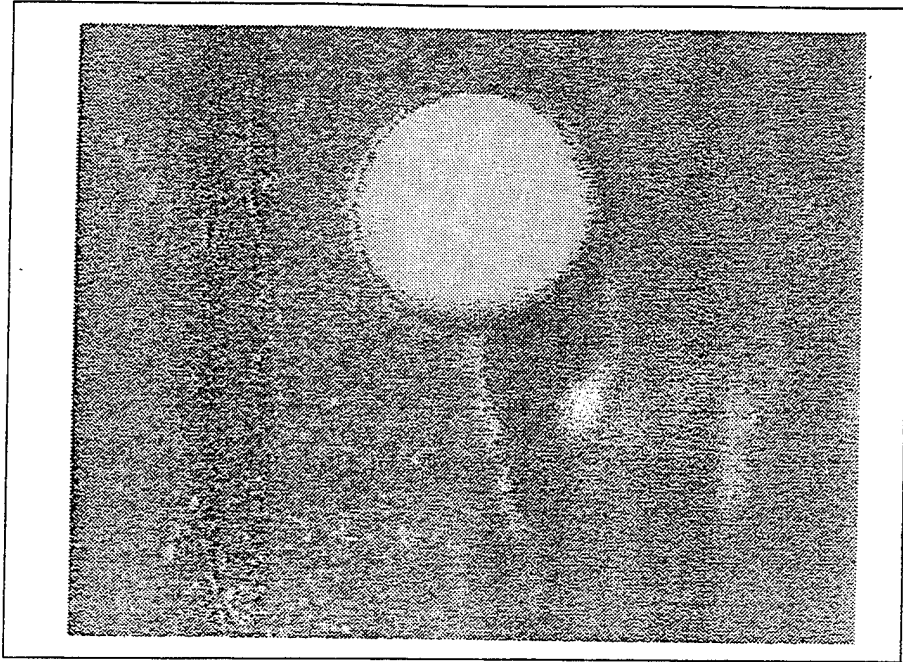


Figure 28 (a) : Optical picture B18, 6 o' clock, 125 cycles

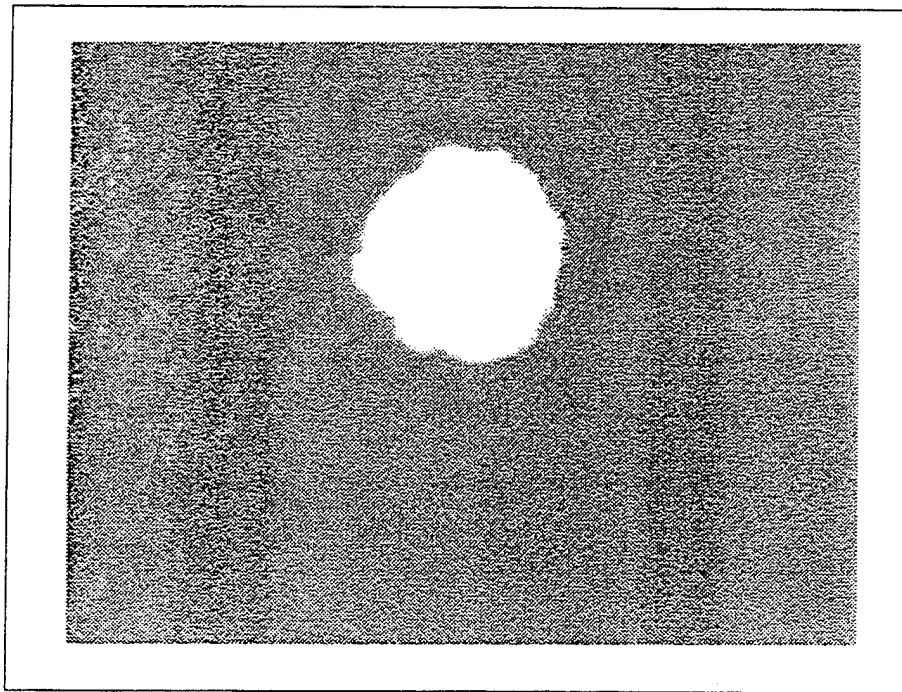


Figure 28 (b) : Optical picture A27, 6 o' clock, 125 cycles

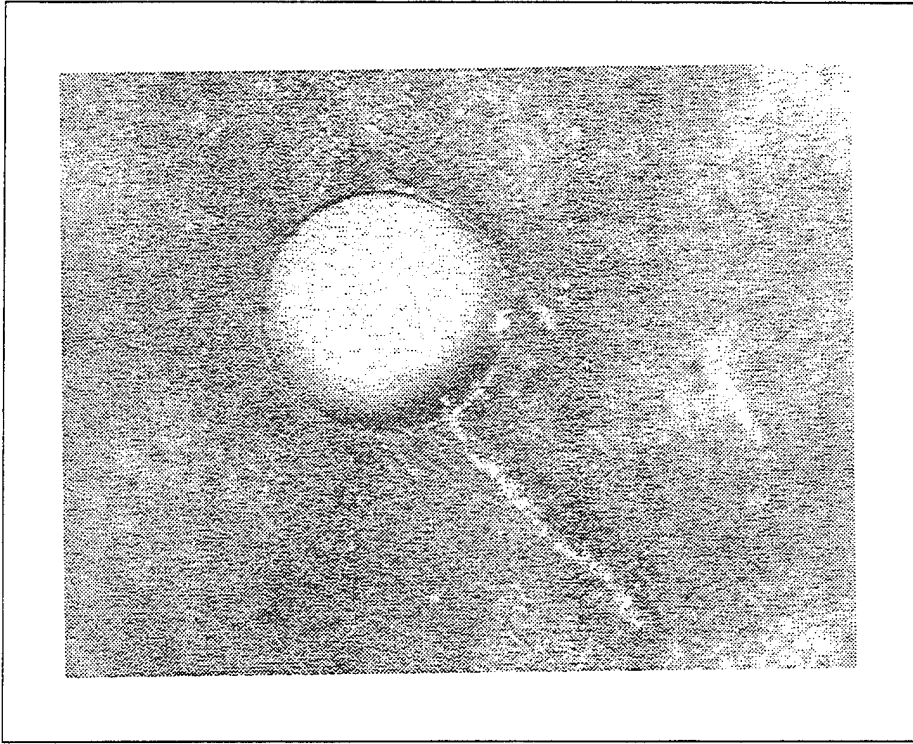


Figure 29 (a) : Optical picture A27, 6 o' clock, 150 cycles

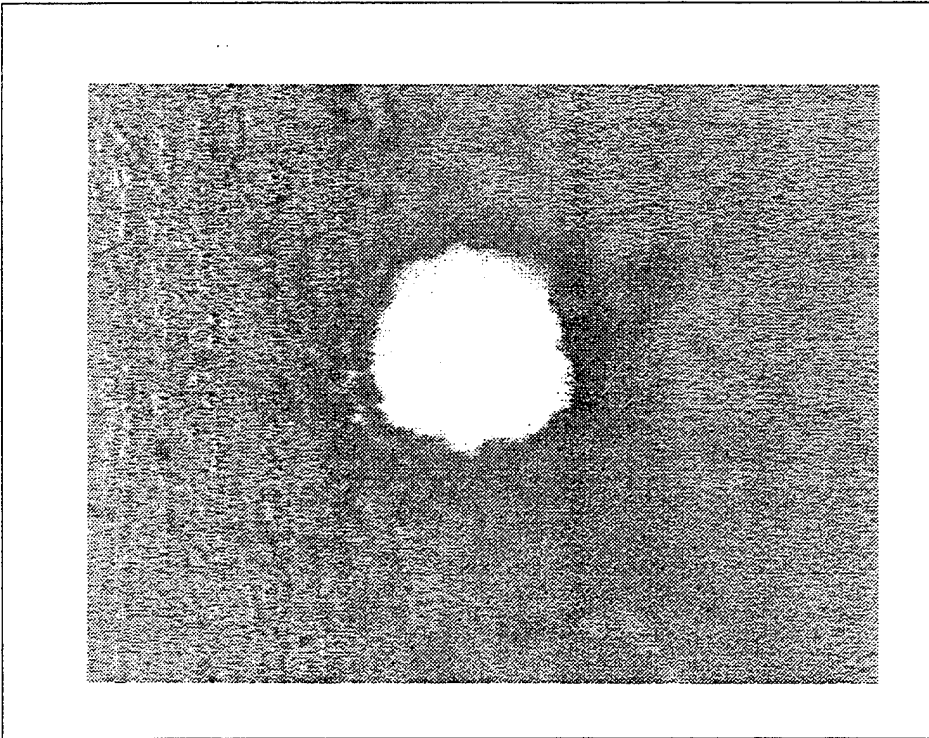


Figure 29 (b) : Optical picture B18, 6 o' clock, 150 cycles

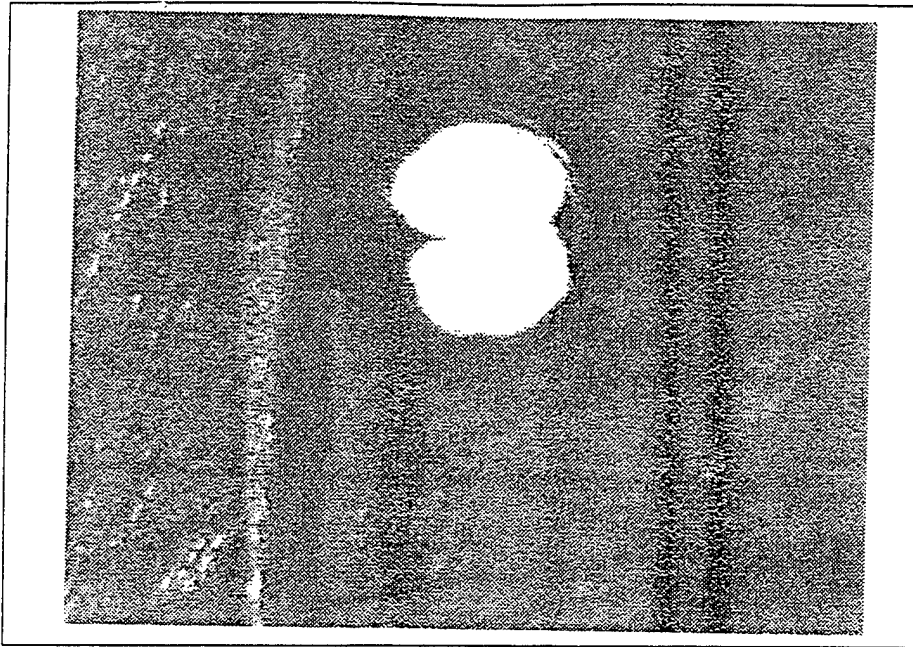


Figure 30 : Optical picture A27, 2 o'clock, 75 cycles.

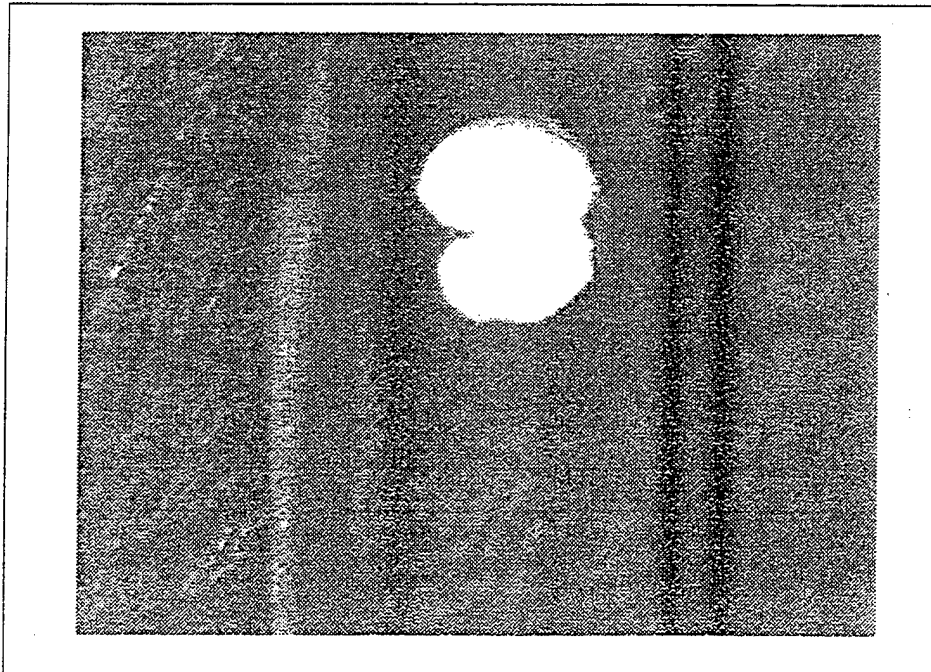


Figure 31 : Optical picture A27, 2 o'clock, 100 cycles.

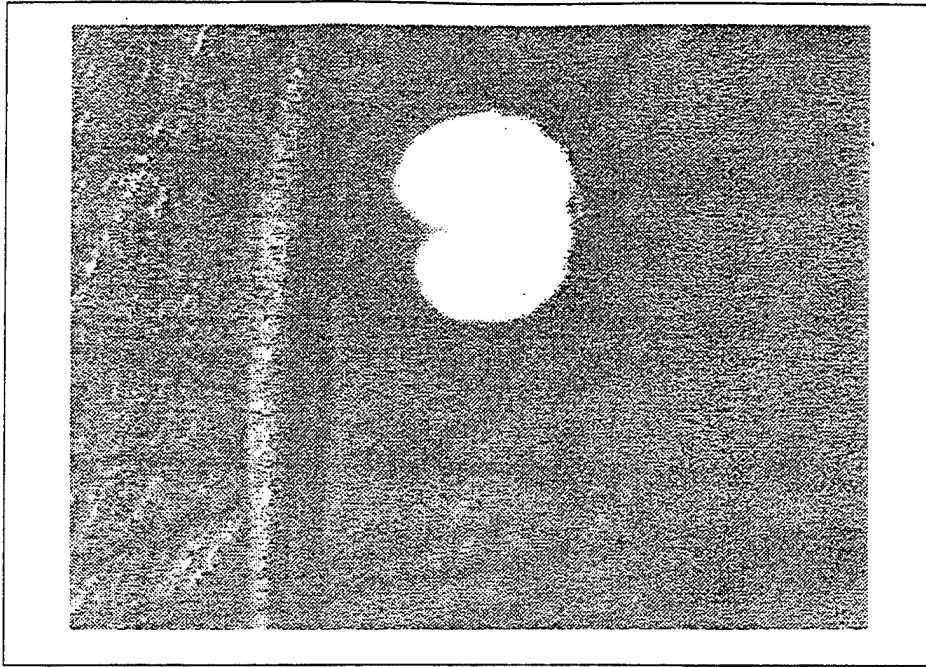


Figure 32 : Optical picture A27, 2 o'clock, 125 cycles

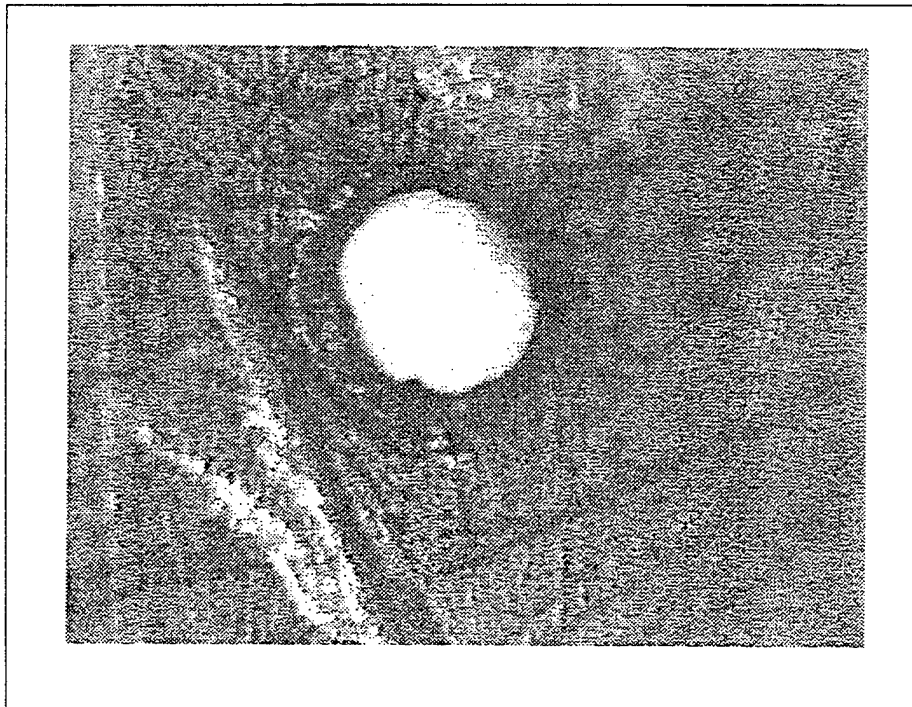


Figure 33 : Optical picture A27, 2 o'clock, 150 cycles

#### D. SEM EXAMINATION

As described in the experimental procedure section of this report, a similar procedure with the optical microscopy examination has been followed in the Scanning Electron Microscopy Examination. In Figures 33 and 34, views of the 12 o'clock position of the virgin A22 and A' 26 swirl plates can be seen. The difference in the surface finishing can be justified for the A' swirl plate, while the texture within the holes seems to have no difference among the A and A' types (Figure 34).

Figure 35 and 36 show the 12 o'clock position for the B and A types. A much smoother surface of the hole in B18 is evident in comparison with the rough texture of the hole's surface in A27 (Figure 36 (a) and (b)) and also the different surface finish (Figure 35 (a) and (b)) can be seen in these figures.

Figures 37 through 40, taken in increasing order of number of cycles performed from virgin plates to 150 cycles for the 12 o'clock position, reveal coking depositions on the hole's surface and mainly around the edge of the swirl plates holes. The same observation can be made considering Figures 41 through 43 and 44 through 46, related with the 3 and 6 o'clock position, respectively. Comparing the surfaces of the holes away from the edge, the deposition of coking did not have the dramatic difference observed at the edges. No significant difference, comparable to that observed at the edges, was evident at the inner surfaces of the swirl plates being in contact with the fuel nozzle's body.

The SEM investigation revealed a major coking accumulation at the edges and on the surface of the holes for both types. The B type, however, has shown much less coking

as compared to the unpolished one. A major interpretation, following from both optical and SEM investigation, is that the surface finish and particularly the degree of roughness of the hole's edge, is quite important, since more depositions are clearly evident on the unpolished swirl plate.

The fact that coking occurs mainly around and on the holes surface, rather than on the swirl plates broad surface, could be attributed to the amount of air available at each case. More air is available around the holes of the swirl plates, after the engine's shut down, compared with the surface. This air contributes to a faster progress of the reactions leading to the formation of gum at the given temperature -time profile. In fact in cases like the one under examination the main parameters leading to the progress of the chemical reactions related to the unburned fuel are the temperature-time profile of the swirl plate and the air and the quantity of air available. Considering the fact that the temperature of the air at the gas turbine after shut down can be different according to the shut down procedure, a possible explanation of the effectiveness of the (HSGI) shut down procedure can be diagnosed. High Speed Ground Idle not only consumes the trapped fuel at the low pressure fuel line of the nozzle but also exposes the swirl plates to a different quantity of air and to a different temperature-time profile.



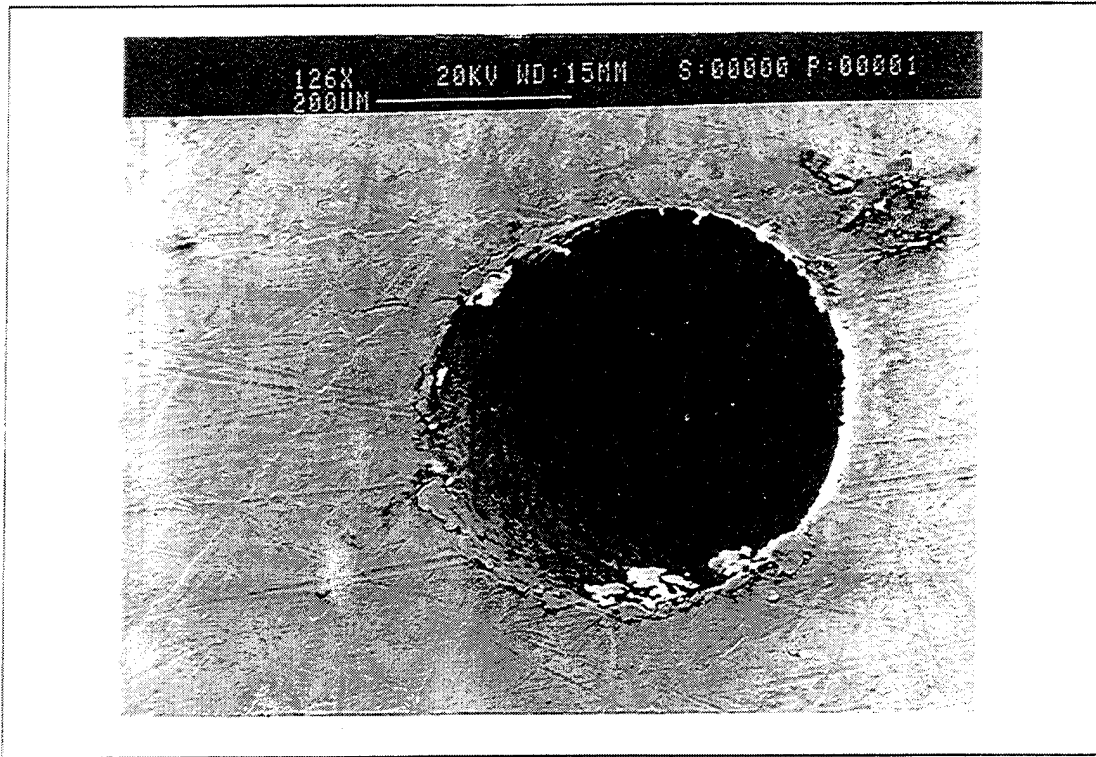


Figure 34 (a) : SEM picture for virgin A22.

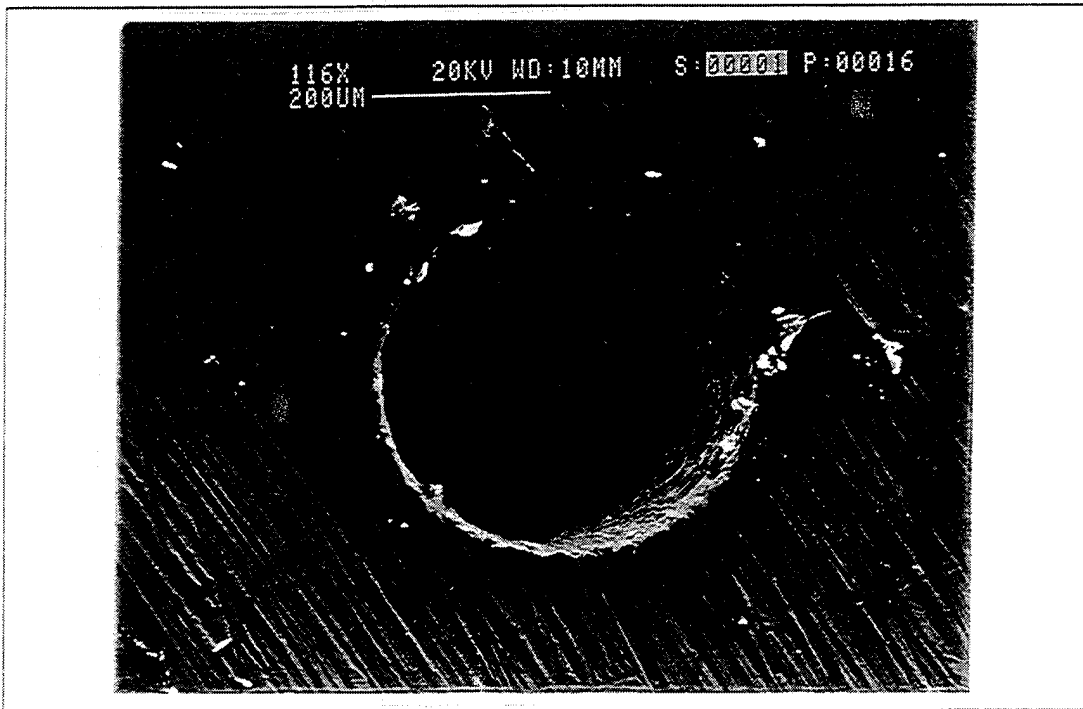


Figure 34 (b) : SEM picture for virgin A'26.

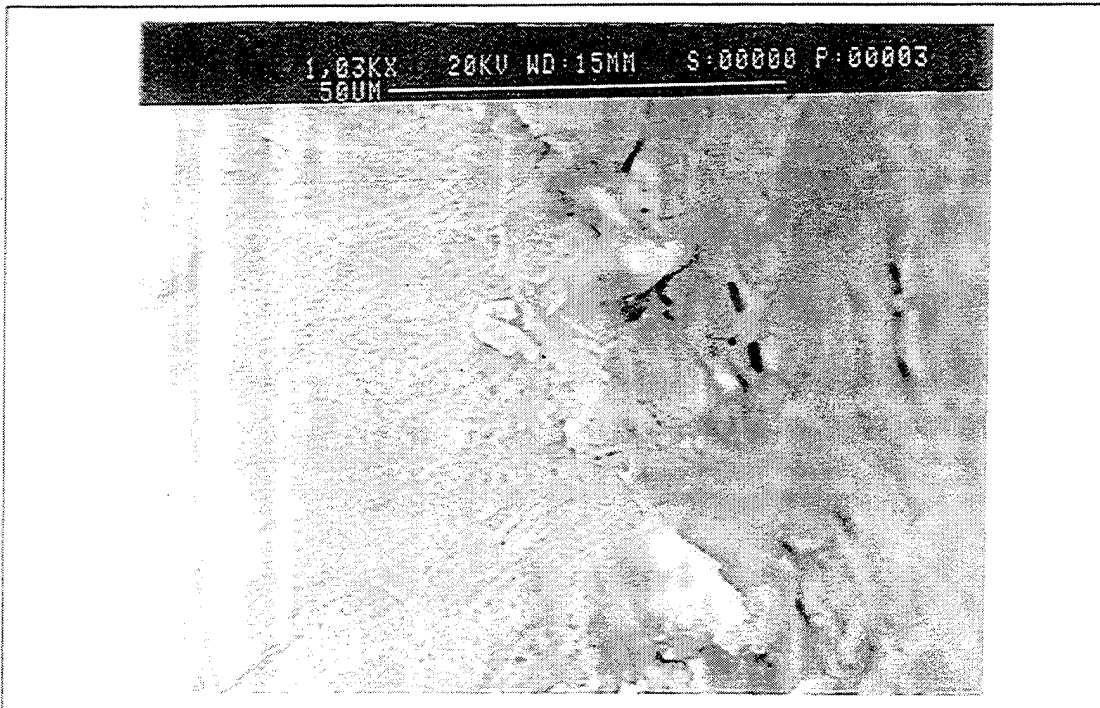


Figure 35 (a) : SEM pictures for virgin A22 (high magnification).

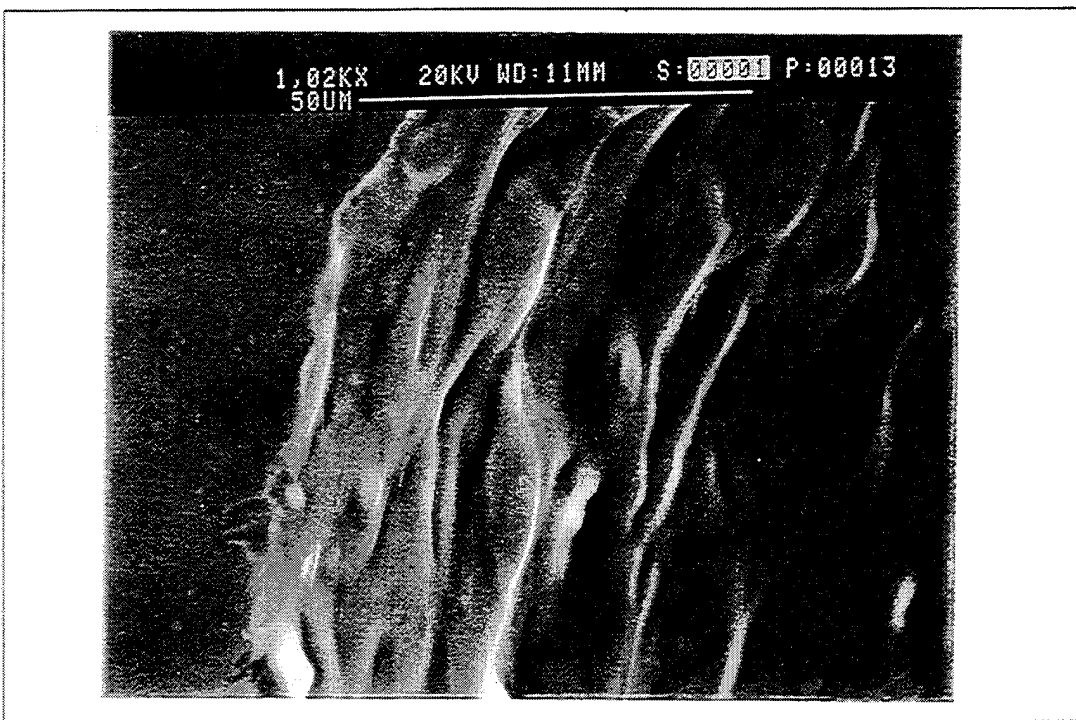


Figure 35(b) : SEM pictures for virgin A'26 (high magnification).



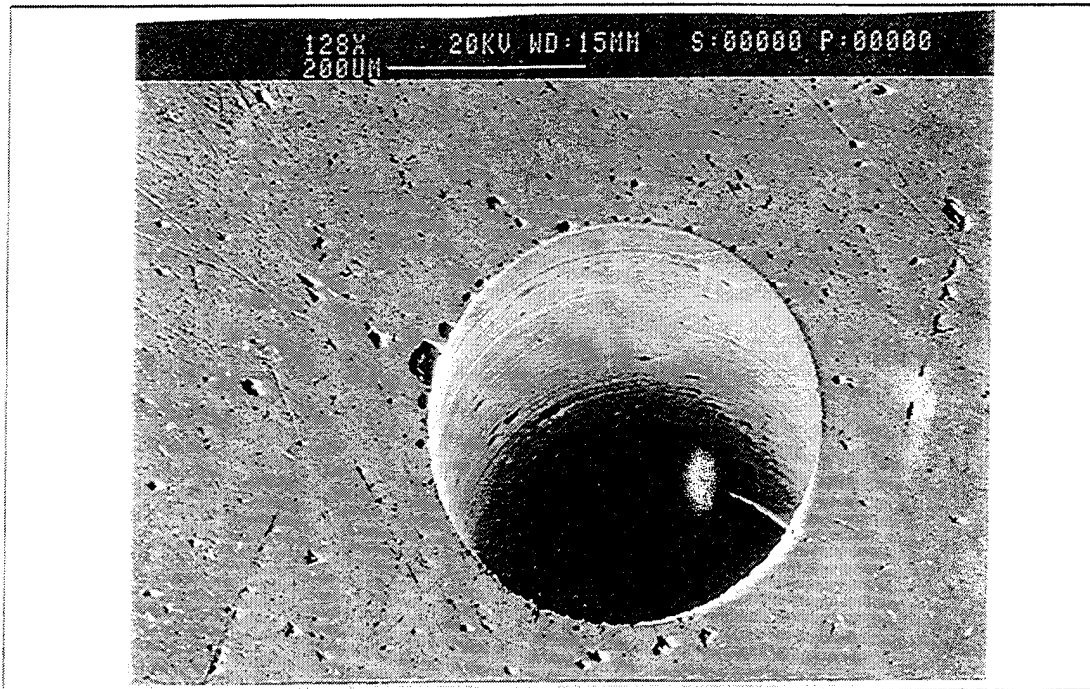


Figure 36(a) : SEM picture virgin B18, 12 o' clock.

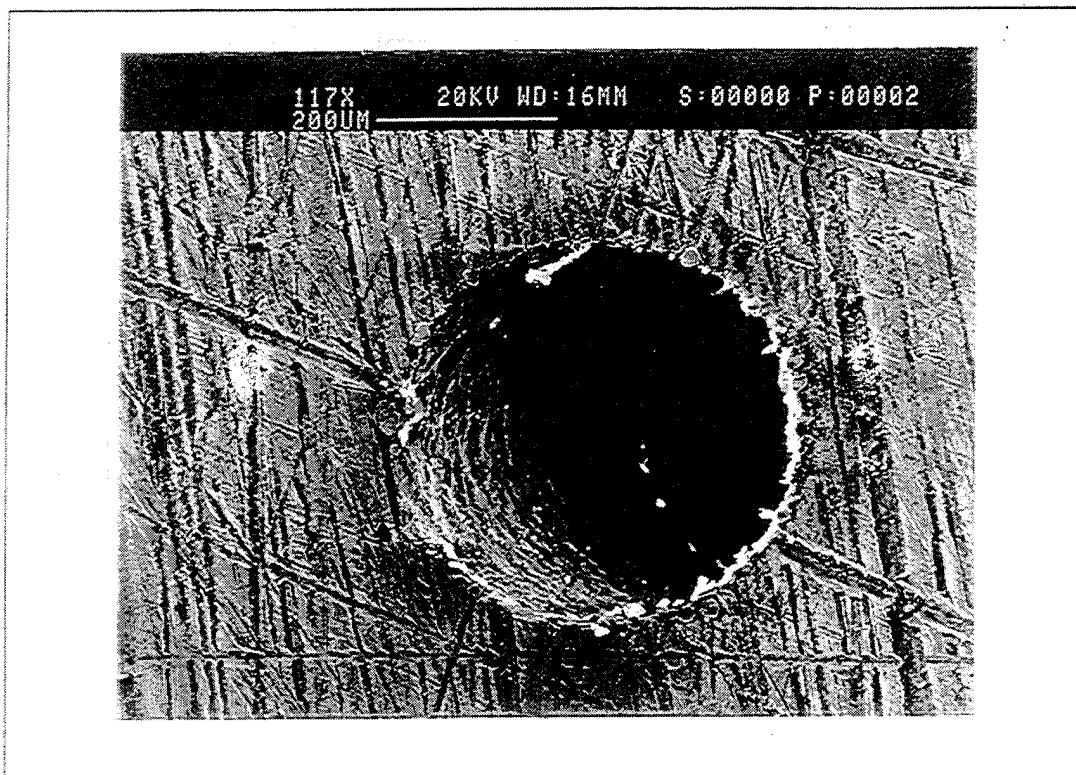


Figure 36(b) : SEM picture virgin A22, 12 o' clock.

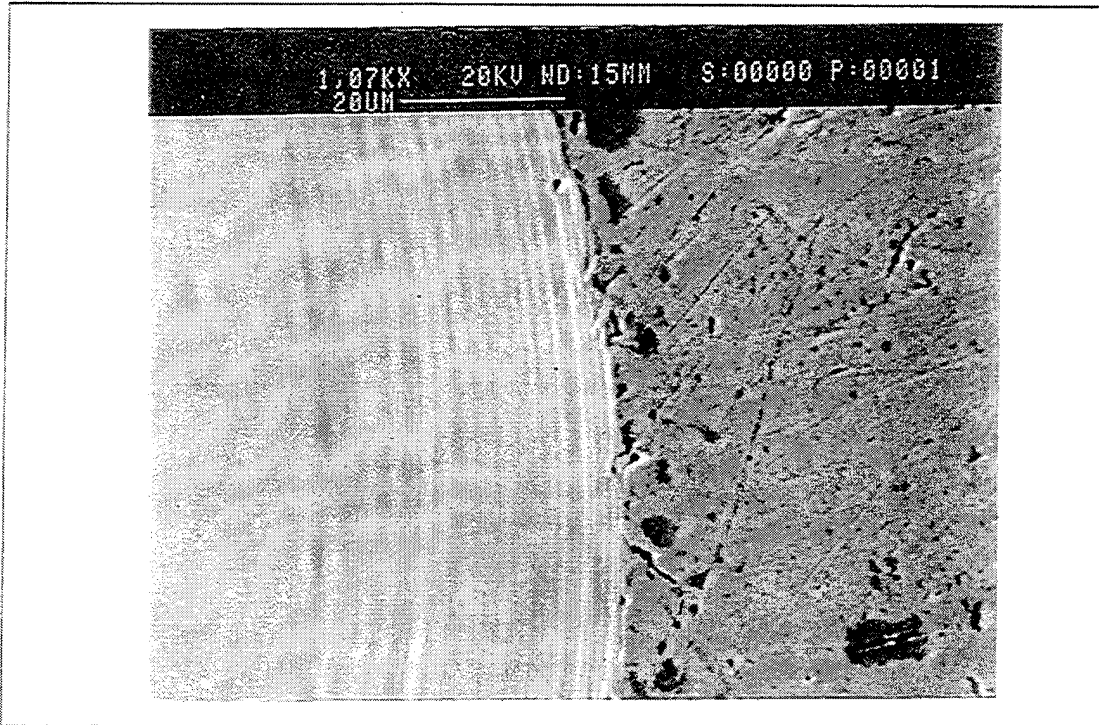


Figure 37(a) : SEM picture virgin B18, 12 o'clock (high magnification)

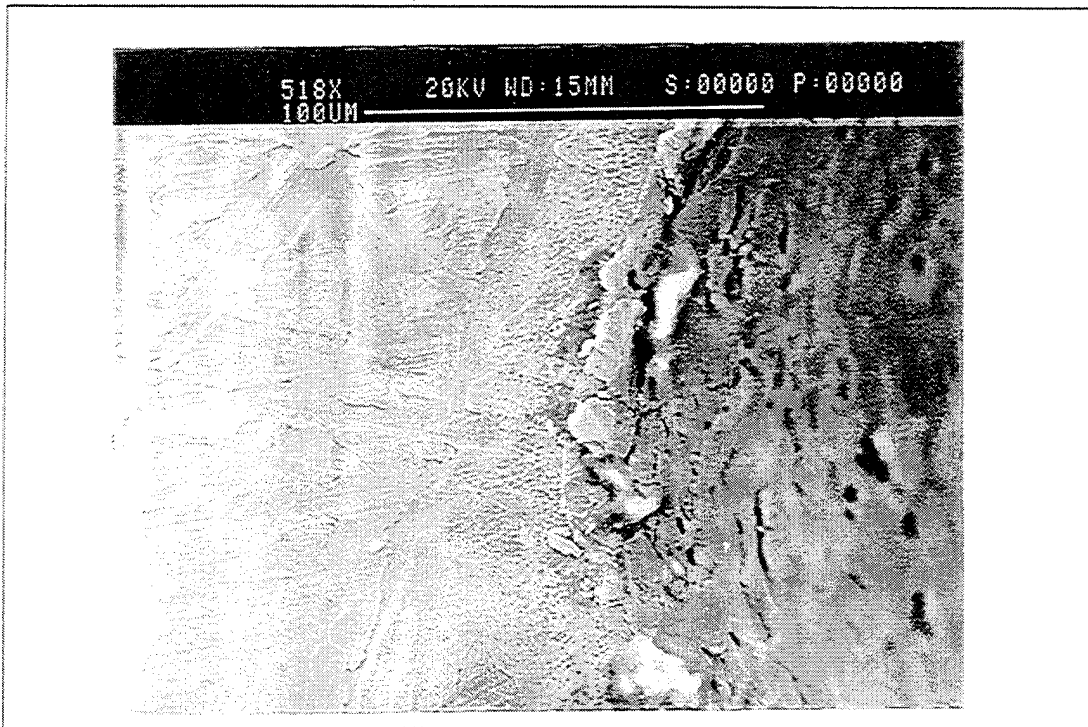


Figure 37 (b) : SEM picture virgin A22, 12 o'clock (high magnification)

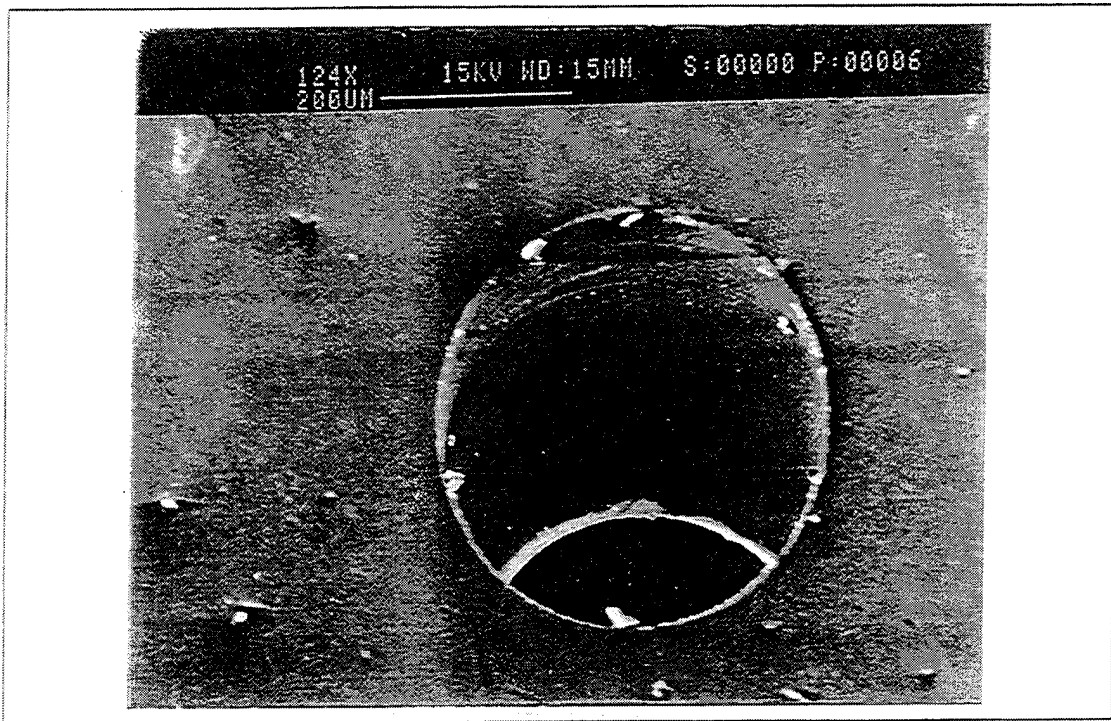


Figure 38 (a) : SEM picture B18, 12 o' clock, 50 cycles

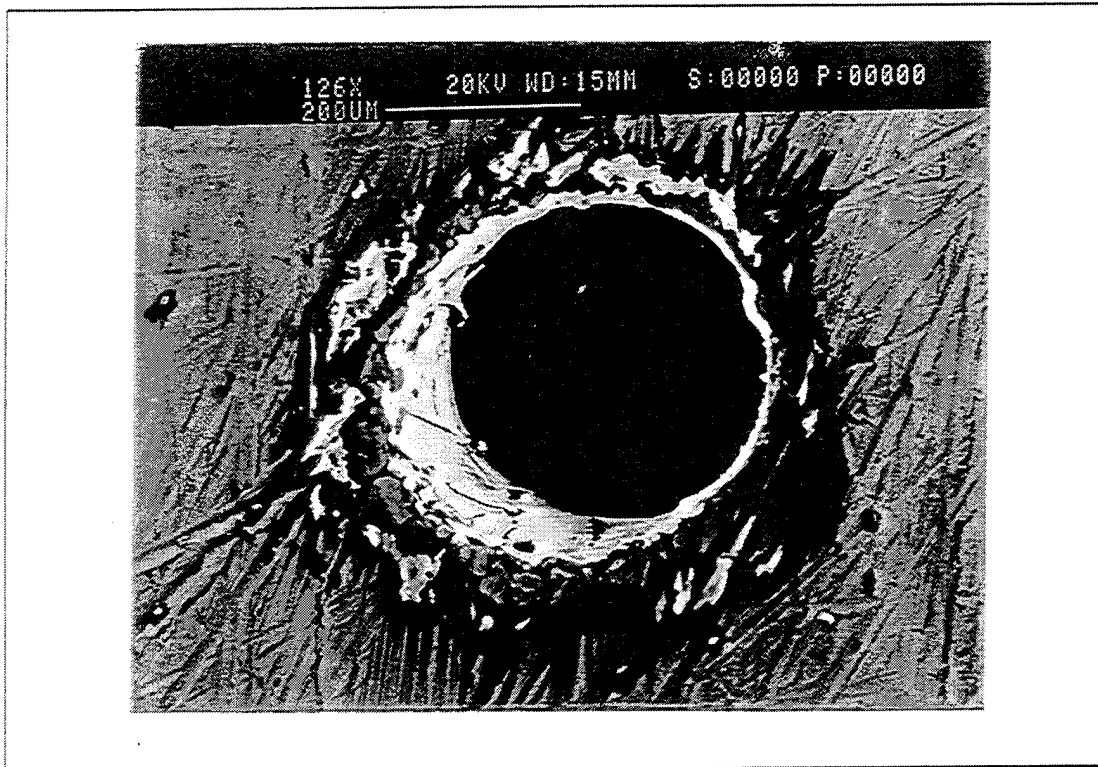


Figure 38(b) : SEM picture A22, 12 o' clock, 50 cycles

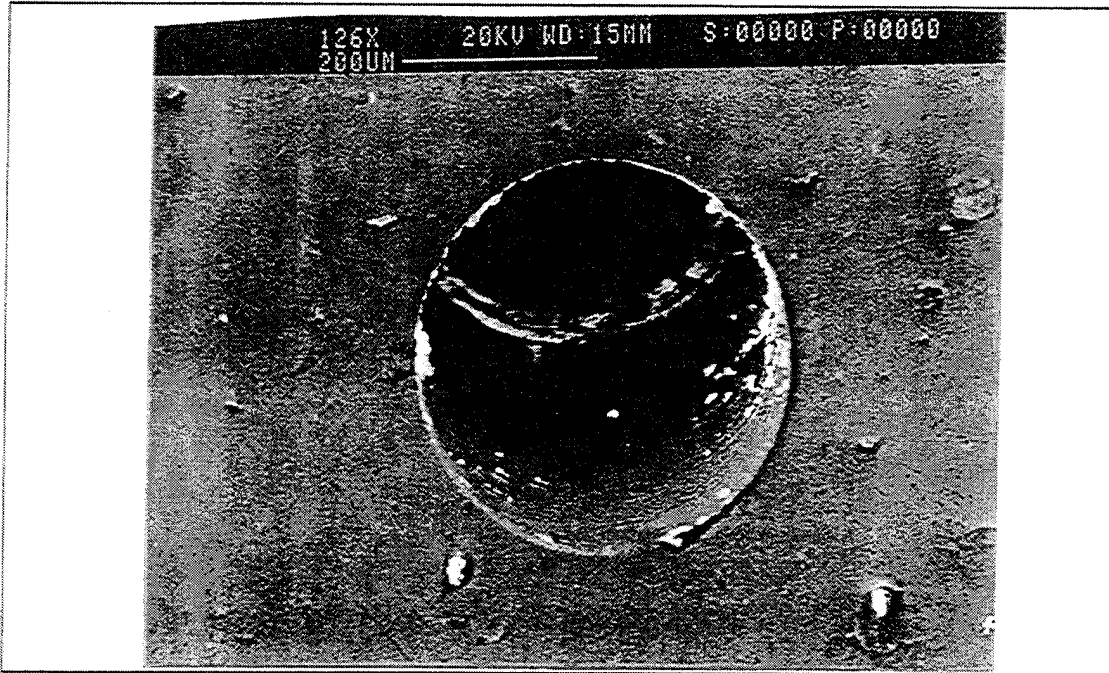


Figure 39 (a) : SEM picture B18, 12 o' clock, 100 cycles

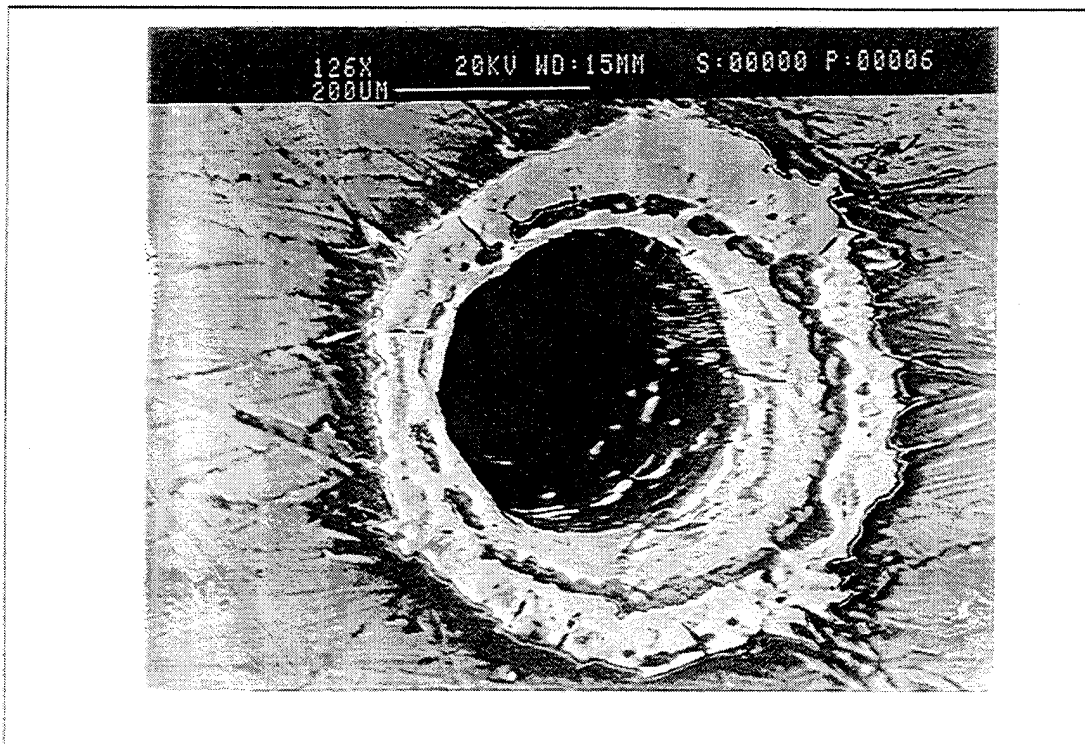


Figure 39 (b) : SEM picture A22, 12 o' clock, 100 cycles

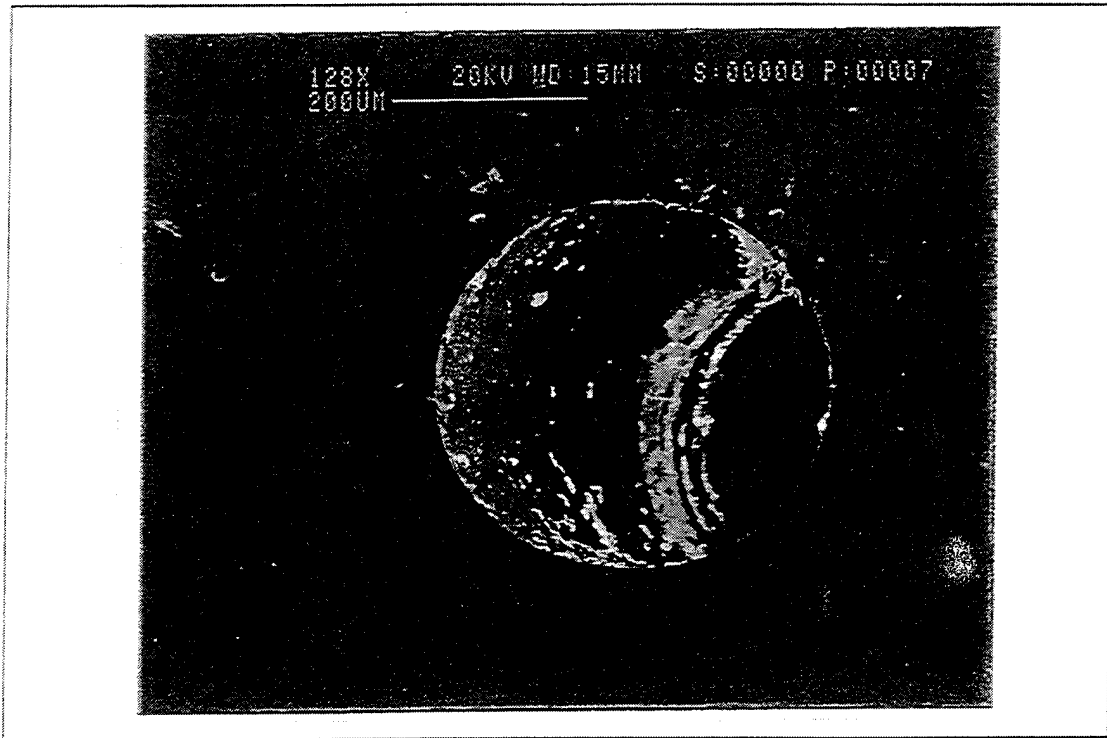


Figure 40 (a) : SEM picture B18, 12 o' clock, 150 cycles

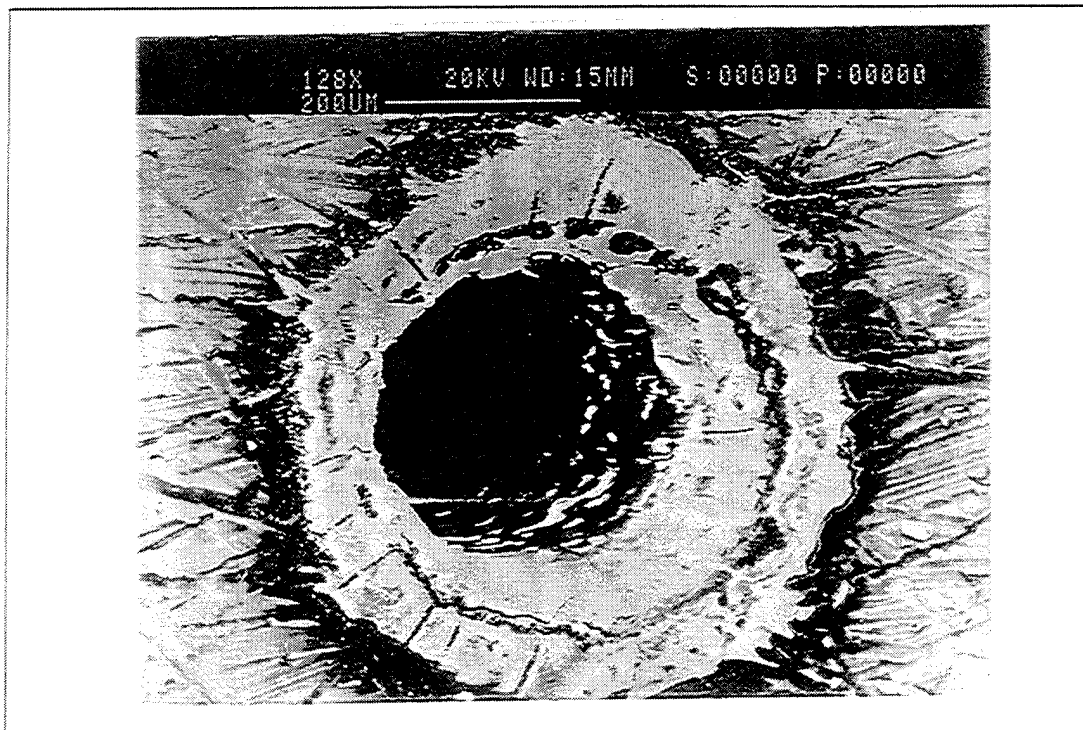


Figure 40 (b) : SEM picture A22, 12 o' clock, 150 cycles



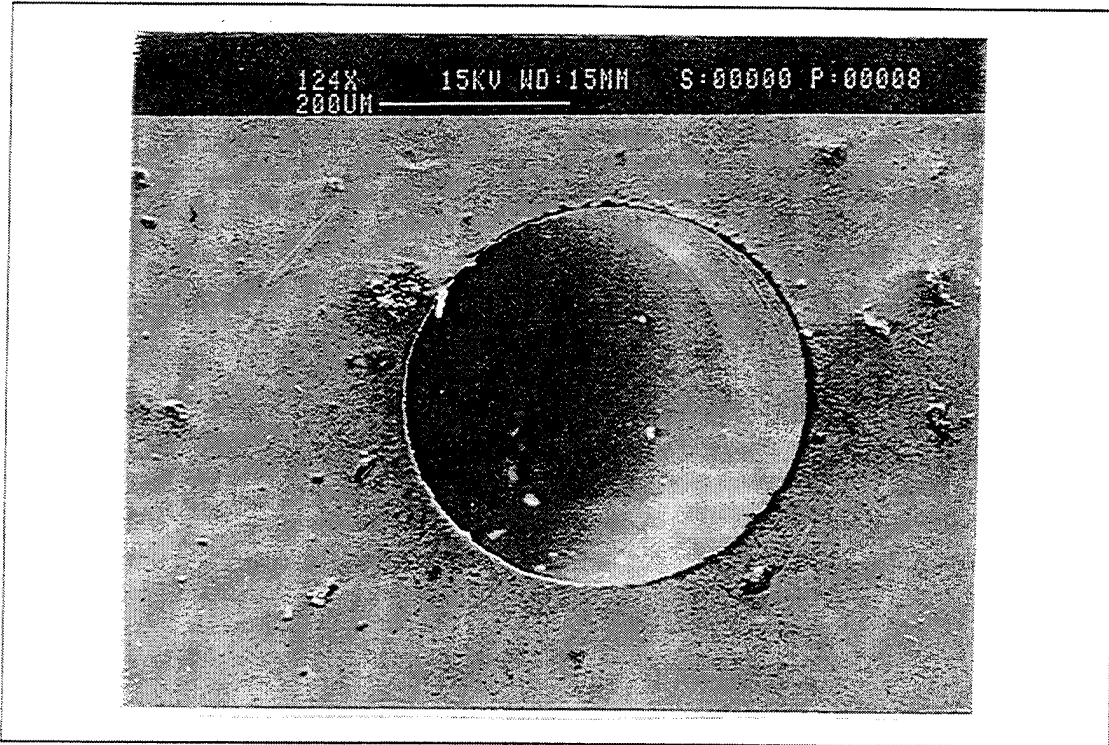


Figure 41 (a) : SEM picture B18, 3 o' clock, 50 cycles

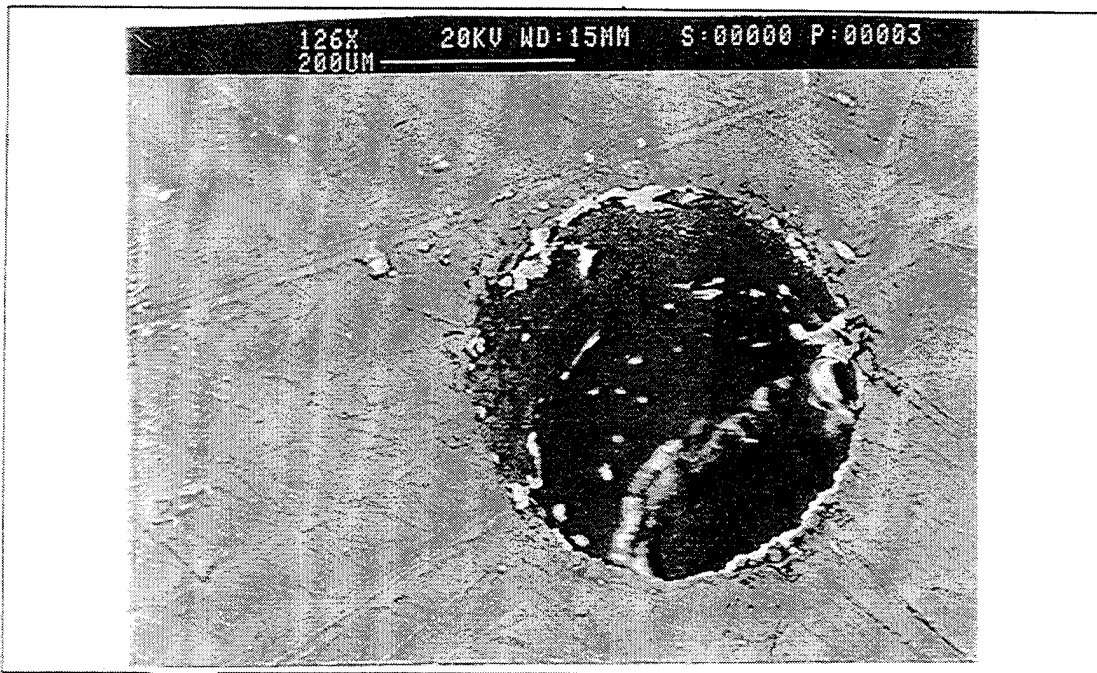


Figure 41 (b) : SEM picture A22, 3 o' clock, 50 cycles

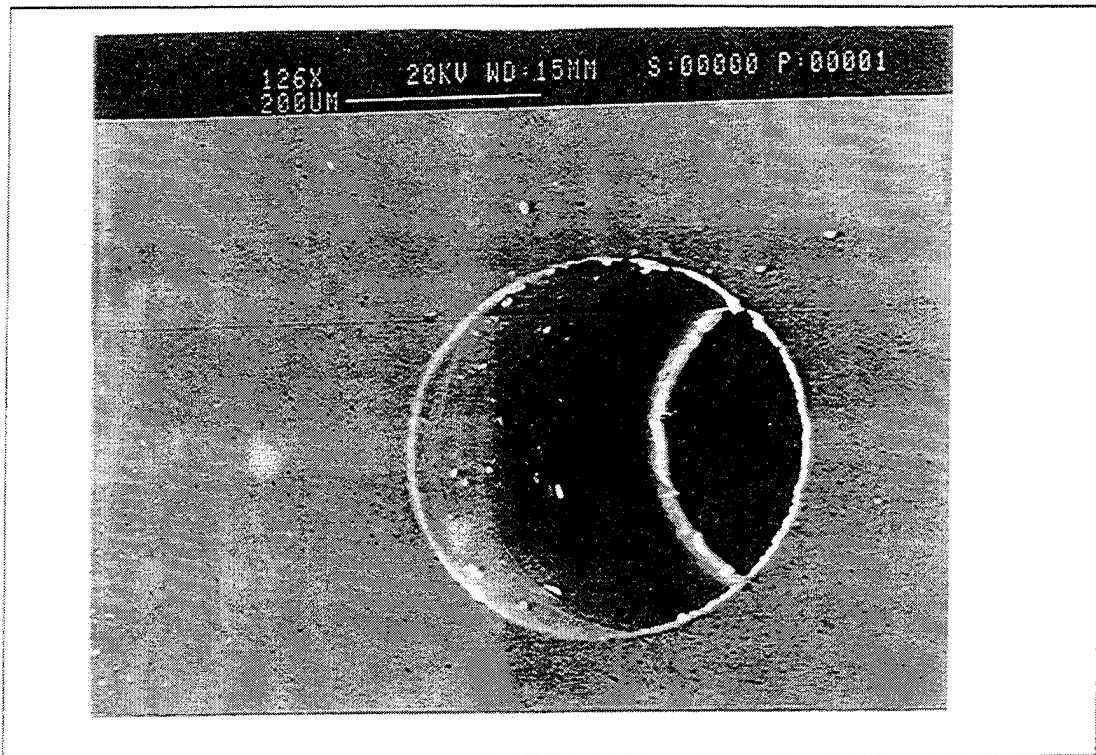


Figure 42 (a) : SEM picture B18, 3 o' clock, 100 cycles

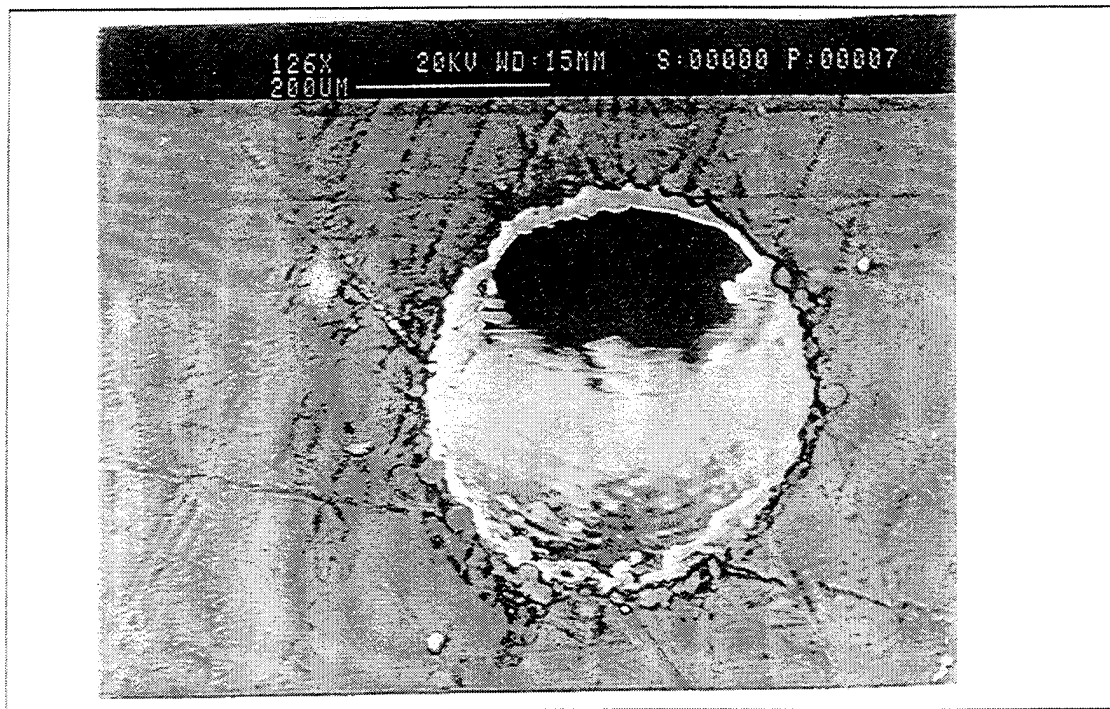


Figure 42 (b) : SEM picture A22, 3 o' clock, 100 cycles

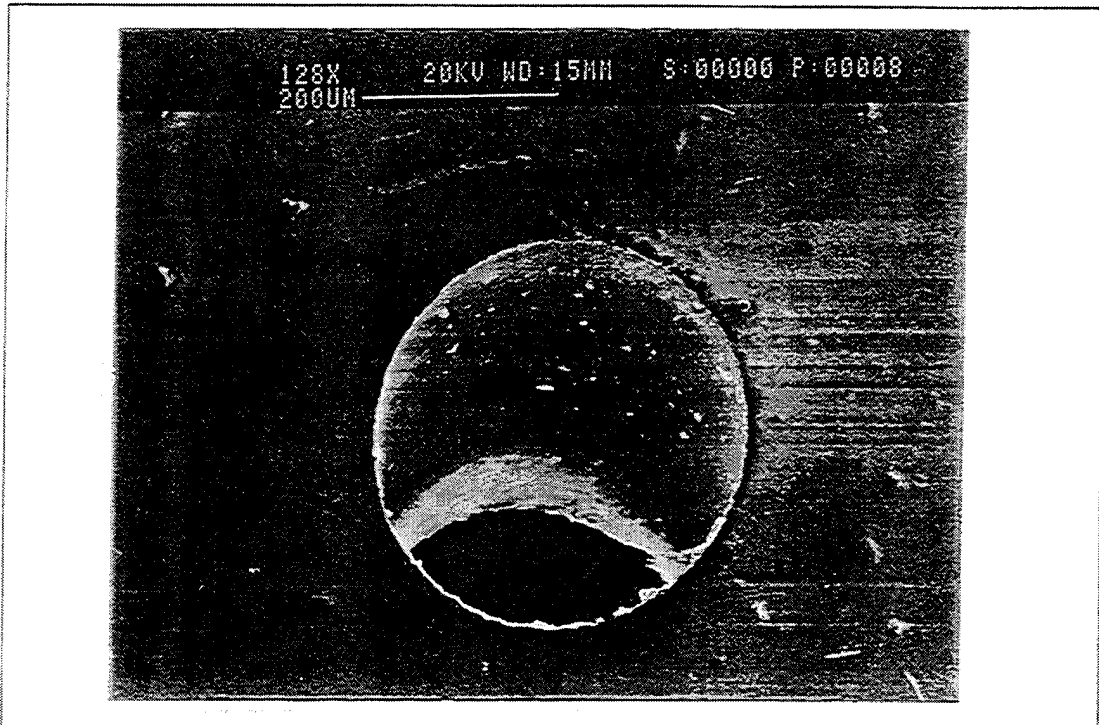


Figure 43 (a) : SEM picture B18, 3 o' clock, 150 cycles

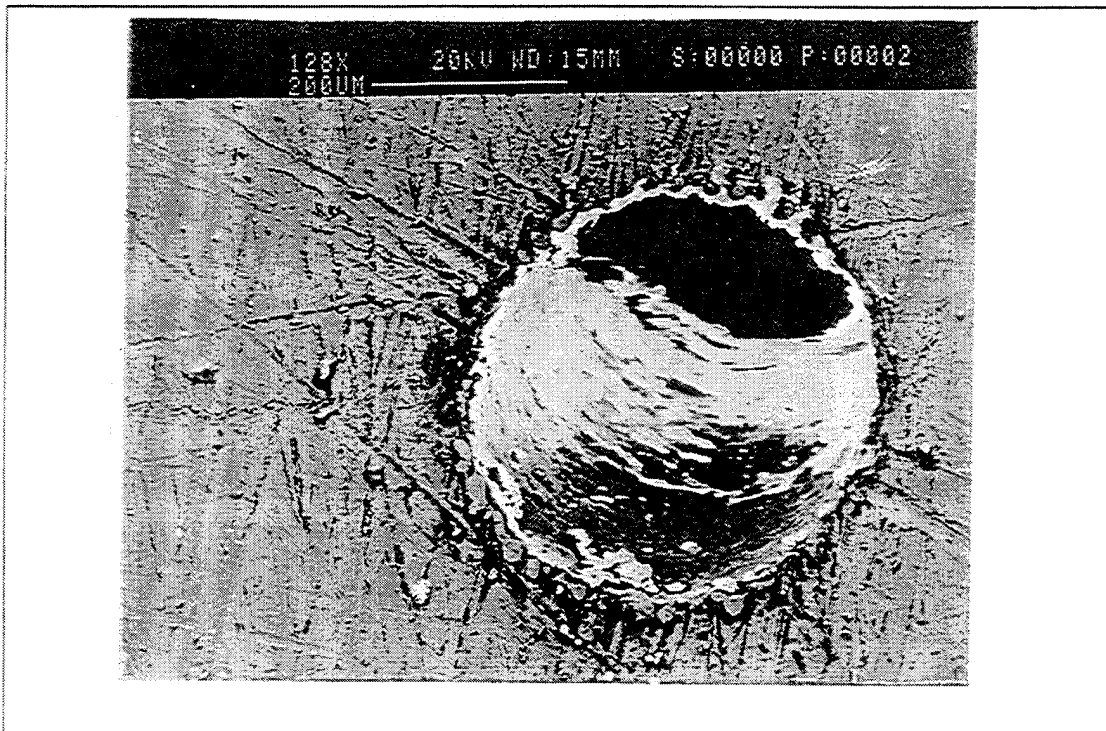


Figure 43 (b) : SEM picture A22, 3 o' clock, 150 cycles



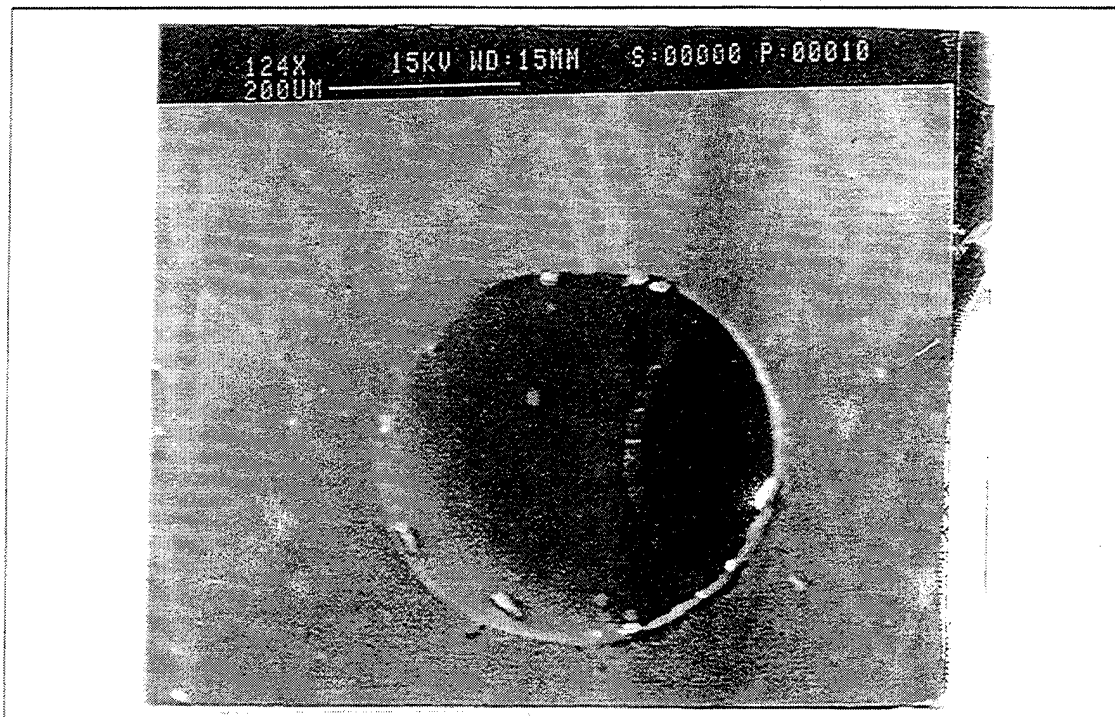


Figure 44 (a) : SEM picture B18, 6 o' clock, 50 cycles

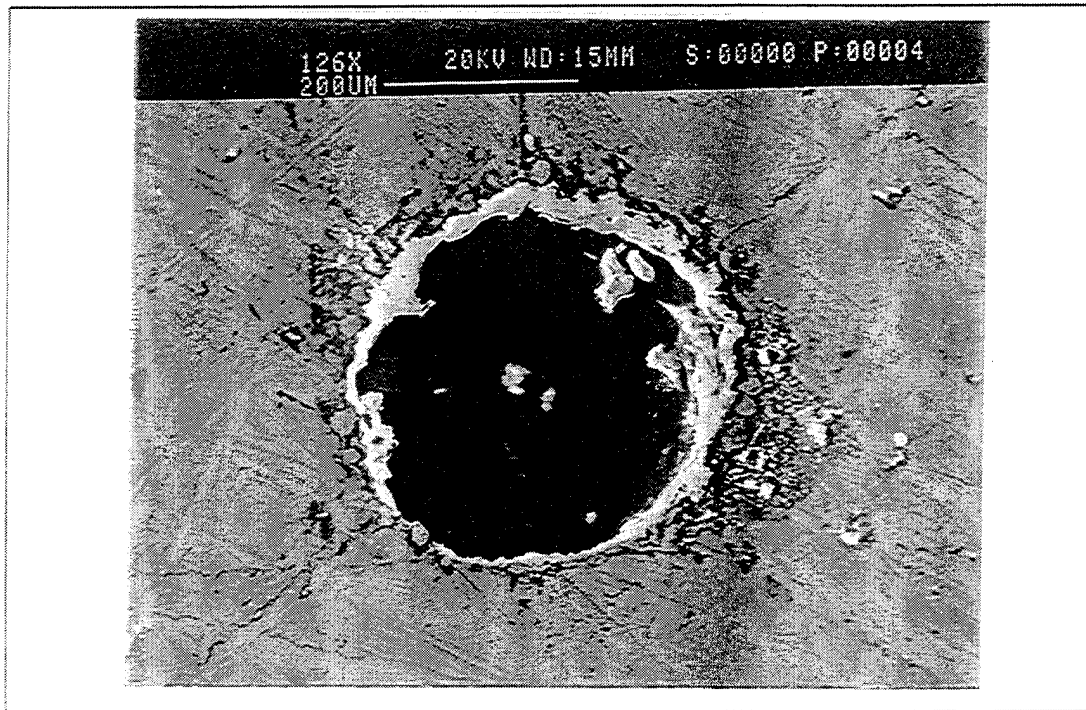


Figure 44 (b) : SEM picture A22, 6 o' clock, 50 cycles

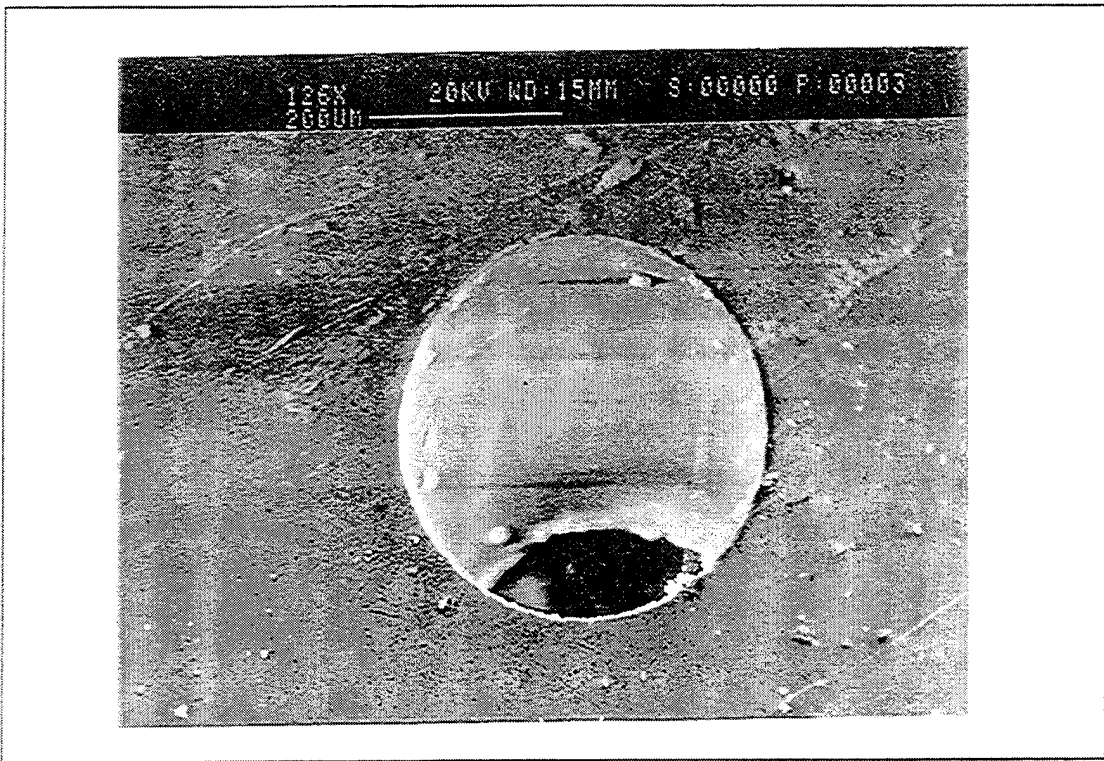


Figure 45 (a) : SEM picture B18, 6 o' clock, 100 cycles

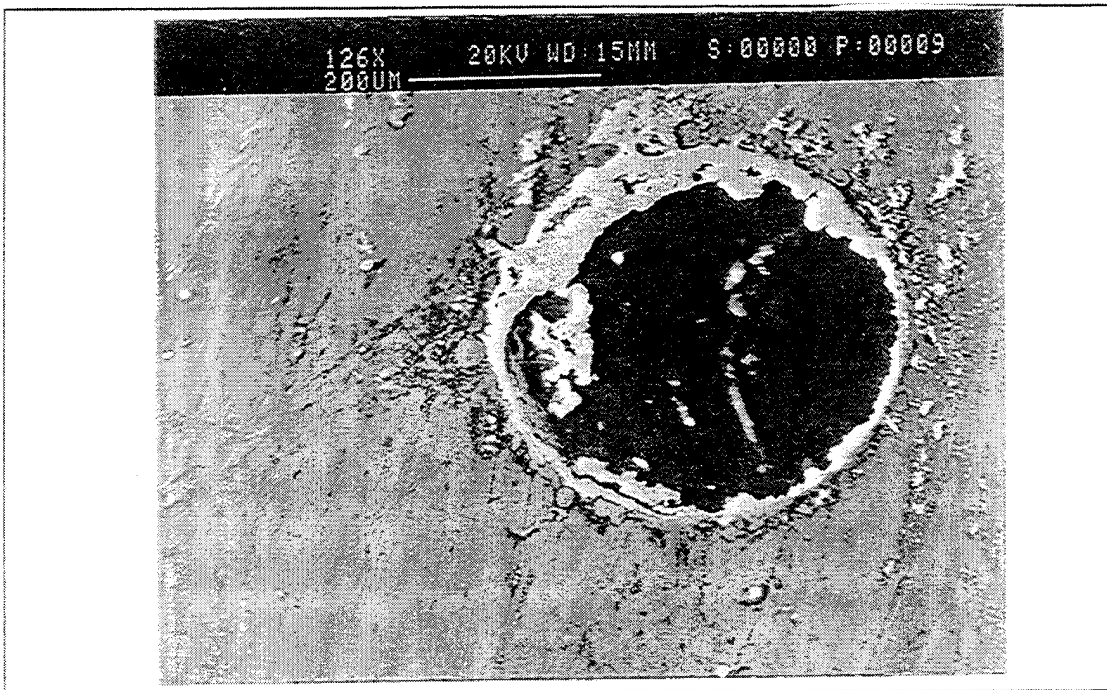


Figure 45 (b) : SEM picture A22, 6 o' clock, 100 cycles

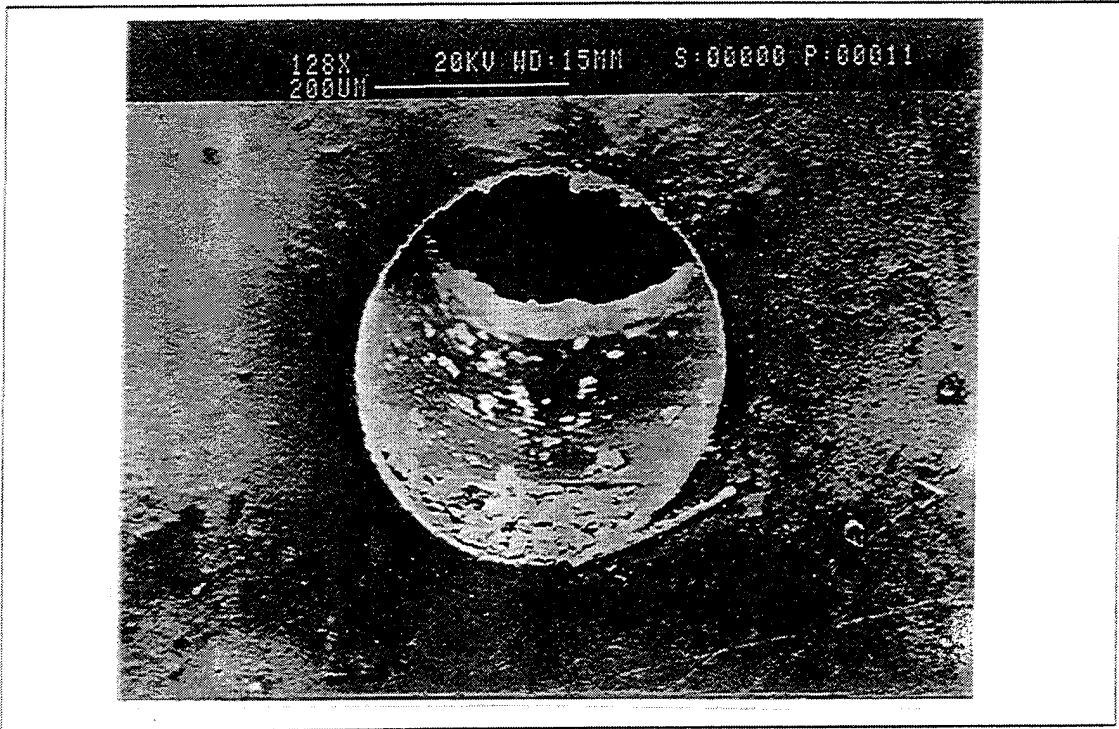


Figure 46 (a) : SEM picture B18, 6 o' clock, 150 cycles

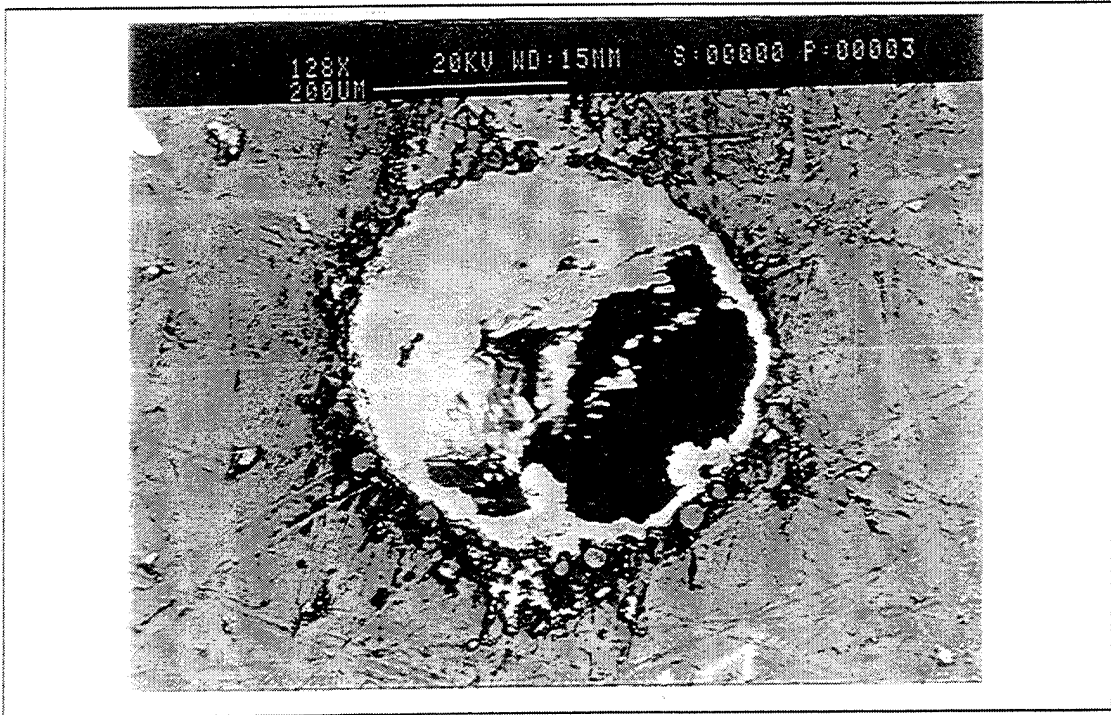


Figure 46 (b) : SEM picture A22, 6 o' clock, 150 cycles

## **E. FLOW- CLOSURE OF HOLES, MEASUREMENTS**

Flow measurements are reported here for the A27 and. B18 swirl plates. The results on the flow measurements and the calculated average percentage of closure of the swirl plate's holes can be seen in Tables 6 and 7.

Figures 46, 47 show the characteristic curves of Flow vs. Pressure drop for different amount of cycles performed. A first order curve fit was performed using the available data for each "family " data points referring to the same cycles. The respective slopes that were obtained showed very slight variation at the ranges of 15 to 25 psi and that was a verification of the initial design method since the isentropic flow model that was adopted was proved to be the right one for this case [Appendix D].

Figure 48 shows the percentage in average closure of the swirl plates holes for the case of the A and B. B18 gives a significantly improved behaviour compared with the A 27 and the average closure of the holes in B18 is much less for the same conditions than the average closure in A27 holes. This result is in agreement with the observations made in both the optical and SEM investigation.

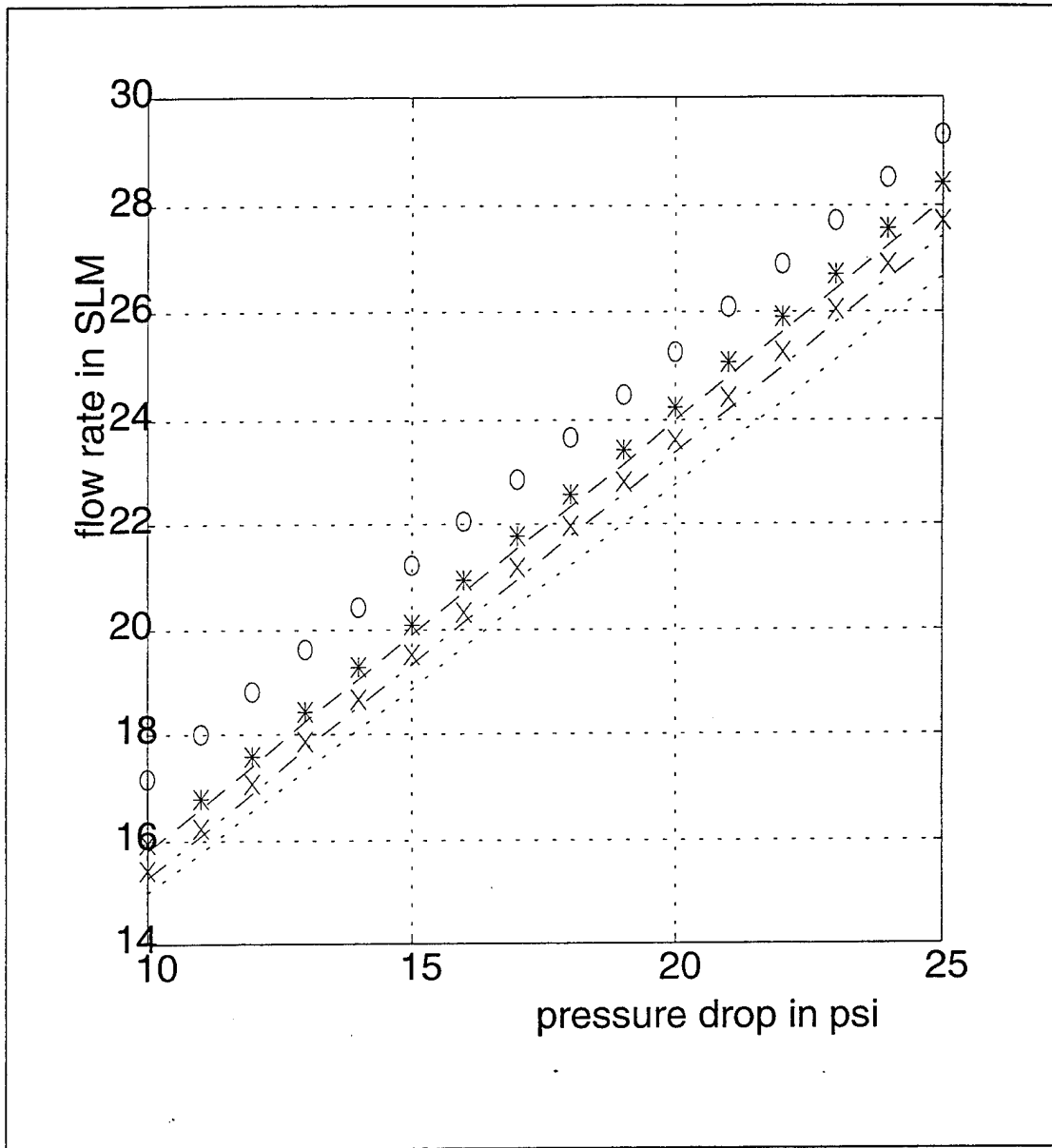


Figure 47: Flow characteristic curves for A22 swirl plate.

- Line ('000') : After 0 cycles performed ( $0.81 \cdot P + 0.96$ ).
- Line ('\*\*\*') : After 50 cycles performed ( $0.83 \cdot P + 7.633$ ).
- Line ('- -') : After 75 cycles performed ( $0.82 \cdot P + 7.567$ ).
- Line ('xxx') : After 100 cycles performed ( $0.82 \cdot P + 7.2$ ).
- Line ('- . - .') : After 125 cycles performed ( $0.81 \cdot P + 7.1667$ ).
- Line ('----') : After 150 cycles performed ( $0.78 \cdot P + 7.1667$ ).

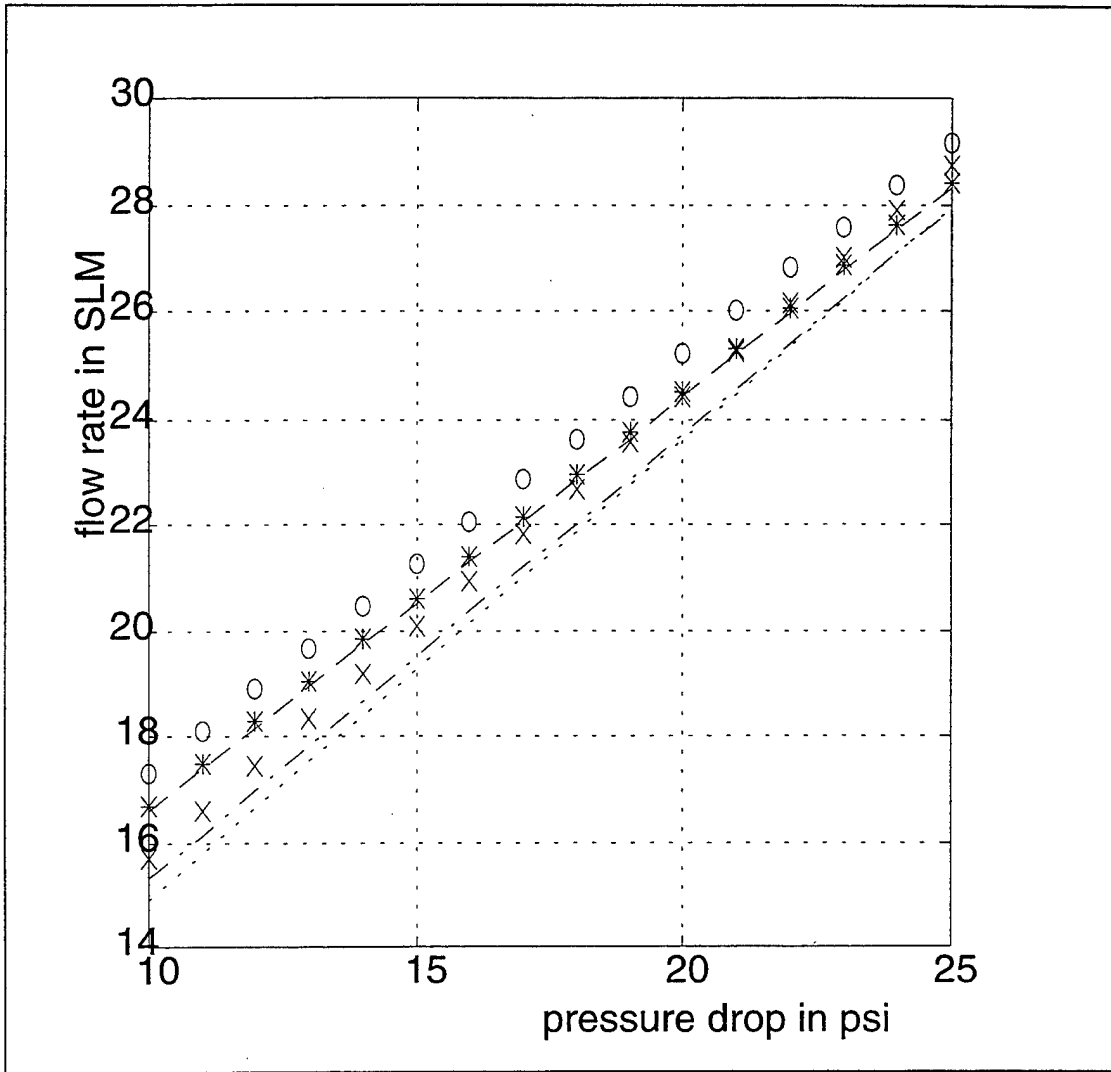


Figure 48: Flow characteristic curves for B18 swirl plate.

- Line ('000') : After 0 cycles performed ( $0.79 \cdot P + 9.4$ ).
- Line ('\*\*\*') : After 50 cycles performed ( $0.78 \cdot P + 8.9$ ).
- Line ('- -') : After 75 cycles performed ( $0.78 \cdot P + 8.8$ ).
- Line ('xxx') : After 100 cycles performed ( $0.87 \cdot P + 7$ ).
- Line ('- . -') : After 125 cycles performed ( $0.84 \cdot P + 6.9$ ).
- Line ('----') : After 150 cycles performed ( $0.87 \cdot P + 6.2$ ).

Cycles Performed	0	24	50	75	100	125	150
Pressure 15 psi	21.3		19.9	19.4	19.2	19	18.7
Pressure 20 psi	25.1	25.2	24.6	24.9	24.2	24	23.1
Pressure 25 psi	29.4		28.2	27.6	27.4	27.1	26.5

Table 6: Flow measurements in SLM at various pressures for A27.

Cycles Performed	0	24	50	75	100	125	150
Pressure 15 psi	21.1		20.3	20.2	20	19.5	19.1
Pressure 20 psi	25.5	25.2	25.1	25	24.5	23.9	23.9
Pressure 25 psi	29		28.1	28	28.7	27.9	27.8

Table 7 : Flow measurements in SLM at various pressures for B18.

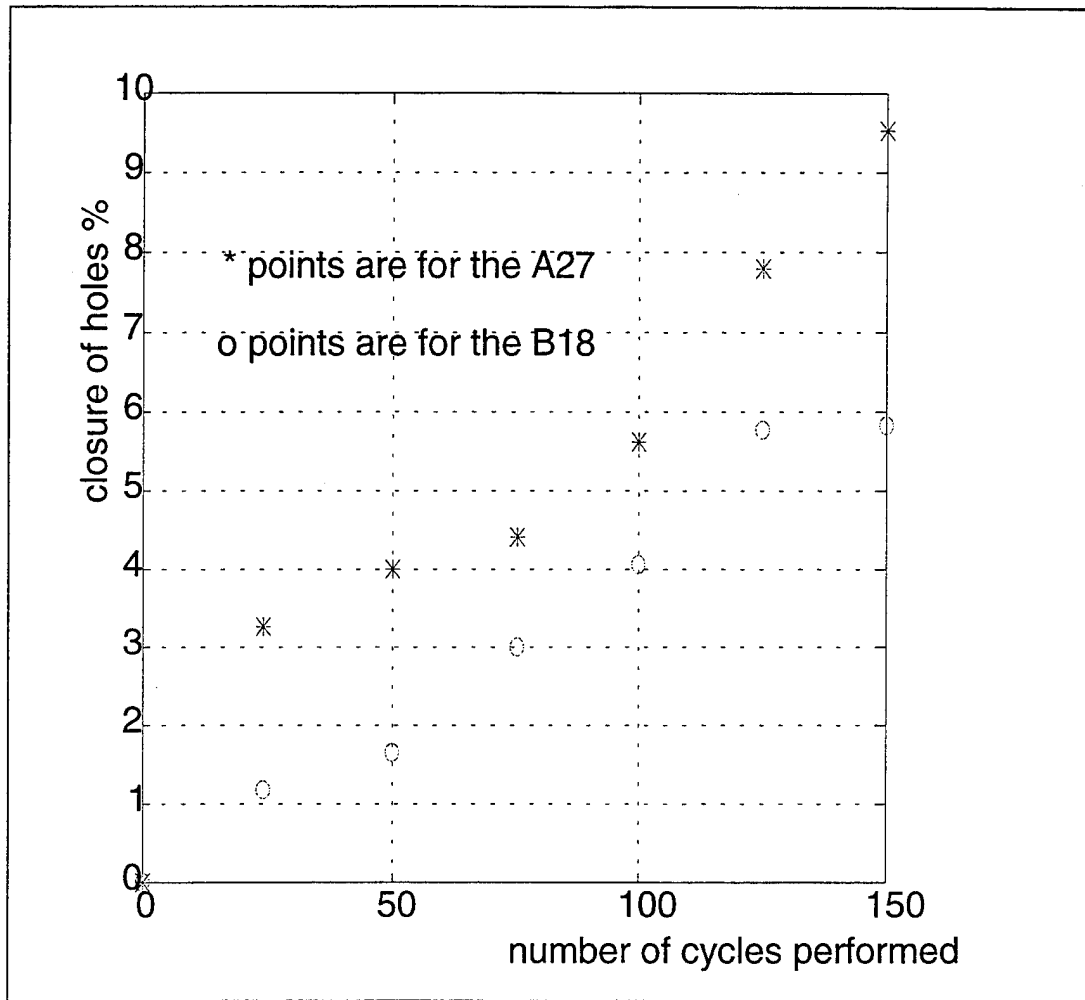


Figure 49: Average percentage closure of swirl plates hole vs. cycles performed

Cycles Performed	0	24	50	75	100	125	150
A27	-	3.26	3.99	4.4	5.61	7.78	11.17
B18	-	1.18	1.64	3.0	4.05	5.77	5.81

Table 8 : Average percentage of hole closure for A27 and B18.





## IV CONCLUSIONS AND RECOMMENDATIONS

### A. CONCLUSIONS

#### 1. Experimental Set-Up, Test Method

1. The testing rig that was developed in this study provides a reliable apparatus that is both easy to use and to modify and is inexpensive and safe in its operation. The test set-up, efficiently serves the purpose of to supplying the NAVY (or any other interested part ) with comparative data relative to similar coking problems of the swirl plates of fuel nozzles in gas turbine engines.
2. Periodic weight measurement of the swirl plate provides information about the rate of accumulation of deposits. It does not give exact coking rate and cannot provide information about the distribution of deposits on the plate surfaces or in holes, but can give a comparative estimation of the potential behaviour of coking accumulation under given conditions.
3. Optical microscopic examination provides information relative to the coking distribution along the edge of the holes. It can also be used to further interpret the estimations made from the weight measurement, either in a qualitative way, by comparing the pictures taken, or in a quantitative way by means of the size of hole calculated from the optical picture using available image software packages (Image Pro etc.).
4. SEM examination provides a detailed view of the holes, holes edges and the broad surfaces of the swirl plates. In this way interpretation of the effects of different surface finish treatments on the coking distribution on both holes and surface can be made. Again, this interpretation can be quantitative or qualitative in the same way as the optical pictures. In this study the qualitative interpretation of the pictures has been used since the hole's size has been measured with the flow measurements method.
5. The flow measurements can be used for the accurate calculation of the average percentage closure of holes. However, the information provided is not directly related to the fuel nozzle's efficiency in a quantitative way. The flow measurements have considered the isentropic-choked flow model, which is an approximation of the actual flow through the holes. Atomization of the fuel molecules and how this is directly affected by the closures has not been considered. Also the effects on the spray pattern due to the closure have not been investigated in this method. More tests related with the factors mentioned above have to be performed before definite conclusions can be made relative to the fuel nozzles efficiency and how is this affected by the swirl plates

depositions . The flow measurements can be used however to compare relative flow differences which can be directly correlated to the hole closure for two different types of swirl plates subjected to similar conditions.

6. The holes position nomenclature used in the experiment has been proved very useful in the case of swirl plates which have holes drilled at different angles depending on the manufacturer.

## **2. A , A' And B Types Of Swirl Plates Behaviour**

1. The weight measurements have shown a significantly lower rate of accumulation of deposits on the B (Du Pont) type of swirl plate as compared with the A (Parker production) type swirl plate that is already in use on the E-2C aircraft, from 50 up to 70% less. Much less difference is observed in the accumulation rate between A and A' (Parker polished swirl plates). A' had a rate of accumulation at 20 % less than A.
2. Optical microscopy investigation showed results that are in agreement with the weight measurements. Much more coking was evident around the edges of the holes for the A type swirl plate compares to the B type swirl plate. (Figures 15 through 29) following the higher accumulation rate observed in A type in comparison with the B type.
3. SEM investigation revealed more coking for the A type than the B type of swirl plate, and that this was mainly accumulated around the hole's and not on the broad surface of the plate (Figures 38-46).
4. The average percentage closure of the holes showed significant closure for the A type of swirl plate in comparison with the B (35% up to 50%), when both subjected to the same conditions.
5. The results have not shown any position. according to the nomenclature described on the swirl plate on which the accumulation of deposits is more favoured.
6. The suggested solution of polishing of the swirl plates has proved to be effective according to the data obtained so far. Weight measurements, optical and SEM investigation and average hole closure has shown much less coking effects on the B type in comparison with the A type. A significant observation revealed from the SEM pictures (Figures 44-46) is that the polishing of the inner hole surface is particularly effective, since the major coking accumulation is taking place around the holes and not on the swirl plates surface.
7. The choice between A' type and B type as a potential solution to the problem seems to favour the B (Du Pont) type of swirl plate. However a final choice may need to also take into consideration the higher cost of production of the B type due to the extremely detailed drilling and polishing procedure, cost which

is based on today's technology, are much more for the B type than the A' type. Thus more data should be obtained for the A' type swirl plate in parallel with the B type. In this way we will be able to conclude which is definitely more advantageous from an economic point of view.

8. The pointed ("spiky") deposition observed in some instances on the A type of swirl plate should not be considered as contributor to the overall holes closure effect, because it has proved to break under usual flow measurement conditions where the pressure of the air flowing through the holes is much smaller than the actual one experienced in service. The effect, however, that might be evident in the overall gas turbine coking problem (combustion chamber etc.) need to be examined further since is not uncommon in the swirl plates deposition (Figures 30-33).

## **B. RECOMMENDATIONS**

### **1. Experimental Set-Up, Method**

1. The NOTEBOOK package that was used to control the furnace has proved to be quite effective but it could also be substituted by another data acquisition package which includes more features in programming and display the data. This would probably widen the range of temperature-time profiles that could be achieved. In the same direction, the use of more strategically placed thermocouples should provide an overall understanding of the temperature gradients and heat flow in the rig at various selected places.
2. Instruments to monitor the quality of air in the rig (measuring humidity and other properties) could be used to assist the understanding of the role that air properties plays in the coking problem.
3. A future modification of the testing rig could also include the design of a controlled ventilation system to adjust quantities of air into the rig in the attempt to approximate working conditions of the fuel nozzle.
4. The results of the method could be used to categorise the quality of swirl plates, as far the coking resistance concerns, according to a scale. In this way the reference to a swirl plate type can be done by using this characterising scaling number which can be directly related with the coking resistance behaviour. This can be done by assigning a percentage on each one of the individual parts of the method, namely the weight increase measurement, the optical and SEM examination and the hole closure calculation. The percentage has to be representative of the extent that this part of the method is considered to contribute to the depositions problem. An easy way to do this is the by the use of a multiplier serving this purpose. By adding the resulting products we get a total number that can be related with the grading scale established.

get a total number that can be related with the grading scale established. Experimental data based on a larger sampling size could be very helpful on this direction (see Appendix F).

## **2. Future Study**

1. The comparative behaviour of A type and A' type of swirl plates has to follow this investigation in parallel with the A type vs. B type and A' type vs. B type in order to give more data based on a larger sample.
2. Different coating methods provided by several manufacturers can be tested in the everlasting attempt of finding the most inexpensive but still effective way to solve the problem. As the modern aircraft industry is designing higher performance engines, the problems of coking may be increased and a compromise has to be found between performance on one side and preventive - repairing maintenance on the other. The  $Ta_2O_5$  and the silica  $SiO_2$  coating (Appendix C) could easily be the first candidates for an investigation following this direction.
3. The testing rig can be used also to study the effects of different kind of fuel types, subjected to the same experimental conditions and various temperature time profiles. The results could be used for the evaluation of alternative type of fuels that are currently investigated [Ref. 17, 3].

## APPENDIX A: CORROSION AND DEPOSITS IN GAS TURBINES

A short description of the corrosion and deposits problem at various parts of a gas turbine, except on the swirl plates, is included in this Appendix.

In principle problems of coking in gas turbines are associated with much higher temperatures. Accordingly, one should consider separately swirl plates problem from the cases of the turbine blades or the combustor area. On Figure 50 a simple representation of a Jet Engine can be seen:

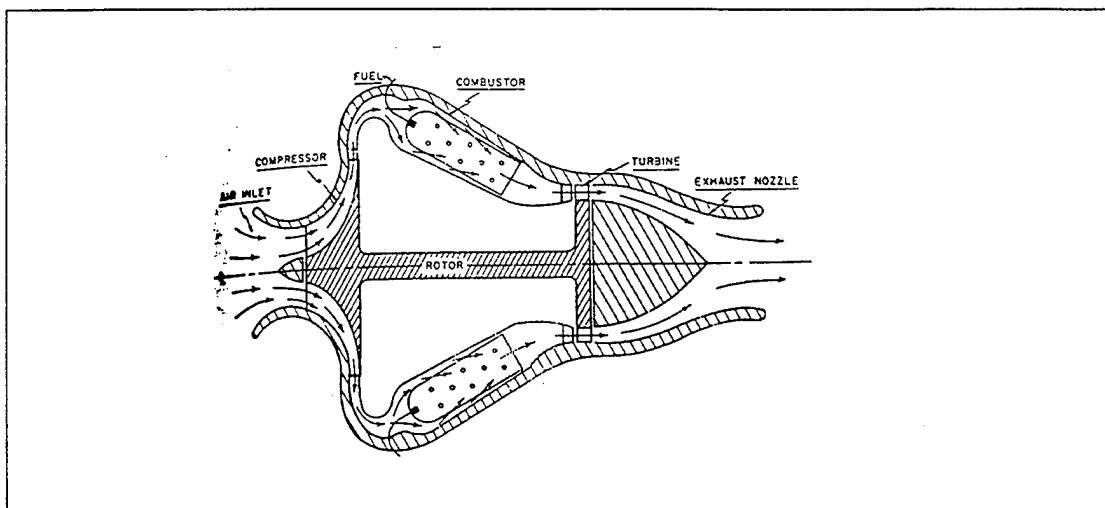


Figure 50 : Schematic representation of a Jet Engine (from [23]).

### A. COMBUSTORS

Studies on the deposits formed within the combustion area have shown that distillate fuels having low ash content tended to form deposits, mainly on atomisers or combustion chamber's walls. These deposits were found to consist mostly of carbon, with the material on the walls being either hard and coke like, because of direct impingement of liquid fuel from distorted spray patterns, or light and sooty from fuel-rich combustion.

The free carbon content of such deposits was found to range from 20 % in the atomiser section when burning kerosene, to 90% downstream of the atomiser when burning a partly aromatic fuel [Ref. 6].

With clean distillate fuels, combustor deposits are related somewhat to the fuel composition, particularly to the content of aromatics. In most cases, however, combustor deposits are the result of poor operating conditions or of shortcomings of the combustion system [Ref. 6]. This can be mainly attributed to the nonuniform mix of the air being present, with the fuel. Depositions of these types have been also reported on the liners of the fuel. The incident of the overriched mixtures, depends on the combustor design, primarily the location and size of the air entry holes. It also depends on nozzle design and spray pattern and on the engine operation conditions. Small changes in these parameters, can change deposition significantly. Deposit tests under apparently identical conditions gave results that differ by almost 20%. Liner surface conditions too have a marked effect on deposition. Differences in conditioning or cleaning may change deposits as much as 30% [Ref. 23].

Carbon that covers the liner holes upsets the mixing of cooling air with the burning gases and causes hot streaks in the exhaust. If the fuel flow is reduced to cool these streaks below limits imposed by the material, the engine gives less power and is less efficient. Deposits can also cause uneven heat flow to the liner. Warming results and airflow are distorted. Deposits that break loose and lodge in the turbine later burn out and overheat the nozzles. [Ref. 23].

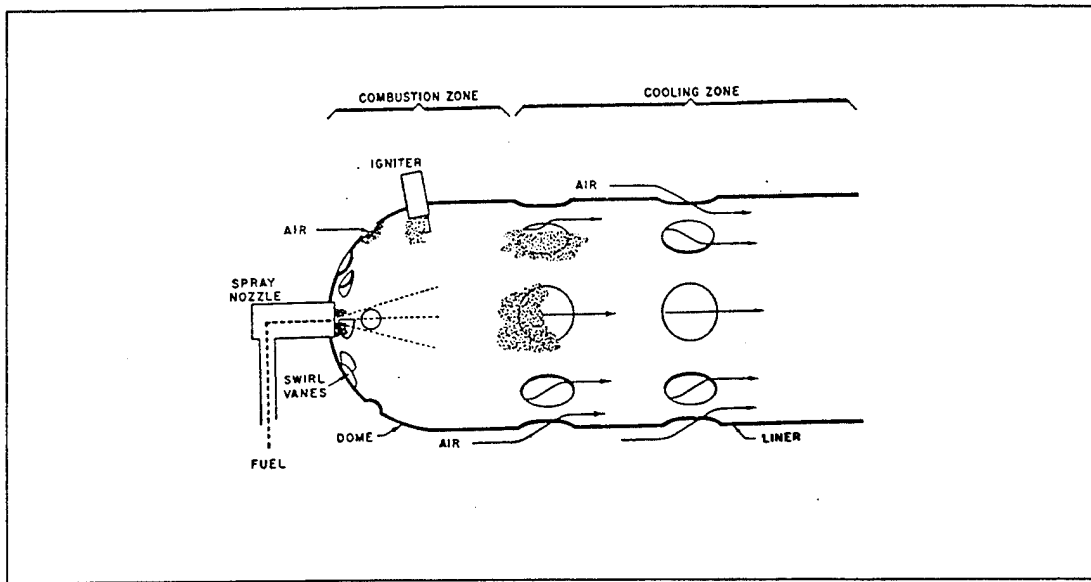


Figure 51: Deposition on Combustion Chamber (From [6]).

## B. ROTORS AND STATORS

Distillate fuels seldom cause trouble with turbine blading. The ash in residual fuels, however, can lead to serious problems, both in forming deposits and in causing corrosion. It was evident that Vanadium commonly accounts for half of such typical deposits and that alkalis are invariably present in at least moderate amounts. A preferential deposition of Sodium was evident, being consistent with the relative vapour of Sodium and Vanadium compounds. ( $\text{Na}_2\text{O}$  and  $\text{V}_2\text{O}_5$  respectively) [Ref. 6, pg. 45].

## C. NOZZLES AND BURNERS

Study of the problems of most concern when burning residual fuel, that refer to corrosion of metal parts by "slag - forming " constituents and deposit formation on nozzles and buckets, has shown that in experimental gas turbines, only 1 to 2 lb. of ash accumulation at the first stage nozzle can cause an appreciable decrease in efficiency and capacity. This study gave some conclusions about what could be the preferable



percentage of Vanadium, Sodium and Calcium in the ash formed. The results of the experiment can be seen on Figure 52 for different cases. More studies are in progress for the same problem [Ref. 6, pg. 46].

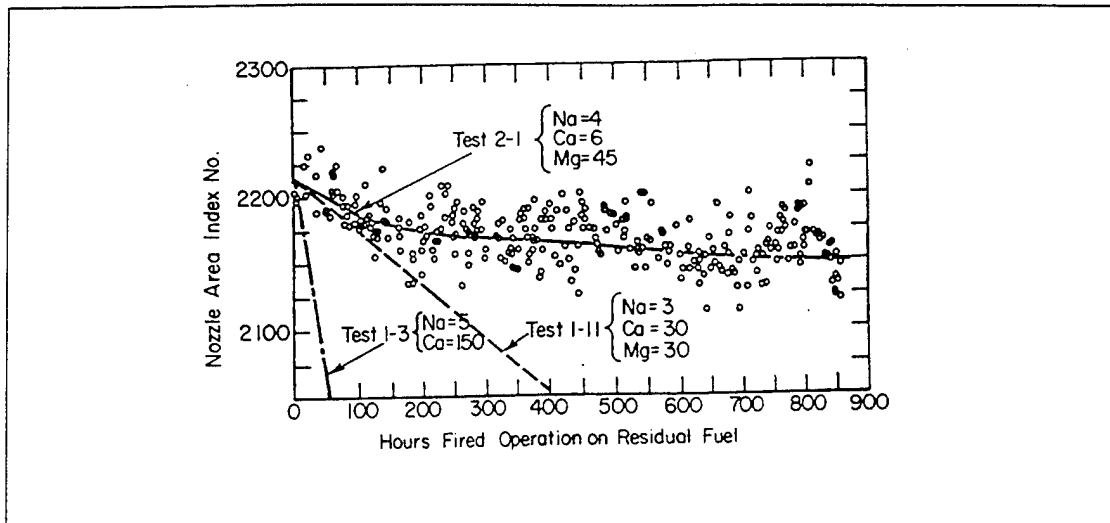


Figure 52: Rate of deposit accumulation in gas turbines burning Bunker C fuel (from [6]).

Jet engines used in aircrafts operate over a wide range of pressures. Ambient pressure ranges from 1 atmosphere at sea level to less than 1/8 of atmosphere at 5000 ft. The burner has to afford complete combustion at high altitude and yet not form deposits at sea level. High altitude combustion is favoured by smaller openings in the dome and consequently less air. But this favours deposition also and so a compromise has to be achieved [Ref. 23].

## **APPENDIX B: CHEMICAL FACTORS**

On the following appendix a description of the major chemical factors participating in the depositions accumulation are described. The major references for this part were from [Ref. 8, 6, 24].

### **A. SINTERING CHARACTERISTICS**

According to a definition, sintering refers to particle coalescence of a powder aggregate by diffusion that is accomplished by firing at an elevated temperature. [Ref. 25, pg. 784]. Although the particles of ash may arrive at a surface by physical transport, accumulation of ash to form massive deposits will depend largely on the adherence of particle to particle. When the adherence is weak, only thin layers of deposits will be formed, those being easy to break and removed (considering flowing gas conditions within the combustion chambers or fuel flow through the nozzle's holes). When the adherence is strong however, ash will continue to build up into thicker and thicker layers [Ref. 6].

The sintering characteristics of the deposits are affected by factors like: chemical composition, nature of minerals in the fuel, time-temperature history during combustion, the atmosphere where the engine is working, the temperature and the time, at which the ash particles are in contact together. Among these, time, temperature and turbulence during combustion are probably the most important. Many of the initial chemical reactions between solids, occur in the "flame", where the higher turbulence ensures frequent collisions between particles and consequently more favourable conditions for chemical reactions. A possible formation of a liquid phase by these reactions leads to

capture of other particles, by the liquid droplet and the eventual formation of a particle large enough to be caught by a surface through inertial impaction. It should be mentioned also, that a liquid phase is more likely to ensure adherence to a solid [Ref. 6].

Some of the particles included in deposits such as  $\text{Si}_2\text{O}_3$ , although not molten, may have a highly viscous surface, even at temperatures as low as 2000 F. Also, a lot of refractory particles sinter well below their melting point. For instance studies have shown that  $\text{Al}_2\text{O}_3$  can be sintered into a thoroughly vitrified body at 3300 F, even though the melting point is 3660 F. In general, these systems, are very complex and that makes it difficult to relate composition to sintering tendency. Empirical and experimental methods have been used to verify a relation of the above type. A general result found was that the sintering behaviour increases, with the alkali content. Less direct relations have been investigated with Sodium and other deposits constituents [Ref. 6].

## **B. FLUXING EFFECT OF ALKALIES**

Sodium and Potassium, can play an important role in inducing sintering. Compounds of these elements are usually highly reactive and the alkalies can form low melting silicates. The alkalies can also form eutectics with  $\text{CaSO}_4$  and  $\text{MgSO}_4$  that might lead to serious fouling problems [Ref. 6].

## **C. CHEMICAL REACTIONS**

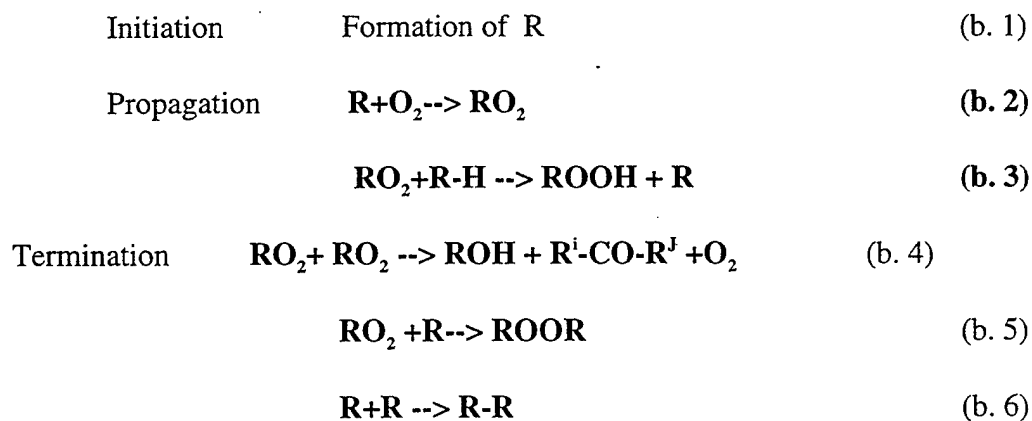
The reaction patterns associated with the combustion of fuel in gas turbines can be based on the basis of two schemes according to a basic study performed by Robert N. Hazlett, James M Hall and Martha Matson ; autoxidation and pyrolysis [Ref. 8]. The latter controls the high temperature reactions 900 F (482 C ) and above and autoxidation

phenomena occur at lower temperatures, 500 F (260C ) and below. In the intermediate regime, above the temperature at which oxygen is completely reacted, but below pyrolysis temperatures, the reactions are more complex. The general features of the three regimes are summarised in the following table and discussed shortly in the following sections.

Regime	Temp F (C)	Reactions	Products
Autooxidation	500 and below (260)	O <sub>2</sub> with C <sub>12</sub>	Hydroperoxides (ROOH)
Intermediate	550-900 (288-482)	(1)ROOH decompos. (2)ROOH init.pyrolysis	Alkohols,ketones+ CO  n-Alkanes, 1 alkenes +H
Pyrolysis	900 and above (482)	C <sub>12</sub> cracking	n-Alkanes, 1 alkenes +H

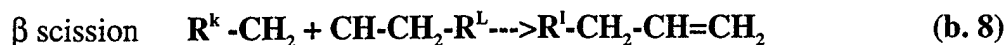
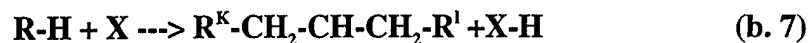
Autooxidation:

The autooxidation reactions are listed in reactions 1-6, and are well established by many studies to explain liquid phase oxidation by elemental oxygen.



## Pyrolysis

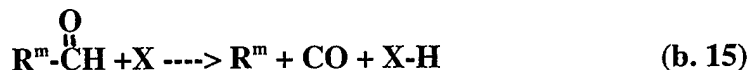
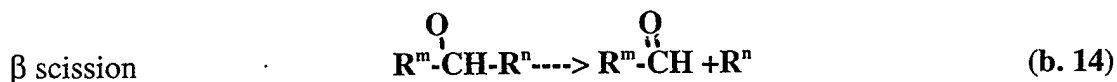
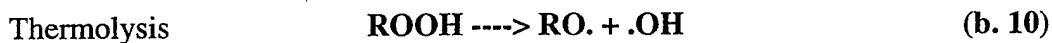
In the pyrolysis regime reactions modified for high pressure conditions can predict the pattern of hydrocarbon products. The sequence of reactions that take place are :



transfer (secondary)

## Intermediate Regime

In the intermediate temperature regime, between autooxidation and hydrocarbon pyrolysis reactions, oxygenated products play an important role. The reactions taking place are the following:



## APPENDIX C: COATED SWIRL PLATES SUGGESTION

In this appendix a short description of the coated swirl plates suggestion in order to prevent coking for the E-2C aircraft fuel nozzles is given. The description is based to the GE.. information package that was available to the NAVAIR [Ref. 12].

The information package which escorts the suggestion mentioned above emphasises the role of the  $Ta_2O_5$  oxide coating film in preventing the formation of sulphides and oxides, which would otherwise develop on bare metal surfaces. The GE study was based on the propagation of the chemical process. The basic concepts that were adopted were :

1. Reactions involving molecular growth must have available high concentrations of the ingredients which provide this growth.
2. The surface is considered to be a source for these ingredients and concentrations.

Reactive fragments produced by the thermal break up of the fuel molecules, contribute to the growth of the coke molecule and the only way to avoid this, is to disperse these fragments. Microcavities, which according to the GE claims, are formed from the sulphides, act as sites for coke formation. A  $Ta_2O_5$  coating film of about 5000 atoms thick (5 microns) applied by Chemical Vapour Deposition Process has been suggested, as the way to avoid the cavities formation and consequently the deposits accumulation on them. On the following pages a schematic representation of the mechanism of coke formation and the suggested solution according to GE can be seen.

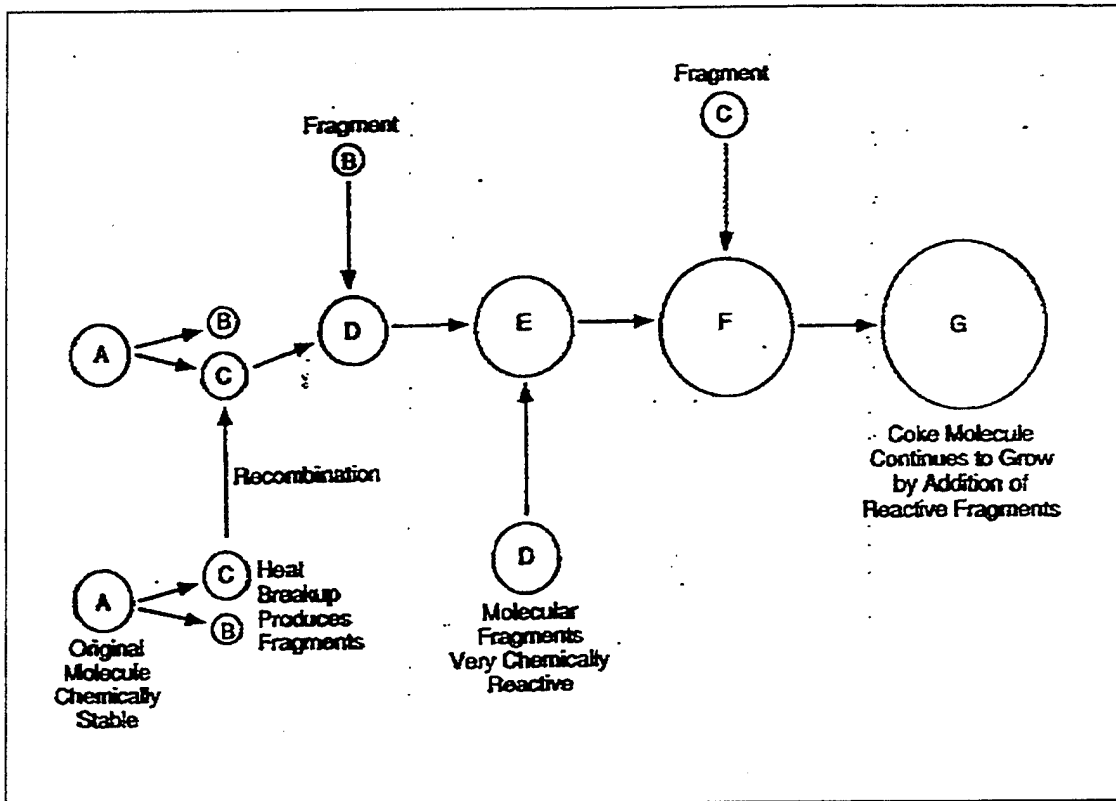


Figure 53 : How coke Forms (Heat break up followed by growth from molecular fragments (from [12])).

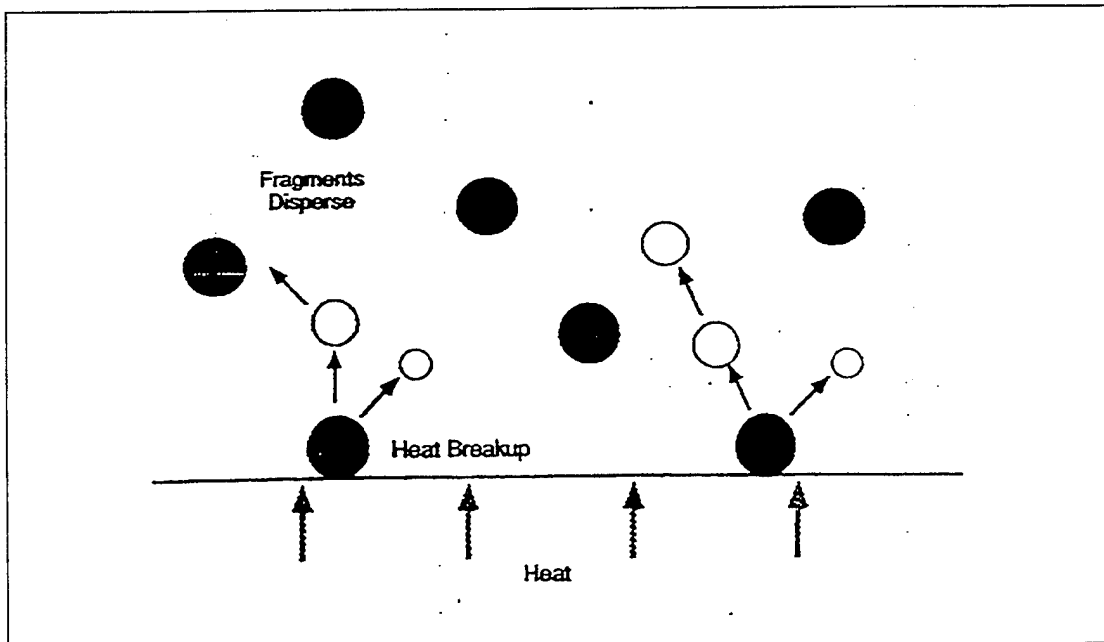


Figure 54: Coke does not grow if fragments can disperse (from [12]).

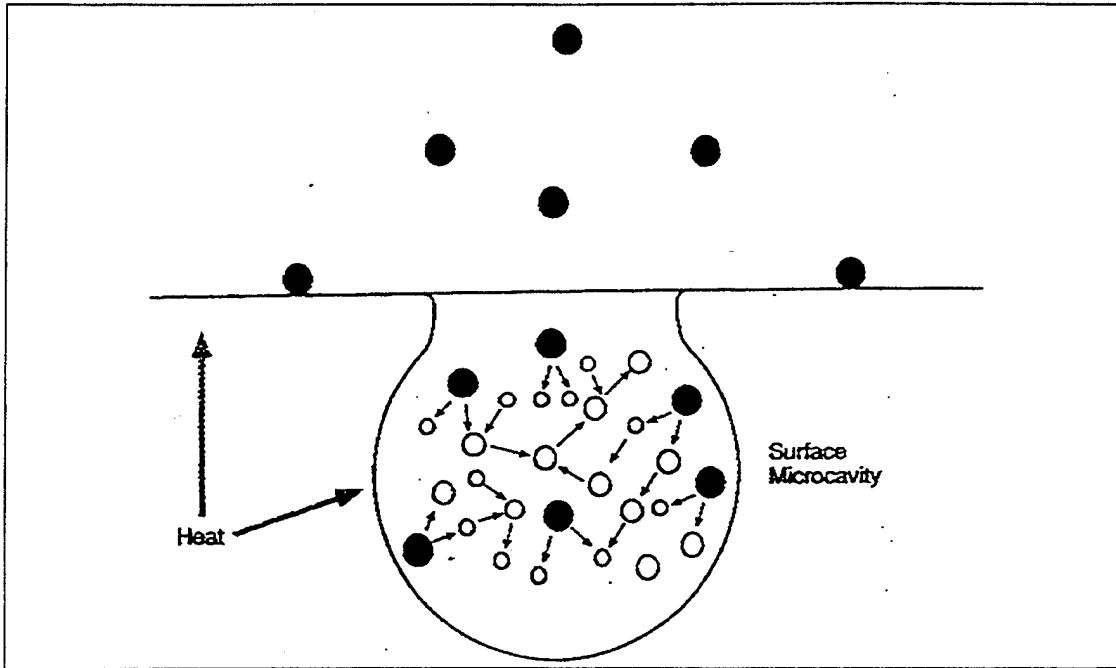


Figure 55 : Surface microcavities contain fragments and permit Coke to grow (from [12]).

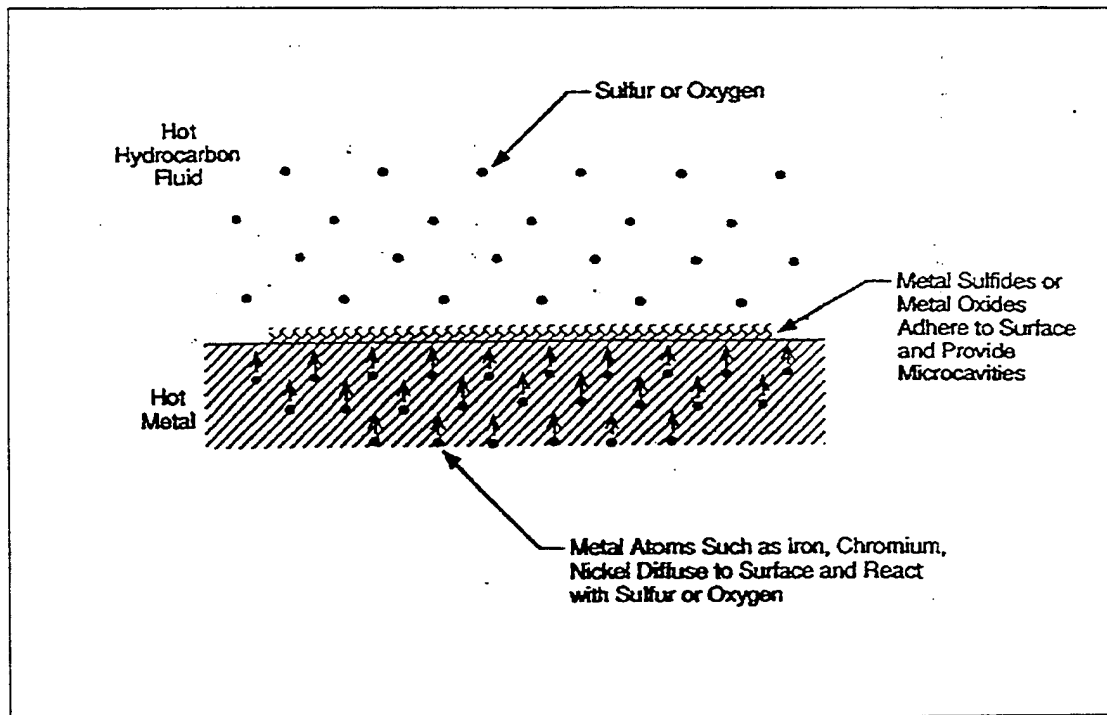


Figure 56 : Sulfur or oxygen in fluid react with metal atoms to form surface microcavities {from [12]}.



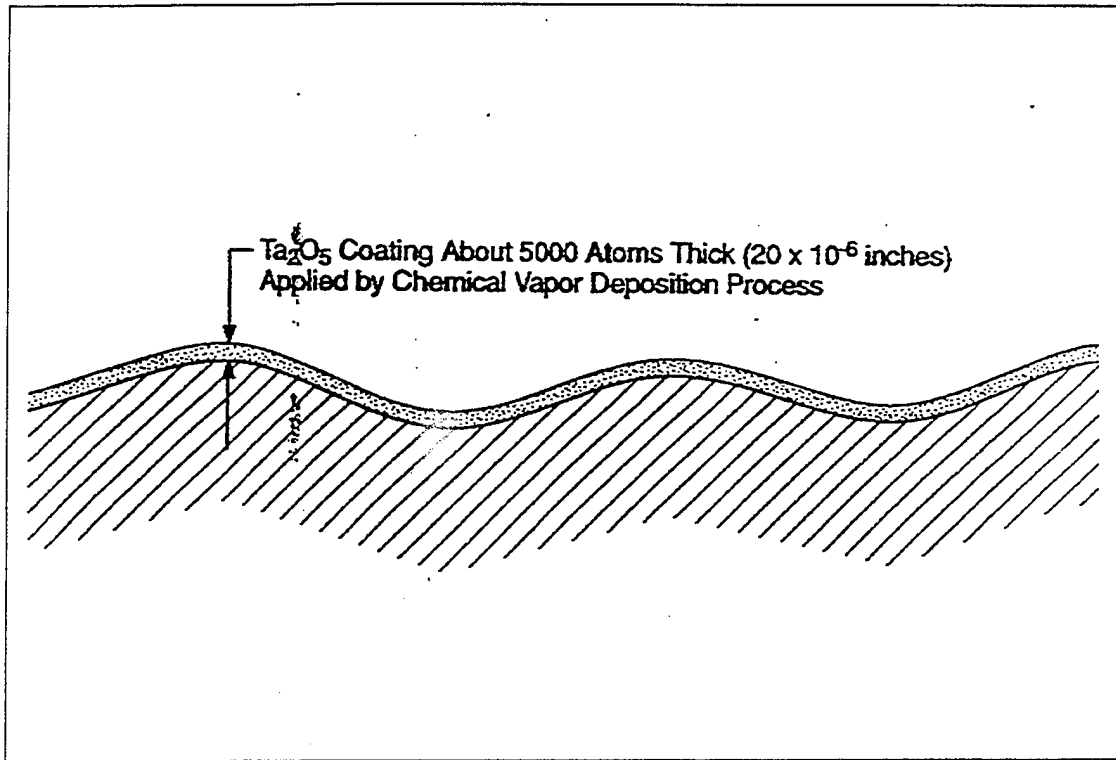


Figure 57 : GE's suggestion of coating film on the surface (from [Ref. 12]).

In the same direction with the Ta<sub>2</sub>O<sub>5</sub> coating Du Pont Lanxide Composites Inc. has suggested a ceramic coating to provide a material at the surface, which is resistant to nucleation of decomposing fuels especially sulfides. The suggested coating is the Cerased SN polymer. At this case coating will have thickness at the range of 25 microns [Ref. 18].

Both suggestions are to be investigated in the near future using the designed NPS testing rig and the results will be compared with A, A' and B types of swirl plates.

## APPENDIX D: ISENTROPIC FLOW AND FLOW MEASUREMENTS

In the present Appendix a short description of the isentropic flow concept and how this was adopted for the design of the flow measurements set-up as a way to measure the average holes closure, is given.

According to [Ref. 26], compressible flow problems are, in general, studied by combining the isentropic and/or adiabatic flow relations with the continuity equation. The one dimensional flow assumption can be used when the change of area in the duct is small and has a large wall radius of curvature [Ref. 26]. The real fluid velocity profile and the one dimensional approximation can be seen in Figure 58 (a) and (b) respectively.

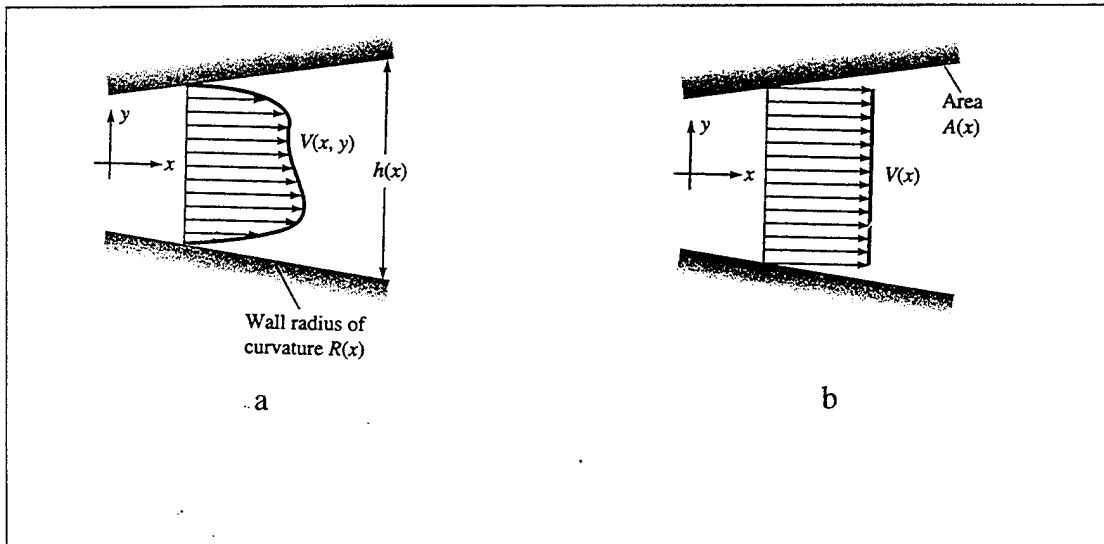


Figure 58 : Compressible flow through a duct : (a) real fluid velocity profile; (b) one dimensional approximation (from [26]).

$$\text{Continuity Equation : } \frac{d\rho}{\rho} + \frac{dV}{V} + \frac{dA}{A} = 0 \quad (\text{d.1})$$

$$\text{Momentum Equation : } \frac{dP}{\rho} + VdV = 0 \quad (\text{d.2})$$

$$\text{Speed of sound Equation : } dP = \alpha^2 d\rho \quad (\text{d.3})$$

Where :        A is the area of the duct

                  P is the pressure of the gas

                  V is the velocity of the gas

$\rho$  is the density of the gas

$\alpha$  is the speed of sound at the given conditions

$$\text{Using equations (d.1), (d.2) and (d.3) we get : } \frac{dV}{V} = \frac{dA}{A} \frac{1}{Ma^2 - 1} = \frac{-dP}{\rho V^2} \quad (\text{d.4})$$

An important parameter in the duct flow studies is the concept of the critical area which is usually termed by  $A^*$ . By this term we infer to the area that is required in order for the duct throat to have sonic flow.

Considering perfect gas relations and  $k=1.4$  White [Ref. 26] concludes to the relation

$$\frac{A}{A^*} = \frac{1}{Ma} \frac{(1+0.2Ma^2)^3}{1.728} \quad (\text{d.5})$$

which produces the plot that can be seen in Figure 59

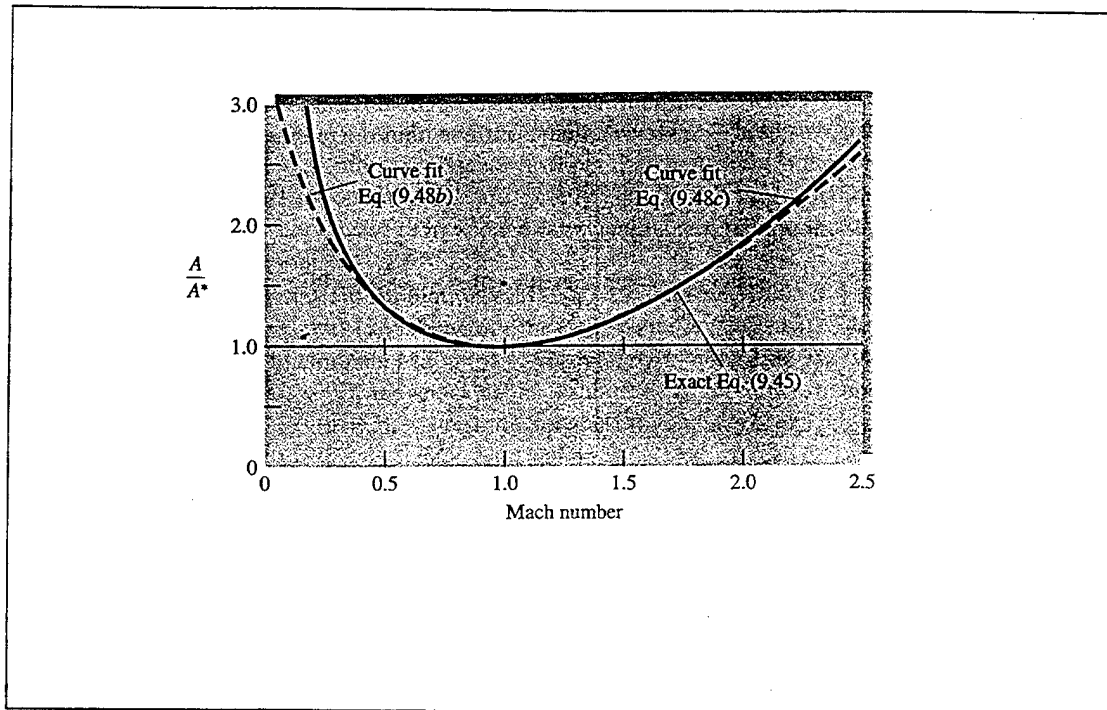


Figure 59 : Area ratio vs. Mach number for isentropic flow of a perfect gas with  $k=1.4$  (From [26]).

This figure shows that the minimum area which can occur in a given isentropic duct flow is the sonic or critical throat area. All other sections must have  $A > A^*$

Considering adiabatic - isentropic flow we get [Ref 26]:

$$\frac{T}{T_0} = \frac{2}{\lambda} \quad (d.6)$$

$$\frac{P}{P_0} = \left[ \frac{2}{\lambda} \right]^{\frac{\gamma}{\gamma-1}} \quad (d.7)$$

$$\frac{\rho}{\rho_0} = \left[ \frac{2}{\lambda} \right]^{\frac{1}{\gamma-1}} \quad (d.8)$$

$$\frac{\alpha}{\alpha_0} = \left[ \frac{2}{\lambda} \right]^{\frac{1}{2}} \quad (d.9)$$

$$\text{where } \lambda = 2 + (\gamma - 1)Ma^2 \quad (d.10)$$

The subscript 0 denotes stagnation properties.

For given stagnation conditions, the maximum possible mass flow passes through a duct is when its throat is at the critical or sonic condition. The duct then is said to be "choked" and can carry no additional mass flow unless the throat is widened. If the throat is constricted farther, the mass flow through the duct must decrease [Ref. 26].

In Figure 60 we can see the relation of Mach number and the  $P/P_0$  and in Figure 61 the relation of Mach number and the  $A/A^*$  ratio for subsonic flow.

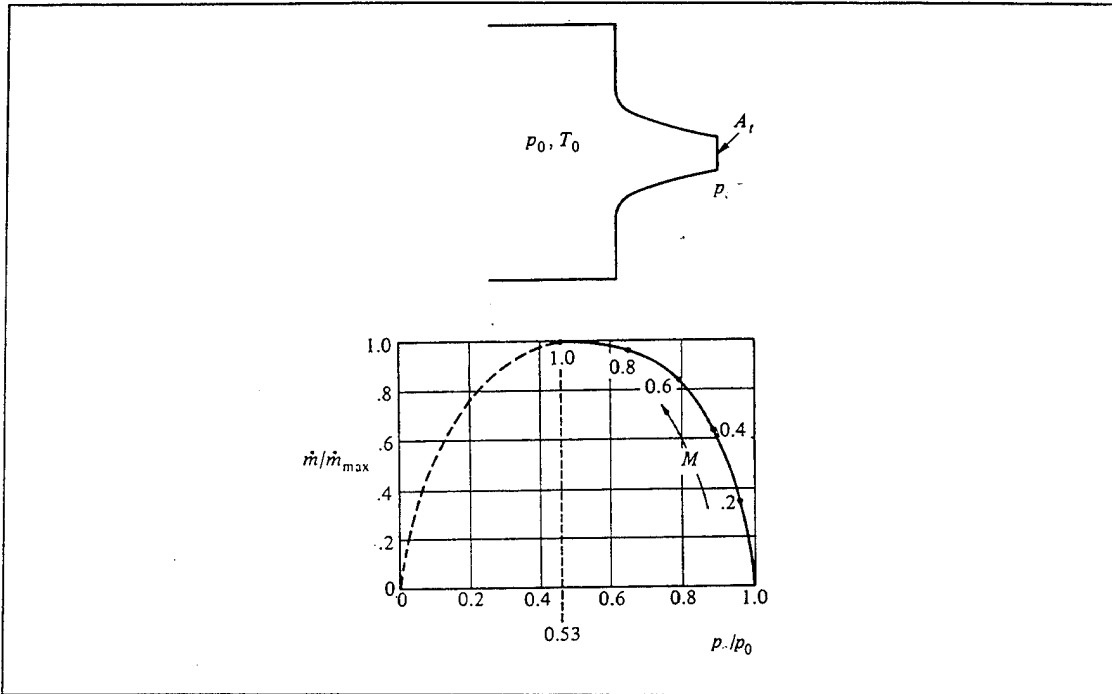


Figure 60 : Various pressure and Mach number configurations for flow through a nozzle (from [27]).

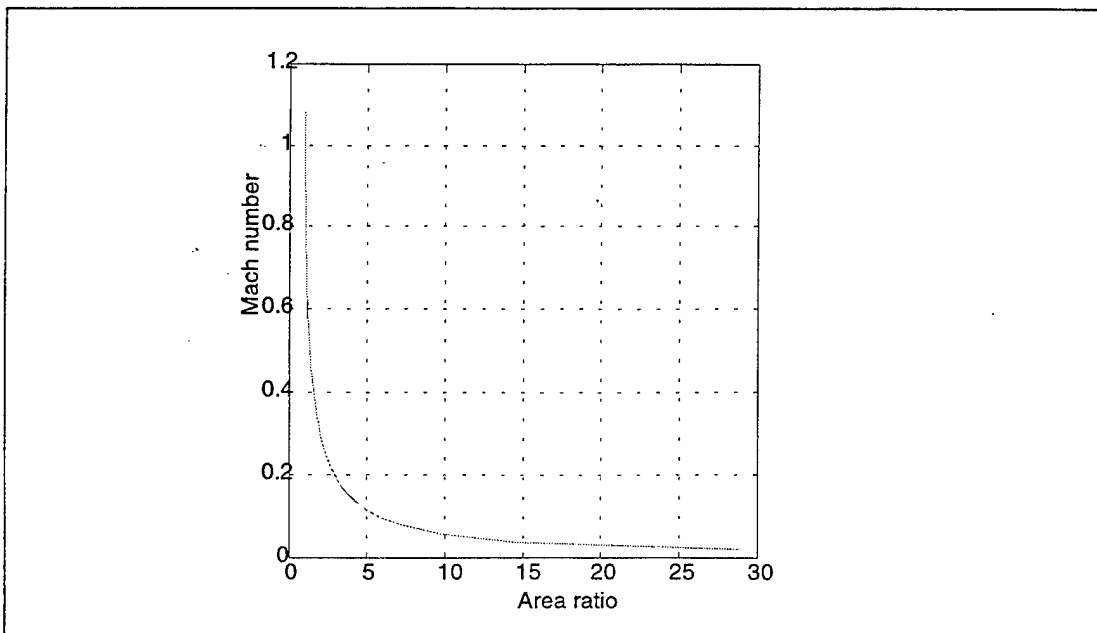


Figure 61 : Area ratio vs. Mach number for subsonic flow (from [26]).

For the case of the converging nozzles, which can be simulated with our case, flow analysis gives the results shown in Figure 62.

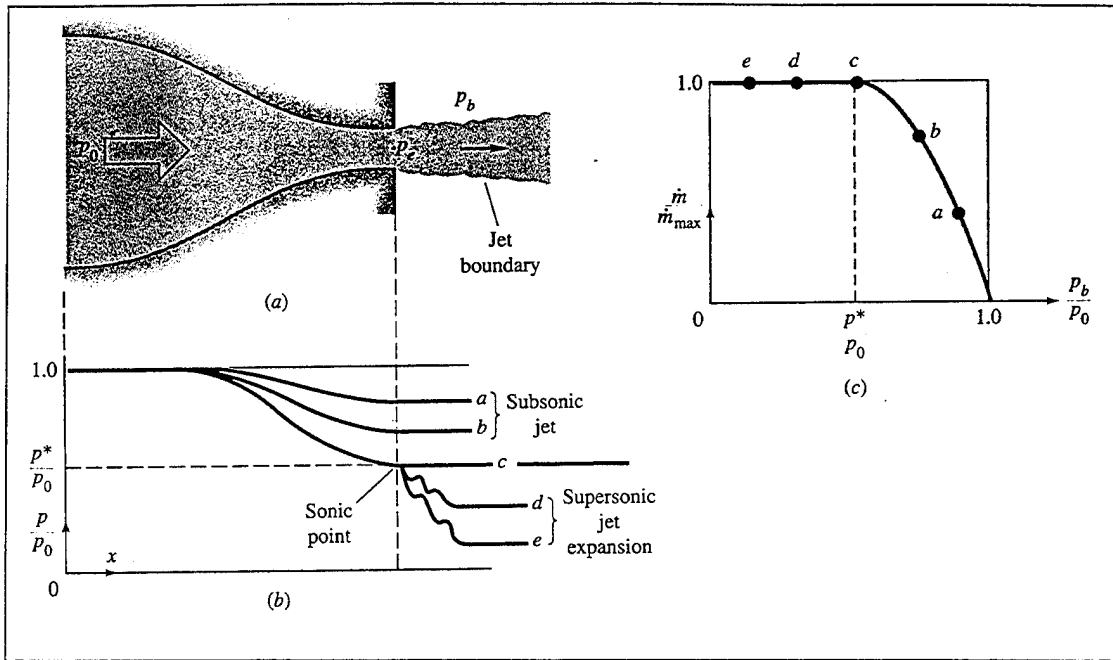


Figure 62 : Operation of converging nozzle (a) nozzle geometry (b) pressure distribution (c) mass flow vs. back pressure.(from [26]).

For a moderate drop in  $p_b$  to states a and b, the throat pressure is higher than the critical value  $p^*$  which could make the throat sonic. The flow in the nozzle is subsonic throughout, and the jet exit pressure  $p_e$  equals the back pressure  $p_b$ . The mass flow is predicted by the subsonic isentropic theory and is less than the critical value  $\hat{m}_{max}$ . (Fig 62 c).

For the condition c, the back pressure exactly equals the critical pressure  $p^*$  of the throat. The throat becomes sonic, the jet exit flow is sonic,  $p_e = p_b$  and the mass flow equals its maximum value. The flow upstream of the throat is subsonic everywhere.

Consequently the design restriction of the set-up was to be able to reproduce sonic flow conditions so that the area measured would be the critical one at each case and representing the maximum flow that can be passed through.

Considering the plots in order to get the sonic flow condition that would allow to obtain a duct flow through the swirl plates holes the following must be satisfied :

$$\frac{P}{P_0} = 0.53 \quad (d.12) \quad \frac{A}{A^*} \geq 6 \quad (d.13) \quad (\text{to verify subsonic flow before the swirl plate})$$

In our case we also have:

$$P = P_{atm} \quad (d.14) \quad P = P_{gage} + P_{atm} \quad (d.15)$$

In our case since the diameter of each hole of the already in use swirl plates is 0.0165 inches we get :

$$A^* = 12 \left[ \pi \frac{0.0165^2}{4} \right]_{144} = 0.0000178 ft^2 \quad (d.16)$$

$$A \geq 6A^* = 1.068 \cdot 10^{-4} ft^2 \quad (d.17)$$

From this result we can find the minimum required diameter for the tube that was used to carry the air to the nozzle in order to obtain a choked flow within the holes of the swirl plate.

Considering the atmospheric pressure being at the range of 101600 to 102500 mbars we can calculate what would be the range of the gage pressures that the gas is a required to have in order to obtain close to sonic flow conditions in our case. After performing the calculations using (d.14), (d.15) and (d.12) the gage pressure required is found to be at any case greater than 13 psi. The gage pressures that were taken in consideration in the experiment were at the 15, 20 and 25 psi.

According to White [Ref. 26] for isentropic flow through a duct, the maximum mass flow possible is proportional to the throat area and stagnation pressure. This is the reason why the plots of the characteristic flow curves for different pressures was performed in our case. It has provided the insurance that the design of the set-up was reproducing almost choked flow conditions for the flow through the swirl plates. As can be inferred from the previous development and the general isentropic flow model the

most accurate measurements are obtained when we are closed to the sonic flow conditions.

The principle of operation of the flow meter is based on the laminar by pass flow, in which most of the gas is forced. The resulting pressure drop within the flow meter forces a small fraction of the flow through the sensor tube.. Since both paths are perfectly laminar the ratio of the total flow  $\hat{m}$  to the sensed flow  $\hat{m}_1$  is exactly constant. A schematic of the operational principle is shown in Figure 63 [Ref. 28].

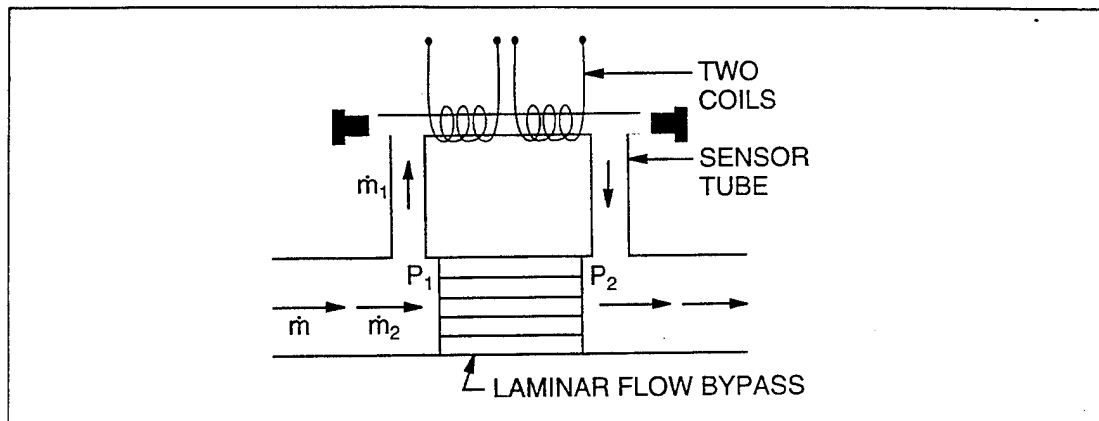


Figure 63 : Schematic of operational principle of flow meter (from [28]).

Two resistance temperature detector (RTD) coils around the sensor tube direct a constant amount of heat into the gas stream. In actual operation, the gas mass flow carries heat from the upstream coil to the downstream coil. The resulting temperature difference  $T_2-T_1$  is detected by the RTD coils and gives the output signal. Since the molecules of the gas carry away the heat, the output signal is directly and linearly proportional to gas mass flow [Ref. 28].



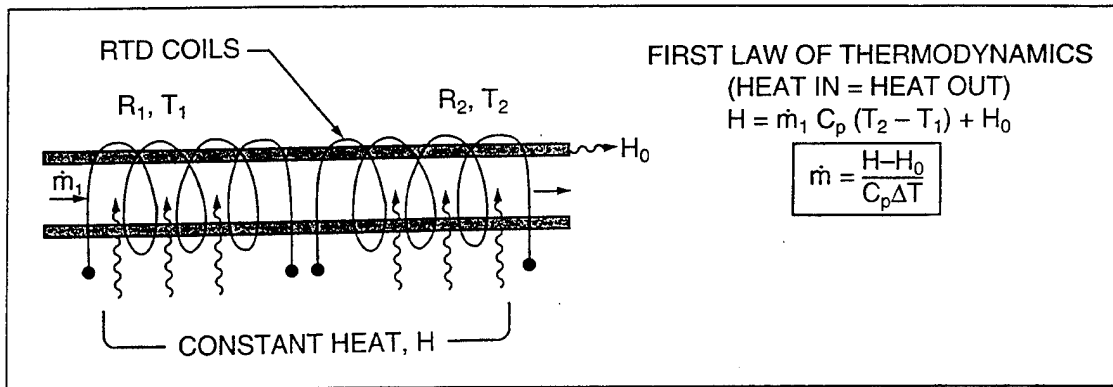


Figure 64 : Operation of coils in the Flow meter (from [28]).

Also the flow meter has to be placed at a minimum distance of 10 inches away from the pressure transducer to reduce turbulence [Ref. 28].

## APPENDIX E: COMPUTER PROGRAMMING DESCRIPTION

On the following Appendix a description of the main points of the programme used to run the testing rig is presented. The references that are associated with this description are [Ref.20] and [Ref. 29].

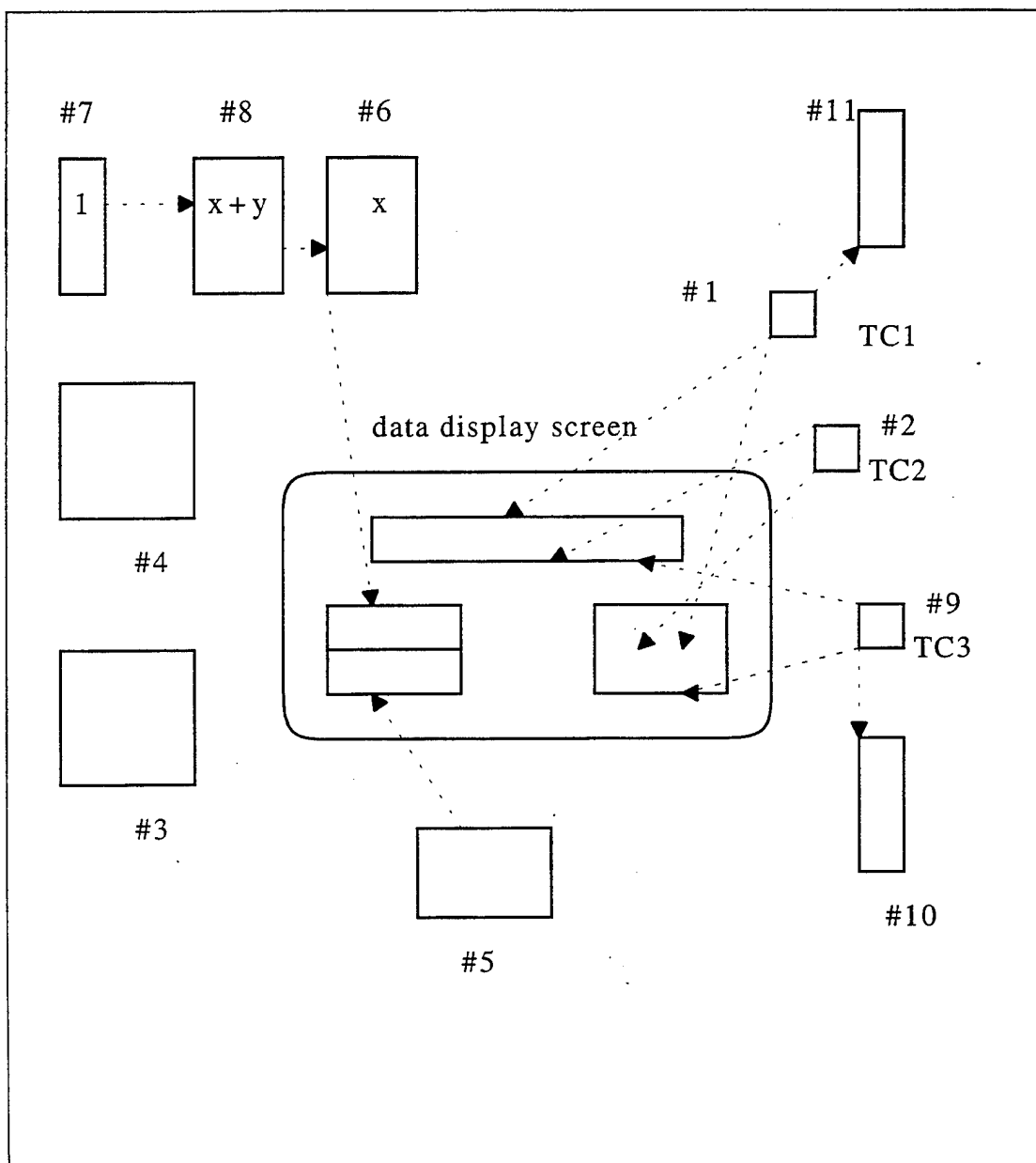


Figure 65: Schematic of the programme used in controlling the furnace.

### Blocks #7, 8, 6

The counting of the cycles performed is done with this three blocks

Block #7 initiates the counting of cycles

Block #8 takes input from Block #7 and #6 and compares with the desired number of cycles to be performed totally

Block #6 adds another cycle if the comparison of the already performed cycles shows that are less than required.

### Block # 4

It is a digital output block activating the relay of the ZIPPETTE pumps

### Block # 3

It is a digital output block activating the three way valve

### Block # 5

A clock counter measuring the time of each cycle and displaying the total time of the experiment.

### Blocks # 1, 2, 3

Thermocouple blocks measuring the temperature in F. Specifically

#1 measures the temperature of the left swirl plate

#2 measures the temperature of the right swirl plate

#9 measures the temperature of the furnace

### Block #10 PID controller

The newly designed testing rig was connected with a PID controller programmable from the NOTEBOOK software package. The new connections were made in such a way so that the control of turning on and off the furnace could be performed through this PID controller. As it is mentioned in the LABTECH NOTEBOOK reference manual the PID controller is based on the PID control equation as follows:

$$O(t) = Pe(t) + I\int e(t')dt' + D\frac{de}{dt}$$

where  $O(t)$  = Output

$e(t)$  = Error (defined as Set point-input)

P = Proportional Constant

I = Integral Constant

D = Derivative Constant

Notebook calculates the error by subtracting the value of the input signal from the setpoint. The proportional, integral, and derivative constants are to be specified for each application. A common way to define these constants is the Zeigler-Nichols method [Ref. 30]).

The furnace that is used in the experiment has variable cooling and heating rates that can be preset. The problem to be solved in our case, was to make the NOTEBOOK PID controller Loop Setpoint compatible with the pre-set rates. The best solution was obtained by using the furnace's temperature as the guiding temperature determining the Loop Setpoint. The choice of the swirl plates temperature as the guiding one has not been proved successful because it lead to unsteady temperature time profiles. On the other hand by guiding the furnace temperature in order to achieve the actual temperature-time

for the swirl plate, the heat inertia of the furnace-nozzles system should be taken into account. Whith htese in mind and after lot of experimental trial and error the best solution was found to be for the following settings:

P=0.3

I=0.01

D=0

Block #11

This block saves the temperatures of the swirl plates anfd the furnacein a file in order to be available for actual verification of the temperature-time profile obtained each time. Different sampling rates can be chosen, according to the usetr's needs.

On Figure 65 we can see a schematic of the data display screen.

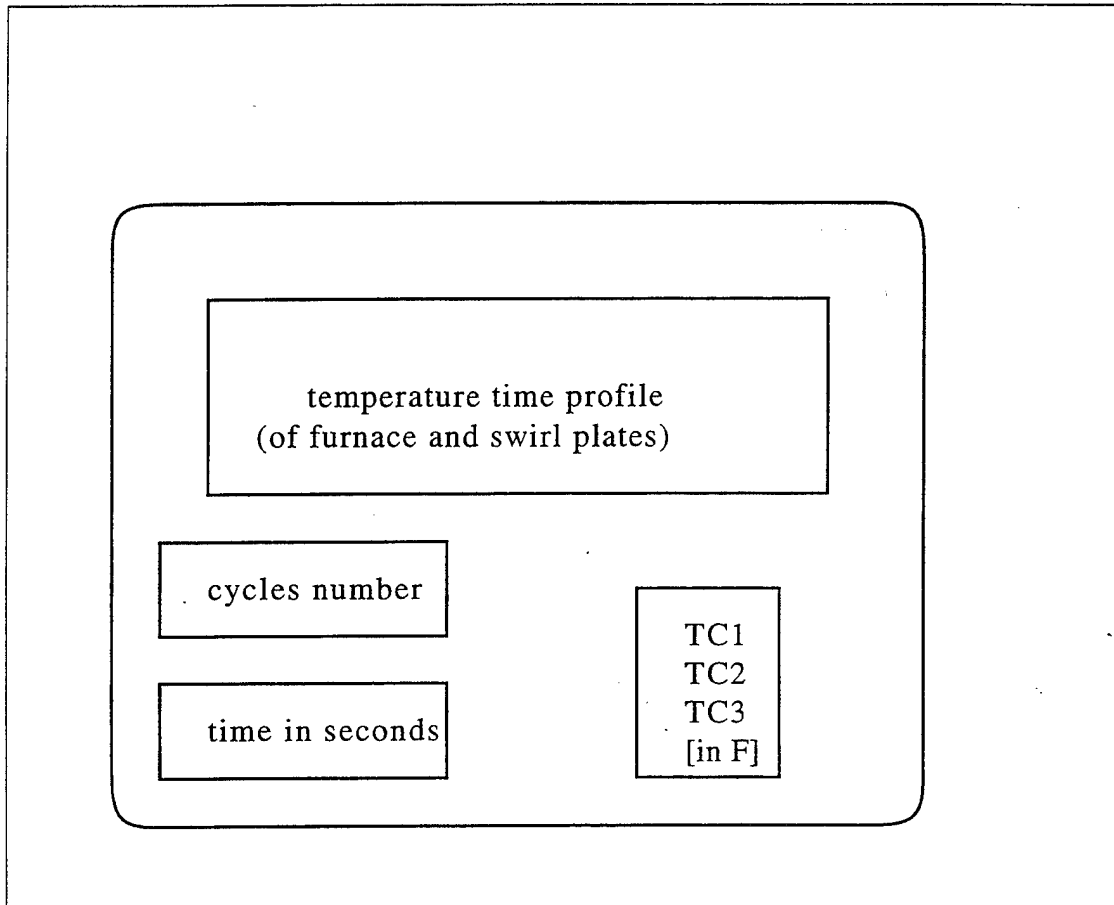


Figure 66 : Schematic of the data display screen.

On Figure 67 the temperature-time profile of the swirl plates along with the furnace temperature (which is controlled by the programme) can be seen.

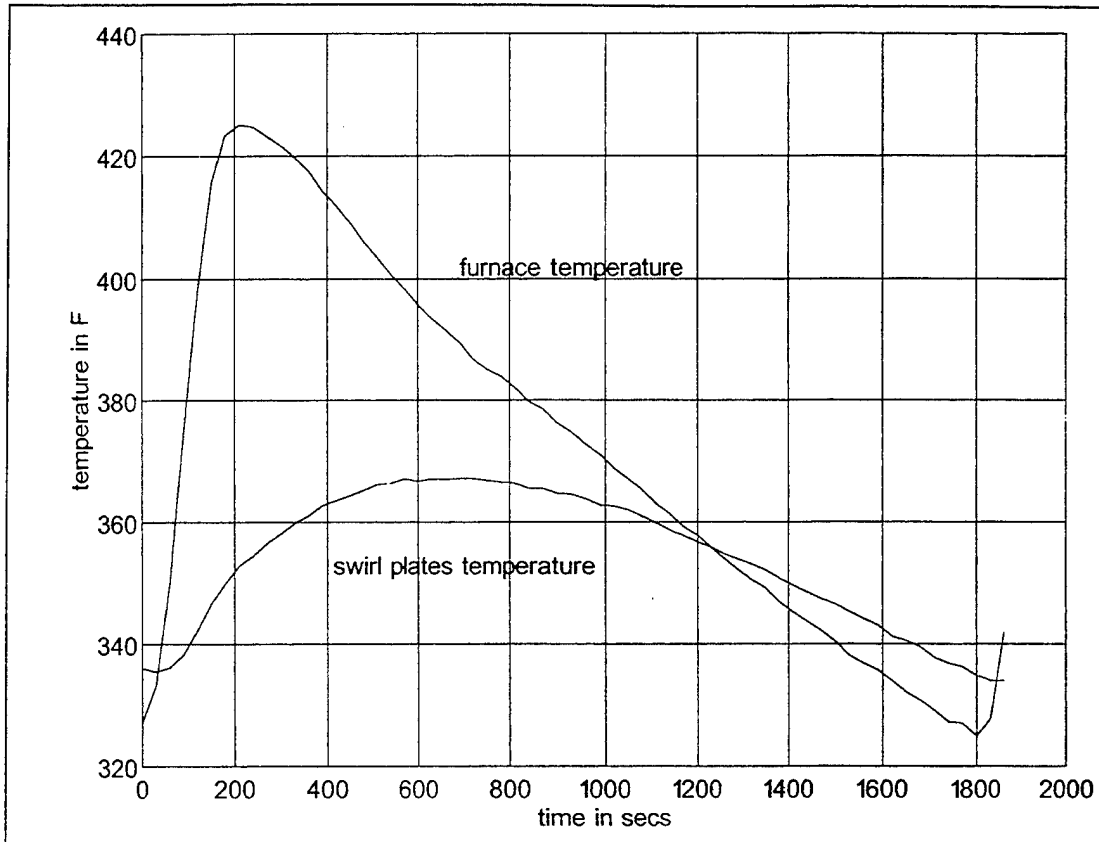


Figure 67: Temperature time profile for the swirl plates and the furnace



## **APPENDIX F: PRINCIPLES FOR A PROPOSED GRADING SYSTEM ON THE COKING RESISTANCE OF SWIRL PLATES**

### **A. GENERAL**

As mentioned in the last part of the recommendations section, the results obtained from the methods described in this study can be incorporated to establish a grading system for the evaluation of coking resistance for the swirl plates. The purpose of this system is to associate the data obtained from several experiments, and come up with a numerical value on a grading scale. In this way the people working on practical applications, who need to know early if the swirl plate suggested is within their expectations, can decide without getting into the details of the experimental results. Instead they have to just refer to the grading scale that has been established and check the number that is available for the questioned swirl plate.

For example in the present programme the experimental method is comprised by four different measurements/examinations: weight measurements, optical examination , SEM examination and flow measurements. Each of these measurements examinations can be associated with a percentage number representing how reliable the measurement is in examining the coking problem. In order for these percentage numbers to be assigned a large number of experiments has to be performed so that a large sampling size is achieved. This number will be characteristic of the method and can be called the "characteristic number".



Considering the results obtained from each kind of measurement examination, one could grade them (or put them in a scale) based on comparison with "model" measurements available and assign them a number. The "model" measurements - examination results can be either pictures from previous experiments at various coking conditions (in the case of the optical or SEM examination ), or weight increase and hole closure numbers (in the case of the weight and flow measurements). The number assigned will be representative of the result and could be called the "scalar factor".

By multiplying the scalar factor with the respective " characteristic number" and adding the products we get a number which can be directly associated with a grading system established in the form of tables with all possible results. This number could be called the "quality number" and could be arranged such that the higher the numerical value, the better the resistance to the potential coking accumulation of the swirl plate is.

## B. EXAMPLE

A simple example of how the method could be incorporated is shown:

Measurement - Examination method	Characteristic number (%)
Weight increase	A
Optical Examination	B
SEM Examination	C
Flow measurements / Hole closure	D

Table 9: "Characteristic numbers" of measurements - examinations

( A+B+C+D=100%)

Measurement-Examination Method	Scalar Factor
Weight increase	a
Optical Examination	b
SEM Examination	c
Flow measurements / Hole closure	d

Table 10 : Scalar Factor of measurements - examinations

According to the suggested method the "quality number" will be:

$$Q = aA + bB + cC + dD$$

and can be associated with an established grading matrix giving information about the behavior of the swirl plate in the coking accumulation problem based on the measurements and examinations performed.



## LIST OF REFERENCES

1. Jane's, All the world's aircrafts 1995-1996.
2. P.J.Hart, Summary of Heat Transfer Work on A427 Fuel Nozzles. Allison Co, July 30, 1991.
3. Prof. Roy Crooks archive. T56-A-427 Engine Fuel Modification.
4. NAVAIRSYSCOM, AIR-5116C, E-2C CLASS DESK, RM 1214, CDR Newman, 4 November 1991.
5. Allison Service Information Letter. Gas Turbine Division, July 29, 1991.
6. William T. Reid External Corrosion and Depositions in Boilers and Gas Turbines. Fuel and Energy Science Series. J.M.Bee'r.
7. Earle H. Kennard, Kinetic Theory of Gases, Mc Graw-Hill, New York, 1938, (p.282).
8. Robert N. Hazlett, James N. Hall, Martha Matson. Reaction of Aerated N-Dodecane Liquid Flowing over Heated Metal Tubes. (Ind. Eng. Chem. Vol 16 No. 2, 1977).
9. Irwin E. Treager, Aircraft Gas Turbine Technology, Second Edition.
10. Burman, De Luca, Fuel Injection and Controls for Internal Combustion Engines / Fuel Systems for Gas Turbines and Jet Engines.
11. Technical Repair Standard for AG9130 Ship Service Gas Turbine Generator.
12. General Information for GE coke barrier coating. Information Package.
13. FAX Veda Inc. NPS Fuel Nozzle Coking Research Project, July 1995.
14. Coordinating Research Council Inc., Aviation Fuel Properties (1983).
15. Maxwell Smith, Aviation Fuels.

16. Purge System, Low Pressure Fuel Nozzle Purge System / Program Preliminary Design Review , June 1994.
17. FAX Veda Inc., 17 JAN 1996.
18. Du Pont Lanxide Composites Inc. Information Package, January 5, 1993
19. Victor L. Streeter, E. Benjamin Wylie, Fluid Mechanics, Eighth Edition (1985)
20. LABTECH NOTEBOOK Reference Manual (11/92).
21. NEY, Box Furnace Installation, Operation and Service Manual (Models 2-90, 2-160, 2-525, 2-1350).
22. IMAGE PRO Reference Manual.
23. D.P. Barnard, Lamont Eltinge, Research Department, Standard Oil Co, Aircraft Turbine Fuel Properties Affecting Combustor Carbon.
24. V. Vassiloyanakopoulos, Study of physical and chemical mechanisms of formation of deposit on metal surface due to burning, evaporation or oxidation of fuel in gas turbines, 5 December 1995.
25. William D. Callister, Jr Materials Science and Engineering. An Introduction. Third Edition, 1994.
26. Frank M. White, Fluid Mechanics, Third Edition 1994.
27. Lames E. A. John, William L. Haberman, Introduction to Fluid Mechanics, Prentice Hall, 1988.
28. Instruction Manual for series 820 Top-Track flow monitoring, Sierra Instruments.
29. Duncan A. Mellichamp Real Time Computing with applications to data acquisition and control . Van Nostrand Reinhold Electrical/Computer Science and Engineering Series.

## INITIAL DISTRIBUTION LIST

	No. of copies
1. Defence Technical Information Center 8725 John J. Kingman Rd., STE 0944 Ft. Belvoir, VA 22304-6145	2
2. Dudley Knox Library Naval Postgraduate School 411 Dyer Rd. Monterey, CA 93943-5002	2
3. Professor Jeff Perkins Code ME/PS Department of Mechanical Engineering Naval Postgraduate School Monterey, California 93943-5004	3
4. CDR Jim Clifton NAVAIR Code 411 1421 Jefferson Davis Hwy. Arlington, Virginia 22243-5169	1
5. Mr. Earl Eck NAVAIR Code 441 1421 Jefferson Davis Hwy. Arlington, Virginia 22243-5169	1
6. Mr. Doug Mearns NAVAIR Code : AIR 4-4 <Mgr. Fuels and Lubricants> Propulsion and Power Division 1421 Jefferson Davis Hwy. Arlington, Virginia 22243-5169	1
7. Mr. Wayne Osgood VEDA Inc. 1800 North Beaurequet St. Alexandria, Virginia 22311-1708	1
8. Dean of Instruction Code 06 Naval Postgraduate School Monterey, California 93943-5000	1
9. Research Administration, Code 08 Naval Postgraduate School Monterey, California 93943-5000	1

10. Department Chairman, Code ME/Mc  
Department of Mechanical Engineering  
Naval Postgraduate School  
Monterey, California 93943-5004 1
11. Naval Engineering Curricular Office, Code 34  
Naval Postgraduate School  
Monterey, California 93943-5004 1
12. Embassy of Greece  
Naval Attaché  
2228 Massachusetts Ave., N.W. 2
13. LTJG Vassilis Vassiloyanakopoulos  
17 Triantafylou St.  
Patissia GR 11255  
Athens, Greece 2